PERGAMON

Aerosol Science 33 (2002) 1667–1679

Journal of
Aerosol Science

www.elsevier.com/locate/jaerosci

Broad range observation of particle deposition on greased and non-greased impaction surfaces using a line-sensing optical microscope

Naomichi Yamamoto[a,*], Minoru Fujii[b], Osamu Endo[c], Kazukiyo Kumagai[a], Yukio Yanagisawa[a]

[a] *Department of Environmental Systems, Institute of Environmental Studies, Graduate School of Frontier Sciences, The University of Tokyo, 5th Building of School of Engineering, Hongo 7-3-1, Bunkyo-ku, Tokyo 113-8656, Japan*
[b] *Department of Chemical System Engineering, School of Engineering, The University of Tokyo, 5th Building of School of Engineering, Hongo 7-3-1, Bunkyo-ku, Tokyo 113-8656, Japan*
[c] *National Institute of Public Health, Shirokanedai, 4-6-1 Minato-Ku, Tokyo 108-8638, Japan*

Received 1 July 2002; received in revised form 21 August 2002; accepted 23 August 2002

Abstract

A computer-automated optical microscope combined with a line-sensing camera was used to capture the entire range of a particle deposit downstream of an individual acceleration nozzle in a hi-volume Andersen sampler. To investigate the particle bounce and reentrainment, particles collected on collocated greased and non-greased Teflon plates on the inlet stage ($d_a > 7$ μm) were observed by an automated particle counting, locating and sizing method. The result confirmed reproducible collection characteristics among nozzles even though application of the grease increased collection efficiency and altered the size distribution of collected particles to the larger side. In these experiments, assuming spherical particles with uniform density, approximately 65% of particle mass and 50% by number were lost from non-greased plates at 54% RH, while 45% by mass and 25% by number were underestimated at 84% RH. The spatial investigation showed that particles were densely deposited around the center of deposition on greased plates while on non-greased plates they were dispersedly distributed. Particle dispersions on the smooth impaction plate were due to bounce and/or reentrainment of small particles especially with $d_{PA} < 10$ μm.

Keywords: Line-sensing optical microscope; Particle bounce and reentrainment; Impaction; Grease

* Corresponding author.
E-mail address: yamamoto@yy.t.u-tokyo.ac.jp (N. Yamamoto).

0021-8502/02/$ - see front matter
PII: S0021-8502(02)00120-9

1. Introduction

Impactors use the principle of inertia to collect and/or separate airborne particles based on their Stokes numbers. In the space between the nozzle exit and impactor plate, accelerated particles tend to continue in a straight line and eventually impact on the flat impaction plate due to their inertia while the air streamlines bend sharply. Although large particles, i.e. ones with Stokes numbers larger than a critical value, tend to be unable to follow the air streamlines due to their inertia, small particles can follow them. Using this mechanism, the cascade impactors, samplers with impactor stages in series, have been widely used for the measurement of particle size distribution by mass because of their capability to separate polydisperse airborne particles based on inertial classification. Many types of cascade impactors including the Lundgren impactor, Andersen sampler, Mercer impactor, and the micro-orifice uniform deposit impactor (MOUDI) (Marple, Rubow, Turner, & Spengler, 1987; Marple, Rubow, & Hehm, 1991) have been developed for aerosol sampling over the past few decades.

In inertial impactors, large, dense and solid particles often bounce on the impaction plates because of their kinetic energy of rebound (Dahneke, 1971). Since the nozzle velocities become greater in subsequent stages, particles once bounced are likely to continue to bounce until they reach the final stage of the cascade impactor, typically an afterfilter. In addition to bounce, particle reentrainment, i.e., blow off of particles by a jet with sufficient force to overcome adhesive forces between particles and impaction surface, is also important (Hinds, 1999). Corn and Stein (1965) used various sizes of glass beads to investigate particle reentrainments in relation to the particle size and bulk air velocity. In their study, particle reentrainments were increased for larger particles and with greater air velocity. For these reasons, particle bounce and reentrainment errors can be often significant in the size-distribution measurement by cascade impactors (Dzubay, Hines, & Stevens, 1976; Cheng & Yeh, 1979). It is known that surface roughness of substrate materials, types of coating materials, particle size, nozzle velocity, and solidity and hardness of particles play important roles in particle bounces and reentrainments (Rao & Whitby, 1978a, b; Reischl & John, 1978; Ellenbecker, Leith, & Price, 1980; Hinds, Liu, & Froines, 1985; Turner & Hering, 1987; Newton, Cheng, Barr, & Yeh, 1990; Chang, Kim, & Sioutas, 1999). Although some impaction substrates such as quartz fiber have relatively soft surfaces, which reduce particle bounce and reentrainment due to some partial entrainment of the impinging air streamlines on the impaction substrate, smooth and solid surface substrates such as aluminum foil or Teflon PTFE filters result in loss of particles from the target stage and contamination by bounced or reentrained particles into subsequent stages. The most commonly used method to reduce particle bounces and reentrainments is the application of high-viscosity grease on impaction surfaces (Rao & Whitby, 1978a, b; Turner & Hering, 1987). Greasing materials, however, may interfere with the chemical analyses of particles collected on the greased substrate. While coating with oil or grease is essential if elimination of large particles were only the purpose of impaction, it is not always applicable especially in cascade impactors for which all the stages are normally intended for subsequent analyses.

To investigate particle loss due to bounces and/or reentrainments, monodisperse fluorescent polymer microspheres were often used in the laboratory experiments (Wall, John, Wang, & Goren, 1990; Chang et al., 1999). The amounts of traceable fluorescent particles collected on the impaction surfaces and afterfilter were subsequently analyzed by fluorescence detectors to compare the mass balance of particles on each medium. Furthermore, this method could investigate the wall loss of particles

by washing sampler walls to extract them (Chang et al., 1999). Provided that a greased impaction surface could completely prevent from particle bounce and reentrainment, afterfilters loaded at the downstream of each greased and non-greased impaction plate in collocated samplers were weighed to compare the amounts of particles even though the wall loss of particles could not be considered in this method.

Many methods have been attempted for quantitative analysis of particle bounces and reentrainments on impaction surface. To our knowledge, however, no study has ever been conducted to visually investigate the entire area of a particle deposition created by an individual acceleration nozzle of an inertial impactor. Since the visual investigation of particles using microscopes is normally performed manually, it is slow, tedious and often inaccurate due to operator error or bias (Hinds, 1999). In addition, the scope of observable area was quite limited in optical microscopes with fixed objective lens and slide. To overcome these problems, the computer-automated optical microscope combined with a line-sensing camera, used in conjunction with a linear motor actuating slide, was used to capture the entire range of a particle deposition. This method was used in this paper to characterize the entire image of a particle deposition on an impaction plate generated by an individual acceleration nozzle of a cascade impactor, and investigate the possible mechanisms of particle bounce and reentrainment by comparing spatial patterns of particles deposited on greased and non-greased Teflon impactor plates. This method could furthermore investigate particle bounce and reentrainment events at real sampling situations, as opposed to laboratory-based experiments using monodisperse aerosols, and identify the size portion of bounced and/or reentrained particles for a given impaction stage.

2. Experimental

In this study, a hi-volume Andersen sampler (Model AH-600, Shibata Scientific Technology Ltd., Tokyo, Japan) was used. Although quartz fiber substrates, designed exclusively for a hi-volume Andersen sampler, were commercially available, PTFE Teflon plates of 1 mm thickness were used as impaction plates to imitate the conditions under which smooth substrates such as aluminum foil or Teflon PTFE filter are used in an inertial impactor. In addition, white Teflon plates made easier to observe particles by an optical microscope because of its contrast with dark color airborne particles composed mostly of black carbon, typical of the Tokyo area (Kaneyasu, 1998). Teflon plates were cut into approximately 1×1 cm^2 pieces and were placed right beneath the nozzle exits from the upper stages of a cascade impactor. A hi-volume Andersen sampler was used because the large stage area (approximately 30 cm of diameter) and sufficient space among each nozzle hole on a sampling stage made it possible to place 1×1 cm^2 pieces of Teflon plates (Fig. 1). Numbers of nozzles, air velocities and diameters of nozzles for each stage are summarized in Table 1.

To investigate the particle bounce and reentrainment, the numbers of deposited particles on non-greased and greased Teflon plates were compared. Since particle bounce and reentrainment were expected to occur mostly on the inlet stage, which collects the largest particles with sufficient energy to bounce and/or re-entrain, the investigation was focused on the inlet stage, i.e. the stage for particles with > 7 μm of aerodynamic diameter, d_a. Both greased and non-greased plates were collocated on the impactor stage (Fig. 1). Three-quarters of the surface area of the stage were covered with a quartz fiber filter as in its normal configuration, while the remaining one-quarter was reserved for 12 Teflon plates. A total of 12 Teflon plates including six greased and six non-greased

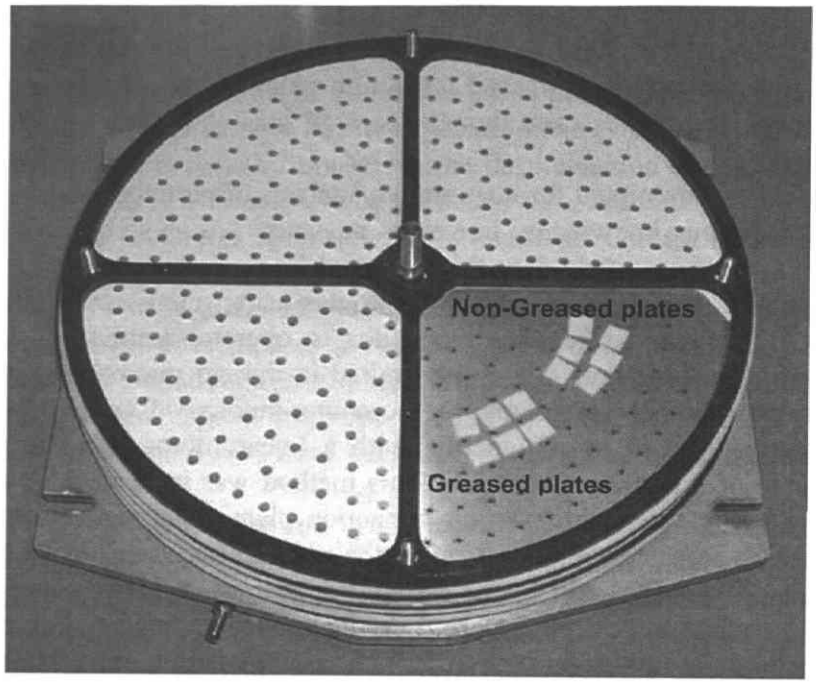

Fig. 1. Greased and non-greased Teflon plates on the impactor stage.

Table 1
Specifications of impactor stages of a hi-volume Andersen sampler, AH-600 Model

Stage Number	Size range d_a (μm)	Jets/stage	Impactor jet diameter, D_j (mm)	Nozzle velocity (m/s)
1	> 7.0	300	3.48	3.31
2	3.3–7.0	296	2.14	8.74
3	2.0–3.3	300	1.54	16.88
4	1.1–2.0	296	1.05	36.31

surfaces were placed immediately beneath the exits of 12 acceleration nozzles. The Teflon plates were directly attached on the steel surface of the impactor stage by double-sided tape. In this experiment, high-vacuum silicone grease (Dow Corning Asia Inc., Kanagawa, Japan) dissolved in acetone was applied onto the impaction surfaces for greased Teflon plates, and allowed to dry. Samplings were conducted on the roof of the building of the National Institute of Public Health, Tokyo, Japan on May 14 and August 7, 2002. Two samplings were performed to observe the effect of relative humidity (RH) on particle bounce and/or reentrainment. Ambient sampling conditions including temperature and RH are shown in Table 2. In these experiments, flow rate was adjusted to 566 l min^{-1} as specified for the sampler, and the air samples were taken for 90 and 45 min for May 14 and August 7 samplings, respectively.

An optical microscope equipped with a line sensor camera, Dot Analyzer DA-6100/LS (Oji Scientific Instruments, Hyogo, Japan), was used to examine the particles collected on greased and

Table 2
Ambient sampling conditions

Sampling date and time	RH (%)	Temperature (°C)
May 14, 2002, 11:30–13:00	54	22
August 6, 2002, 7:00–7:45	84	28

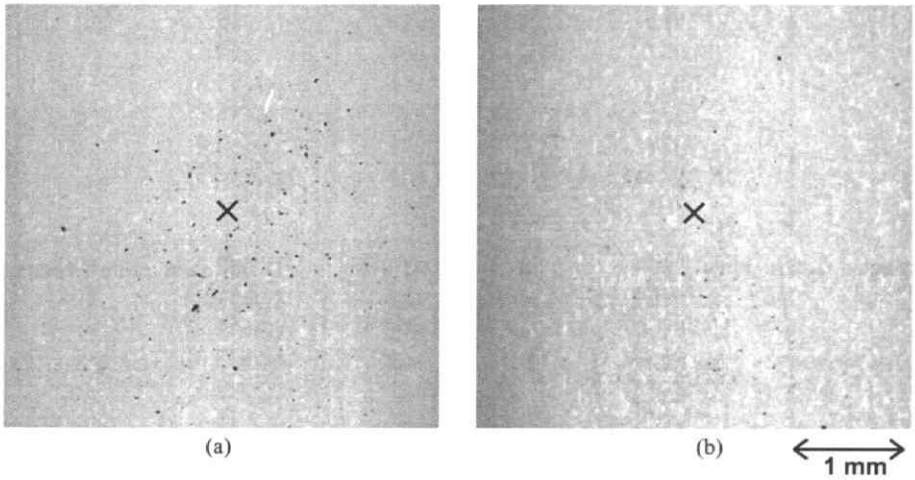

Fig. 2. Images of particle depositions on (a) greased and (b) non-greased Teflon impaction plates with calculated centers of particle depositions.

non-greased Teflon impaction plates. Using its advantage of line-sensing mechanism, accomplished with its linear motor actuating slide, to capture broad ranges of target materials, an entire area of a particle deposition created by each individual acceleration nozzle could be observed. Captured images were then segmented into black and white pixels ($2.747 \times 2.747\ \mu m^2$/pixel) by the image analysis software, DA-6000, bundled with the optical microscope (Oji Scientific Instruments, Hyogo, Japan) to process sizes, numbers and locations of deposited particles.

3. Results and discussion

The images of particle deposits on greased and non-greased Teflon impaction plates captured by the Dot Analyzer DA-6100/LS are shown in Fig. 2. The particle numbers and size distributions based on their projected area diameters, d_{PA}, on greased and non-greased Teflon impaction plates at 54% and 84% RH are summarized in Tables 3 and 4. The result indicated that the variability of particle numbers collected on each type of impaction surfaces was small among nozzles ($N = 245 \pm 24$ and 119 ± 18 for greased and non-greased plates at 54% RH, and $N = 488 \pm 53$ and 368 ± 77 at 84% RH, respectively). The size distributions of particles in d_{PA} on each type of plates were also consistent among nozzles, ranging 13.8–15.8 and 11.2–13.4 μm of geometric mean particle diameters for greased and non-greased impaction plates at 54% RH, and 11.8–13.0

Table 3
Numbers and size distributions of particles collected on greased and non-greased Teflon impaction plates at 54% RH

Impaction substrate	Sample[b] ID	Numbers of particles, N	Size distribution[a]	
			Geometric mean diameter, d_{PA} (μm)	GSD
Greased Teflon plate	G1	269	13.8	1.7
	G2	257	15.2	1.7
	G3	216	14.6	1.6
	G4	235	15.8	1.6
	G5	223	15.8	1.7
	G6	270	15.0	1.6
	Mean	245	15.0	1.7
	SD	24		
Non-greased Teflon Plate	NG1	117	12.7	1.6
	NG2	103	11.2	1.8
	NG3	127	12.7	1.8
	NG4	104	13.0	1.6
	NG5	152	12.5	1.6
	NG6	111	13.4	1.8
	Mean	119	12.6	1.8
	SD	18		

[a]Based on particle's projected area diameters.
[b]Each sample was taken beneath each individual nozzle jet.

and 10.8–11.7 μm of the diameters at 84% RH, respectively. Geometric standard deviations (GSDs) of size distributions of collected particles were 1.6–1.7 and 1.6–1.8 for greased and non-greased plates at 54% RH, and 1.6–1.7 and 1.6–1.7 at 84% RH, respectively. In Figs. 3 and 4, the size distributions of particles on greased and non-grease plates are shown, with calculated frequency of lost particles defined as differences between particle numbers on greased and non-greased plates within each particle size interval. The size distributions in Figs. 3 and 4 were obtained from the ambient air of 1.02 and 0.51 m^3 collected through six nozzles (total 300 nozzles/stage) with a flow rate of 566 l min^{-1} for 90 and 45 min, respectively. Results indicated that larger particles were selectively lost from the non-greased impaction plates. In these experiments, assuming all the particles were spheres with uniform density, approximately 65% of particle mass and 50% by number were lost from non-greased plates at 54% RH, while 45% by mass and 25% by number were underestimated at 84% RH. These findings suggest that errors in the size distribution measurement due to particle bounces and/or reentrainments affected, to a higher degree, mass rather than number concentrations. In addition, it was found in this study that particle loss due to bounce and/or reentrainment occurred more significantly at the lower RH condition, which has been studied by many investigators using non-microscopic methods (Owens, 1923; Winkler, 1974; Stein, Turpin, Cai, Huang, & McMurry, 1994; Vasiliou, Sorensen, & McMurry, 1999). The size distributions in Tables 3 and 4 and Figs. 3 and 4 were, however, based on particle projected area diameters and

Table 4
Numbers and size distributions of particles collected on greased and non-greased Teflon impaction plates at 84% RH

Impaction substrate	Sample[b] ID	Numbers of particles, N	Size distribution[a]	
			Geometric mean diameter, d_{PA} (μm)	GSD
Greased Teflon plate	G1	471	12.0	1.6
	G2	424	13.0	1.7
	G3	466	11.8	1.7
	G4	473	12.1	1.6
	G5	516	12.2	1.7
	G6	579	12.3	1.7
	Mean	488	12.2	1.7
	SD	53		
Non-greased Teflon plate	NG1	510	11.2	1.6
	NG2	281	10.8	1.6
	NG3	376	11.1	1.6
	NG4	344	11.7	1.7
	NG5	329	11.1	1.6
	NG6	368	11.2	1.6
	Mean	368	11.2	1.6
	SD	77		

[a]Based on particle's projected area diameters.
[b]Each sample was taken beneath each individual nozzle jet.

might be distorted by the deformation of particles at the moment of impaction. Since the particle deformation energy may be altered with the application of greasing materials, the particle size distributions on greased and non-greased plates might be affected differently. The effect of the application of grease to particle deformation is an issue that requires further investigation, for instance, using three-dimensional profile microscopes. The result, however, could confirm the reproducible collection characteristics among the nozzles even though the application of the grease increased the collection efficiency and altered the size distribution of collected particles to the larger side.

Particle deposition patterns were characterized along the distance from the central point of a particle deposition, i.e. the point at which the jet centerline intersected the impaction plate. Since it was inaccurate to externally determine the center of particle deposition using measurement tools such as micrometers, the point was defined based on the spatial distribution of particles on the impaction plane. Since the particle deposit pattern was circular for the impactors with circular jets, the point at which the jet centerline intersected the impaction plate should be the same at the center of particle deposit of circular shape. Using the image analysis software, X and Y values were automatically given to each particle based on their horizontal and vertical locations on the image captured by the microscope. Since the particle distribution was symmetric, i.e. circular, we defined the means of all the particle location, i.e. mean X and Y values of all the particle, as a center of deposition on that

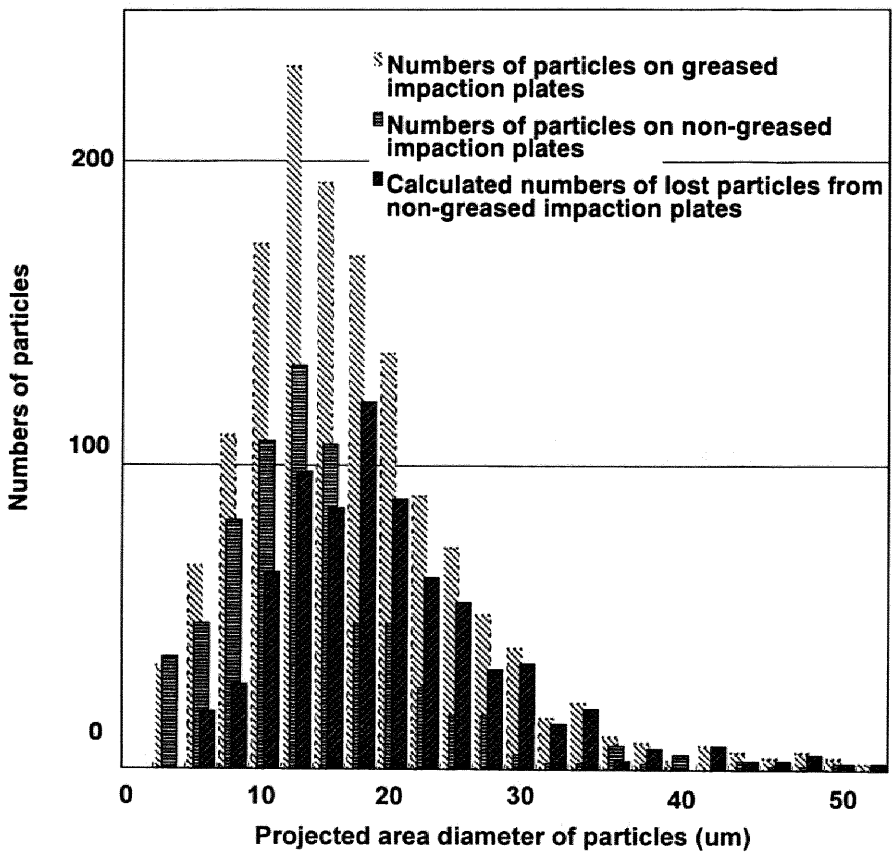

Fig. 3. Size distributions of particles deposited on greased and non-greased impaction plates collected through six nozzles at 54% RH. Numbers of lost particles were calculated as differences between particle numbers on greased and non-greased plates.

image. To reduce the influence of the particles located at outlier points on estimation of the center of deposition, geometric means, instead of arithmetic means, were used. Geometric means were calculated separately for X and Y coordinates using each X and Y value of particles, and the mean X and Y calculated individually were combined to be a point as a central point of particle deposit (Fig. 2). The distances of each particle from the central point of the deposition were determined based on the pair of X and Y values calculated in this manner.

The particle deposit densities per unit area (numbers/mm^2) were examined along the distance from the central point of particle deposition (Fig. 5). The result indicated that particles were densely deposited around the center of deposition on greased impaction plates while they were dispersedly distributed on non-greased plates. Furthermore, particle deposit densities on greased and non-greased impaction plates were inverted approximately around 2.6 mm of the distance. Assuming that no relocation of particles occurred on greased impaction plates, this result suggests some particles, once impacted on the inner part of deposition on non-greased surface, may hereafter relocate themselves to the outer part. In addition to the particle deposit density, the particle numbers in each concentric annulus with the constant radius interval step, i.e. 0.2175 mm, from the center of deposition are

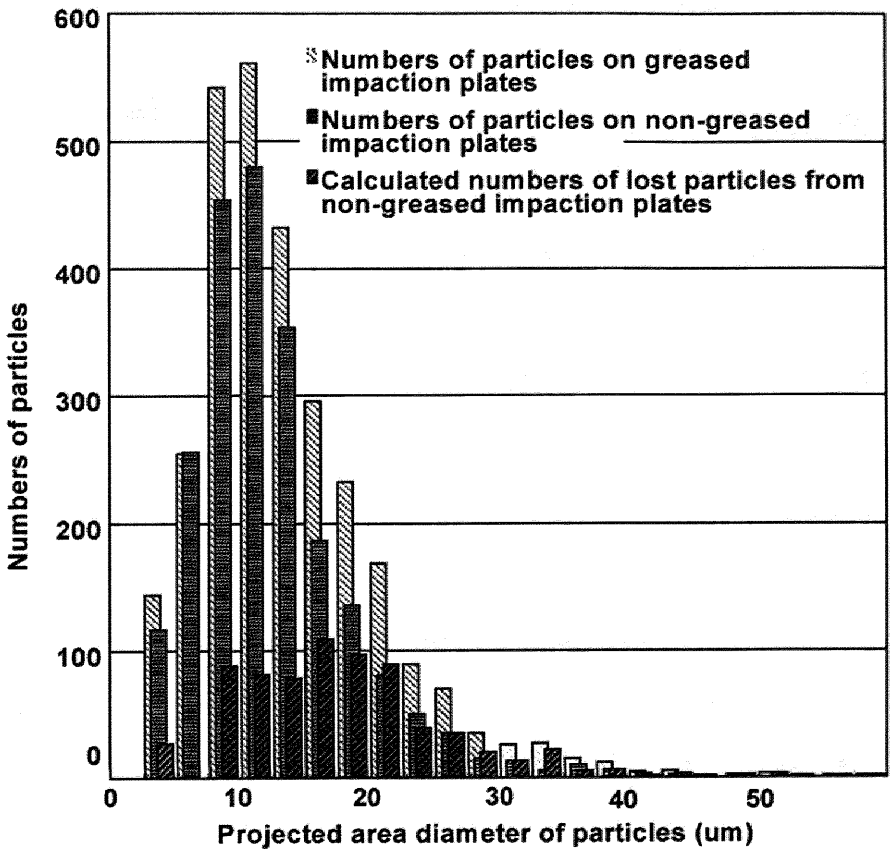

Fig. 4. Size distributions of particles deposited on greased and non-greased impaction plates collected through six nozzles at 84% RH. Numbers of lost particles were calculated as differences between particle numbers on greased and non-greased plates.

shown in Fig. 6. Gray and black bars in Fig. 6 represent differences of particle numbers on greased and non-greased impaction plates. As noted earlier, the differences observed within each distance category could not provide the fractions of instantaneous particle loss on those area portions because the location of particles represented the final landing points, and not necessarily the first impaction points.

The particle deposition patterns on impaction plates were also investigated for size fractionated particle groups (Fig. 7). Particles were classified into six groups, with 5 μm intervals of d_{PA}, i.e. d_{PA} of < 10, 10–15, 15–20, 20–25, 25–30 and $30 <$ μm. The results plotted in Fig. 7 suggest significant amounts of small particles, especially with $d_{PA} < 10$ μm, may be captured further away from the jet centerline, while large particles, especially with $d_{PA} > 20$ μm, which would be expected to be captured closer to the jet centerline, were not even recaptured on the stage. Thus, the overall dispersion of particles on the smooth impaction plate was due to bounces and/or reentrainments of small particles. On the other hand, large particles tended to be completely lost from the stage.

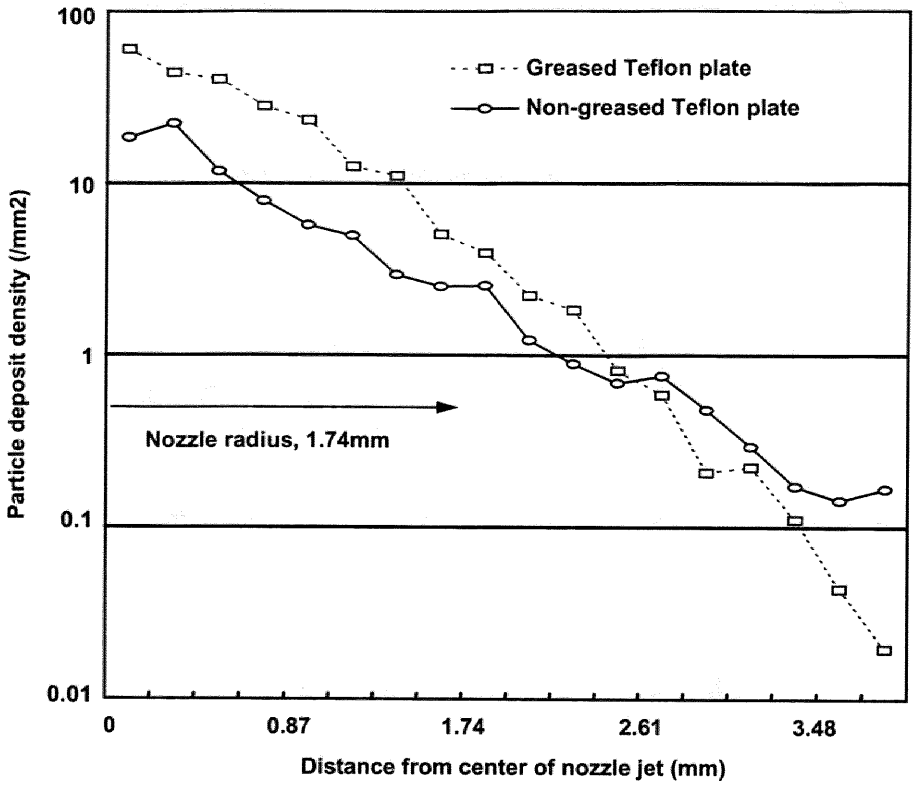

Fig. 5. Particle deposit density along the distances from jet centerline on greased and non-greased Teflon impaction plates at 54% RH.

4. Summary and conclusions

A line-sensing optical microscope, Dot Analyzer DA-6100/LS, was used to investigate an entire area of a particle deposit generated by an individual acceleration nozzle in a hi-volume Andersen sampler. Using its advantage of line-sensing mechanism to capture broad ranges of target materials, the spatial distributions of particles deposited on greased and non-greased Teflon impaction surfaces were investigated. Numbers, sizes and locations of particles on greased and non-greased plates were compared to characterize particle loss from smooth impaction surfaces. Particles deposited on impaction plates were automatically counted, sized and located by the microscope in cooperation with the image analysis software bundled. The result confirmed reproducible collection characteristics among nozzles even though application of the greasing material increased the collection efficiency ($N = 245 \pm 24$ and 119 ± 18 for greased and non-greased plates at 54% RH, and $N = 488 \pm 53$ and 368 ± 77 at 84% RH, respectively) and altered the size distribution of collected particles to the larger side (15.0 and 12.6 μm of the particle geometric mean diameters for greased and non-greased impaction plates at 54% RH, and 12.2 and 11.2 μm of the diameters at 84% RH, respectively). In these experiments, assuming spherical particles with uniform density, approximately 65% of particle mass and 50% by number were lost from non-greased plates at 54% RH, while 45% by mass and 25% by number were underestimated at 84% RH. This result indicated that errors in the size

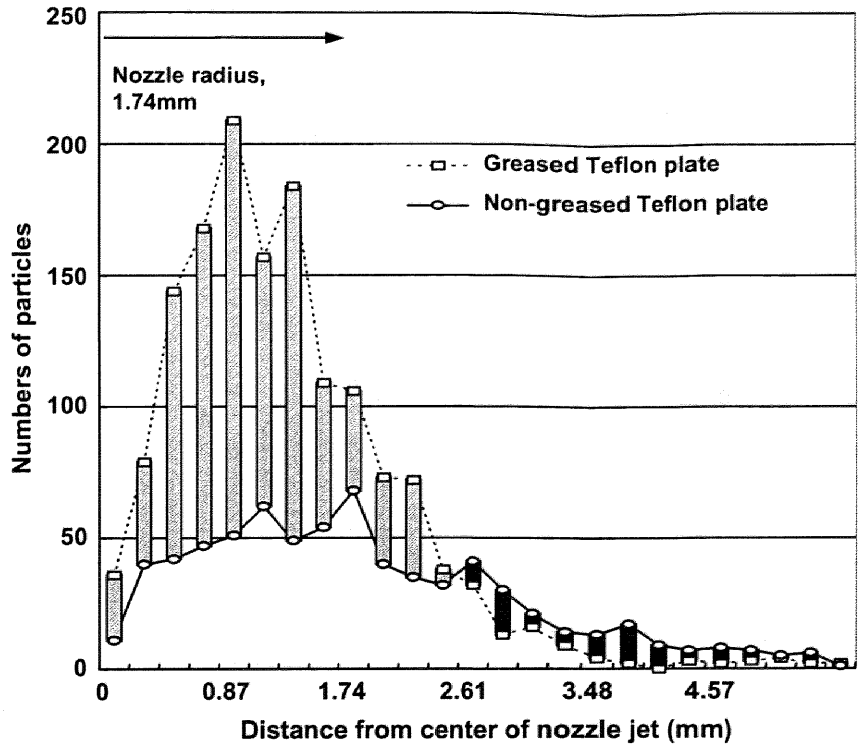

Fig. 6. Numbers of total particles deposited on concentric annuli from the center of the nozzle jet on greased and non-greased impaction plates collected through six nozzles at 54% RH (gray and black bars represent differences of particle numbers on greased and non-greased impaction plates).

distribution measurement due to particle bounces and/or reentrainments were more significant for mass rather than for number concentration measurements. Large particles appeared to be selectively lost from non-greased impaction plates. In addition, it was found in this study that particle loss due to bounce and/or reentrainment occurred more significantly at the lower RH condition. The particle size distributions on the impaction plate may be distorted by the effect of the application of grease on particle deformation.

Microscopic analysis showed that the particles were densely deposited around the centerline of the impaction jet on greased impaction plates while on non-greased plates they were dispersedly distributed. Moreover, it was found that particle deposit densities on greased and non-greased impaction plates were inverted approximately around 2.6 mm of the distance from the central point of the deposition. The particle deposition patterns were also investigated for size-fractionated particle groups. The results of spatial distributions by particle size suggest that dispersion of particle on the impaction plate is due to bounce and/or reentrainment of smaller particles especially with $d_{PA} < 10$ μm.

Acknowledgements

This work was partly funded by the Steel Industry Foundation for the Advancement of Environmental Protection Technology, Japan under Grant No. 12-27-45.

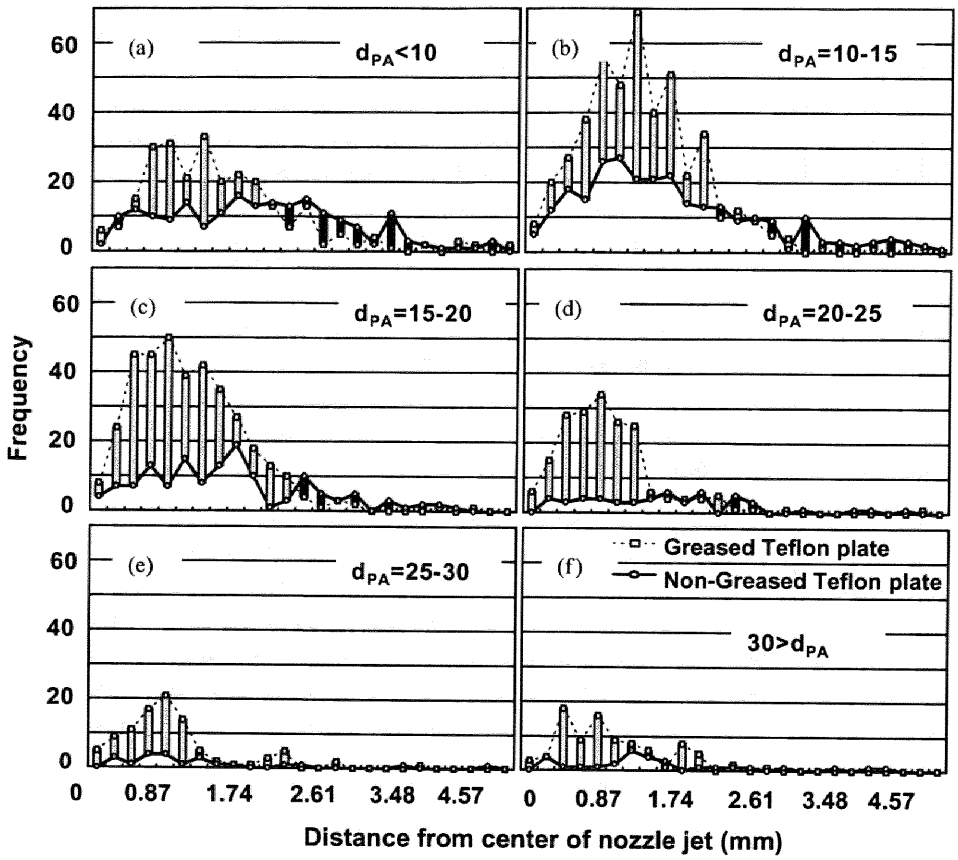

Fig. 7. Numbers of deposited particles with d_{PA} of: (a) < 10, (b) 10–15, (c) 15–20, (d) 20–25, (e) 25–30, and (f) 30 < μm on concentric annuli from the center of the nozzle jet on greased and non-greased impaction plates collected through six nozzles (at 54% RH) (gray and black bars represent differences of particle numbers on greased and non-greased impaction plates).

References

Chang, M., Kim, S., & Sioutas, C. (1999). Experimental studies on particle impaction and bounce: Effects of substrate design and material. *Atmospheric Environment, 33*, 2313–2322.

Cheng, Y. S., & Yeh, H. C. (1979). Particle bounce in cascade impactors. *Environmental Science and Technology, 13*, 1392–1396.

Corn, M., & Stein, F. (1965). Re-entrainment of particles from a plane surface. *American Industrial Hygiene Association Journal, 26*, 325–336.

Dahneke, B. (1971). The capture of aerosol particles by surfaces. *Journal of Colloid Interface Science, 37*, 342–353.

Dzubay, T. H., Hines, L. E., & Stevens, R. K. (1976). Particle bounce error in cascade impactors. *Atmospheric Environment, 10*, 229–234.

Ellenbecker, M. J., Leith, D., & Price, J. M. (1980). Impaction and particle bounce at high stokes numbers. *Journal of Air Pollution Control Association, 30*, 1224–1227.

Hinds, W. C. (1999). *Aerosol technology: Properties, behavior, and measurement of airborne Particles* (2nd ed.). New York: Wiley.

Hinds, W. C., Liu, W. V., & Froines, J. R. (1985). Particle bounce in a personal cascade impactor: A field evaluation. *American Industrial Hygiene Association Journal, 46*, 517–523.

Kaneyasu, N. (1998). Wide ranged measurement of elemental carbon in atmospheric aerosols using spot samples on the tape filter mounted in automated SPM monitors. *Journal of Japanese Society for Atmospheric Environment, 33*(6), 344–356.

Marple, V. A., Rubow, K. L., & Hehm, S. M. (1991). A micro-orifice uniform deposit impactor (MOUDI): Description, calibration, and use. *Aerosol Science and Technology, 14*, 434–446.

Marple, V. A., Rubow, K. L., Turner, W., & Spengler, J. D. (1987). Low flow rate sharp cut impactors for indoor air sampling: Design and calibration. *Journal of Air Pollution Control Association, 37*, 1303–1307.

Newton, G. J., Cheng, Y. S., Barr, E. B., & Yeh, H. C. (1990). Effects of collection substrates on performance and wall losses in cascade impactor. *Journal of Aerosol Science, 21*, 467–470.

Owens, J. S. (1923). Jet dust counting apparatus. *Journal of Industrial Hygiene, 4*, 522–534.

Rao, A. K., & Whitby, K. T. (1978a). Non-ideal collection characteristics of inertial impactors—I. Single-stage impactors and solid particles. *Journal of Aerosol Science, 9*, 77–86.

Rao, A. K., & Whitby, K. T. (1978b). Non-ideal collection characteristics of inertial impactors—II. Cascade impactors. *Journal of Aerosol Science, 9*, 87–100.

Reischl, G. P., & John, W. (1978). The collection efficiency of impaction surface. *Staub-Reinhaltung der Luft, 38*, 55.

Stein, S. W., Turpin, B. J., Cai, X. P., Huang, C. P. F., & McMurry, P. H. (1994). Measurements of relative humidity-dependent bounce and density for atmospheric particles using the DMA-impactor technique. *Atmospheric Environment, 28*(10), 1739–1746.

Turner, C. J., & Hering, S. V. (1987). Greased and oiled substrate as bounce-free impaction surfaces. *Journal of Aerosol Science, 18*, 215–224.

Vasiliou, J. G., Sorensen, D., & McMurry, P. H. (1999). Sampling at controlled relative humidity with a cascade impactor. *Atmospheric Environment, 33*, 1049–1056.

Wall, S., John, W., Wang, H.-C., & Goren, S. (1990). Measurements of kinetic energy loss for particles impacting surfaces. *Aerosol Science and Technology, 12*, 926–946.

Winkler, P. (1974). Relative humidity and the adhesion of atmospheric particles to the plates of impactors. *Aerosol Science, 5*, 235–240.

APPENDIX A.2.

N. Yamamoto et al., *J. Aerosol Sci.* 35, 731 (2004)

ELSEVIER

Aerosol Science 35 (2004) 731–741

Journal of
Aerosol Science

www.elsevier.com/locate/jaerosci

Time course shift in particle penetration characteristics through capillary pore membrane filters

Naomichi Yamamoto[a,*], Minoru Fujii[b], Kazukiyo Kumagai[a], Yukio Yanagisawa[a]

[a] *Department of Environmental System, Institute of Environmental Studies, Graduate School of Frontier Sciences, The University of Tokyo, Hongo 7-3-1, Bunkyo-ku, Tokyo 113-8656, Japan*
[b] *National Institute for Environmental Studies, Onogawa 16-2, Tsukuba-Shi, Ibaraki 305-8506, Japan*

Received 11 July 2003; received in revised form 3 December 2003; accepted 5 December 2003

Abstract

The time course change in particle penetration through capillary pore membrane filters was investigated for relatively short filtration periods. In the laboratory experiments, penetration efficiencies of the 0.3 and 1.0 μm standard particles through the 2.0 μm capillary filter were continuously monitored. While penetration efficiencies of both 0.3 and 1.0 μm particles decreased, 1.0 μm particles became selectively captured by the filter. Furthermore, even small amount of collected particles (coverage fractions less than 1% of the filter surface) was found to alter particle penetration characteristics possibly because of the intense accumulations around the rims of capillary pores due to significance of particle interception. No distinct effect by addition of clogging particles of 2.0 μm diameter was observed, indicating the change in particle penetration characteristics was initiated even when particle clogs became important. The present study showed the size distribution of collected particles by capillary pore membrane filters could be biased with time even for short sampling duration.

Keywords: Time course shift; Penetration efficiency; Standard particle; Size distribution; Interception

1. Introduction

Filtration is a widely used method for particle collection. Although there are two types, fibrous and porous filters, both use the same mechanical processes for particle collection, diffusion, interception and impaction, within the filter structures. By means of these collection mechanisms, particles are captured within a filter although the filtration efficiency may be of concern. Capillary pore membrane

* Corresponding author. Tel.: +81-358-417335; fax: +81-358-418583.
E-mail address: naomichi.yamamoto@yy.t.u-tokyo.ac.jp (N. Yamamoto).

0021-8502/$ - see front matter © 2003 Elsevier Ltd. All rights reserved.
doi:10.1016/j.jaerosci.2003.12.001

filters are ones with bundles of microscopic cylindrical holes of uniform diameter, commonly used for chemotaxis, bioassay, air and particle monitoring, microscopic analyses and so on. Because of their smooth surfaces, this type of filters is particularly useful for observation by a scanning electron microscope.

Many researches have been conducted to characterize filtration performance of capillary pore membrane filters. Spurny, Lodge, Frank, and Sheesley (1969a,b), for instance, investigated the filtration performance in relation to particle and pore sizes, pressure drop, porosity of filters and temperature. Kanaoka, Emi, and Aikura (1979) examined the particle collection efficiency through micro-perforated plates. Caroff, Choudhary, and Gentry (1973) theoretically explored the relationship between the capillary pore and particle sizes and filtration efficiencies while Smutek and Pich (1974) suggested the model of low-speed fluid flow in the capillary of a membrane filter. To characterize the performance of commercially available capillary pore filters, Nuclepore filters, Manton (1978, 1979) characterized various particle collection mechanisms such as Brownian diffusion and impaction within the structures of Nuclepore filters. Montassier, Dupin, and Boulaud (1996), on the other hand, experimentally characterized penetrations of various types of particles through the Isopore filters in relation to their pressure drop.

The objective of the present study is to experimentally investigate the particle penetration characteristics through capillary pore membrane filters. In particular, the study aims to identify the time course change in the particle penetration characteristics. Although many researches on capillary pore membrane filters have been performed, few studies have been conducted to characterize filtration performance in time-series. Because of the time course change in aerodynamic properties of the filter due to particle clogs and accumulations, penetration performance may be altered with time. This can result in the biased size distributions of the collected particles. In case of the actual ambient aerosols, in particular, this can lead to the biased chemical concentrations due to inherent size dependency of their chemical compositions. It is, therefore, necessary to characterize the time course shift of penetrated particle sizes. In the present study, standard particles of highly uniform sizes were used to filter through the capillary pore membrane filters in the laboratory experiments. The mixtures of various sizes of standard particles were continuously filtered to observe the time course shift of sizes of the penetrated standard particles. In addition, actual ambient particles were also filtered to examine under the real sampling situation.

2. Experimental

2.1. Materials

Capillary pore membrane filters of 47 mm diameter with 0.8, 1.2 and 2.0 μm pore sizes (Isopore® membrane filter, Nihon Millipore Ltd., Tokyo, Japan) were used. The filters consisted of polycarbonate films of 20 μm thickness with porosities ranging 5–20%. An aluminum filter holder with a stainless steel support (SKC Inc., PA, USA) was used to minimize the effect of electric charge. In the laboratory experiments, polystyrene latex particles with 0.294, 0.603, 1.008 and 2.047 μm diameters (STADEX and DYNOSPHERE, JSR Corp., Tokyo, Japan) were used as standard particles. In this paper, these particles will be referred as the 0.3, 0.6, 1.0 and 2.0 μm particles, respectively. Their sizes, shapes and densities are highly uniform (particle size accuracy within ±3%). The particle

densities reported by the manufacture are 1.054, 1.051, 1.053 and 1.051 g cm^{-3}, respectively, which are nearly equal to the density of water. Therefore, the particles used in this study can be regarded as solid particles of aerodynamic equivalent spheres.

To produce known concentrations of standard particles in a monodisperse manner, an aerosol generator (Aeromaster-V, JSR Corp., Tokyo, Japan) capable to maintain the concentrations constant was used. The particle generation was achieved by pressurized spraying and drying. The standard particles suspended in ultra pure water were diluted, and a bottle containing their suspension was installed to the Aeromaster-V for aerosol generation. Particle concentrations were controlled by changing concentrations of diluted particle suspensions, and the generated concentrations were highly stable (within $\pm 10\%$). To release electrical charge of the particles, a charge neutralizer was built in the generator as a standard equipment. Using a light scattering particle counter, standard aerosols supplied from the aerosol generator were counted. A light scattering particle counter with size channels of 0.3, 0.5, 1, 2 and 5 μm (Model KC-01B, RION Ltd., Tokyo, Japan) was used in the present investigation.

2.2. Penetrations of standard particles

To characterize the particle penetration efficiencies of the clean filters, several experiments changing combinations of particle and capillary sizes were performed. The standard particles with 0.3, 0.6, 1.0 and 2.0 μm diameters were filtered through the capillary pore membrane filters with 0.8, 1.2 and 2.0 μm pore diameters. Using the particle counter, the standard particles supplied from the aerosol generator were counted at the downstream of the filter as penetrated particles. Measurements were performed for 24 min (12 cycles of 2 min measurements by the particle counter) for each experiment. Particle concentrations without filtration were also measured for 12 min (6 cycles of 2 min measurements) immediately before and after the filtration experiment to count entering particles to the filter and confirm stability of particle concentrations. Flow rate through the filter was adjusted at 500 ml min^{-1} (face velocity of gas at filter, q, was 0.48 cm s^{-1}) as specified for the particle counter.

Time course changes in penetration efficiencies were monitored for mixtures of several sizes of standard particles to examine possible competition among various sizes of particles. Experiments were performed under two different conditions: (1) standard particles small enough to penetrate through the filter capillaries were filtered; (2) standard particles large enough to clog the capillaries were added. In the first experiment, the standard particles with 0.3 and 1.0 μm diameters were filtered through the 2.0 μm capillary filter. The number concentrations of 0.3 and 1.0 μm particles were adjusted approximately at 1.6×10^5 and 1.2×10^4 l^{-1}, respectively. In the second experiment, the standard particles with 2.0 μm diameter were added to the aerosol used in the first experiment. The number concentrations of 0.3, 1.0 and added 2.0 μm particles were adjusted approximately at 1.4×10^5, 1.1×10^4 and 6.5×10^3 l^{-1}, respectively. Both samplings were taken about 5 h and flow rates were adjusted at 500 ml min^{-1}. Particle concentrations without filtration were also measured for 30 min immediately before and after the filtration experiment to confirm the stability of concentrations of entering particles to the filter throughout the experiments.

2.3. Penetrations of actual ambient particles

Actual ambient particles were also filtered through the 2.0 μm capillary filter to examine the time course change of filtration performance under the real sampling situation. An alternate sampling

of filtration and non-filtration was conducted. Using the particle counter with a measurement cycle of 34 s, concentrations of size fractionated ambient particles were continuously and interchangeably monitored with and without filtration. A sampling cycle of 3 min non-filtration and 6 min filtration was repeated approximately for 6 h. Mean concentrations measured by non-filtration samplings were defined as the ambient particle concentration for the period the filtration sampling was undertaken in between.

3. Results and discussion

3.1. Relationship between particle and capillary sizes

Particle penetration efficiencies in relation to particle and capillary diameter sizes are shown in Fig. 1. All experiments were performed at $q = 0.48\ \mathrm{cm\,s^{-1}}$. Almost all particles were collected by the filter in case particle and capillary sizes were equal. For instance, the penetration efficiency of the particles with 2.0 μm diameter through the filter of 2.0 μm capillary pore diameter was less than 0.1%. In addition, even though the particle size was smaller than the capillary size, smaller particles tended to be more easily captured by the filter. For example, while the penetration efficiency of the 1.0 μm particles through the 2.0 μm capillary filter was approximately 17%, the efficiency of the 0.6 μm particles through the 1.2 μm capillary filter was less than 1%. In both cases, the ratio of particle and capillary diameters was 0.5.

3.2. Time dependency of penetration of standard particles

First, the standard particles with 0.3 and 1.0 μm diameters, small enough to penetrate through capillaries, were selected to filter through the 2.0 μm capillary filter based on the previous experiment (penetration efficiencies of 55% and 17%, respectively) (Fig. 1). The time course penetration efficiencies of the 0.3 and 1.0 μm particles through the 2.0 μm capillary filter are shown in Fig. 2. Penetration efficiencies of both sizes of particles decreased with time. To examine the time course shift in the size distribution of penetrated particles, number ratios of the 0.3 and 1.0 μm particles penetrated through the filter are plotted in Fig. 3. The ratios were increased with time, suggesting the larger particles (1.0 μm) became selectively captured by the filter.

Second, the standard particles large enough to clog the 2.0 μm capillaries were added to the particle mixture used in the previous experiment. The particles of 2.0 μm diameter is known to be incapable to penetrate through the 2.0 μm capillary filter (Fig. 1). In this experiment, penetration efficiencies of both the 0.3 and 1.0 μm particles decreased with time (Fig. 4). To clarify the time course shift in penetrated particle size distribution, number ratios of the 0.3 and 1.0 μm particles penetrated are plotted in Fig. 5. The ratios were increased with time, suggesting the larger particles (1.0 μm) became selectively captured by the filter.

To explain the time course shift of the size distribution of penetrated particles, the contributions of each particle collection mechanisms, diffusion to the pore walls, interception at the rims of the pores and inertial impaction at the filter face, were roughly estimated using the models described by Spurny et al. (1969a,b) and Gentry, Spurny, and Schoermann (1982). First, the constituent penetrations due

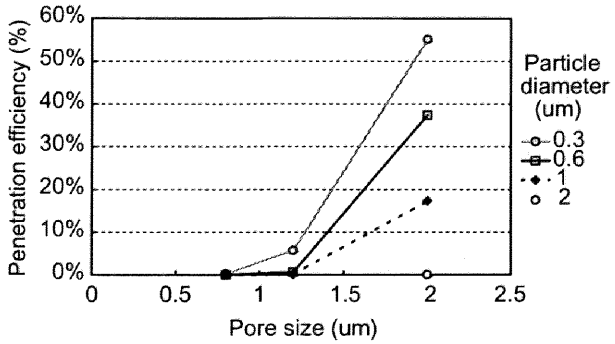

Fig. 1. Penetration efficiencies of standard particles through capillary pore filters, $q = 0.48\ \mathrm{cm\,s^{-1}}$.

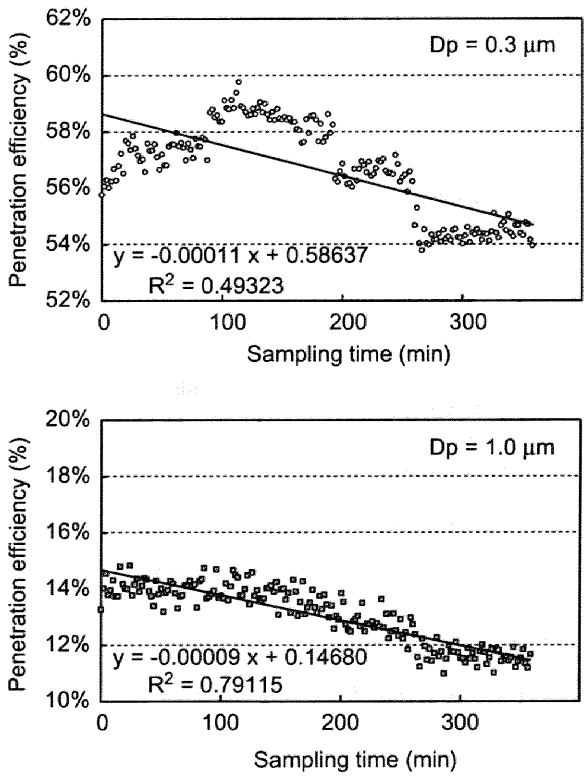

Fig. 2. Penetration efficiencies of 0.3 and 1.0 μm standard particles through a capillary filter with 2.0 μm pores, $q = 0.48\ \mathrm{cm\,s^{-1}}$.

to diffusion alone, Pt_D, were calculated using the Gormley–Kennedy formula:

$$Pt_D = 1 - 2.56Pe^{-2/3} + 1.2Pe^{-1} + 0.177Pe^{-4/3} \quad \text{for } Pe > 25, \tag{1}$$

where the Peclet number, Pe, is given by

$$Pe = \frac{R^2 q}{LDP}, \tag{2}$$

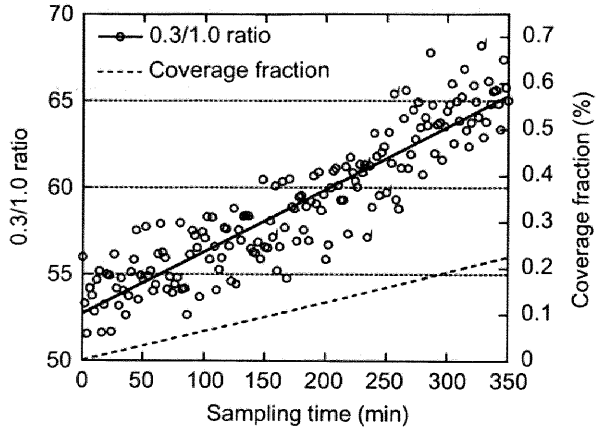

Fig. 3. Number ratios of 0.3 to 1.0 μm standard particles penetrating through a capillary filter with 2.0 μm pores, and particle coverage fractions on filter.

where L is the filter thickness, D is the aerosol particle diffusivity, P is the filter porosity and R is the pore radius of filter. Under the present filtration condition, the values of Pe were far larger than 25. Similarly, the constituent penetrations due to interception alone, Pt_R, were computed using the Natanson expression:

$$Pt_R = 1 - (2N_R - N_R^2), \tag{3}$$

where

$$N_R = r/R \tag{4}$$

and r is the particle radius. Finally, the constituent penetrations due to impaction alone, Pt_I, was calculated using the equation given by Pich (1964):

$$Pt_I = 1 - \frac{2\varepsilon_i'}{1+\xi} + \frac{\varepsilon_i'^2}{(1+\xi)^2}, \tag{5}$$

$$\varepsilon_i' = 2\mathrm{Stk}\sqrt{\xi} + 2\mathrm{Stk}^2\xi \exp\left[-\frac{1}{\mathrm{Stk}\sqrt{\xi}}\right] - 2\mathrm{Stk}^2\xi, \tag{6}$$

where

$$\xi = \frac{\sqrt{P}}{1-\sqrt{P}}, \tag{7}$$

$$\mathrm{Stk} = \frac{mq}{6\eta r R}, \tag{8}$$

where m is the mass of a single particle and η is the gas viscosity. Combining all three particle collection mechanisms, overall penetration efficiencies given by

$$Pt = Pt_D \times Pt_R \times Pt_I \tag{9}$$

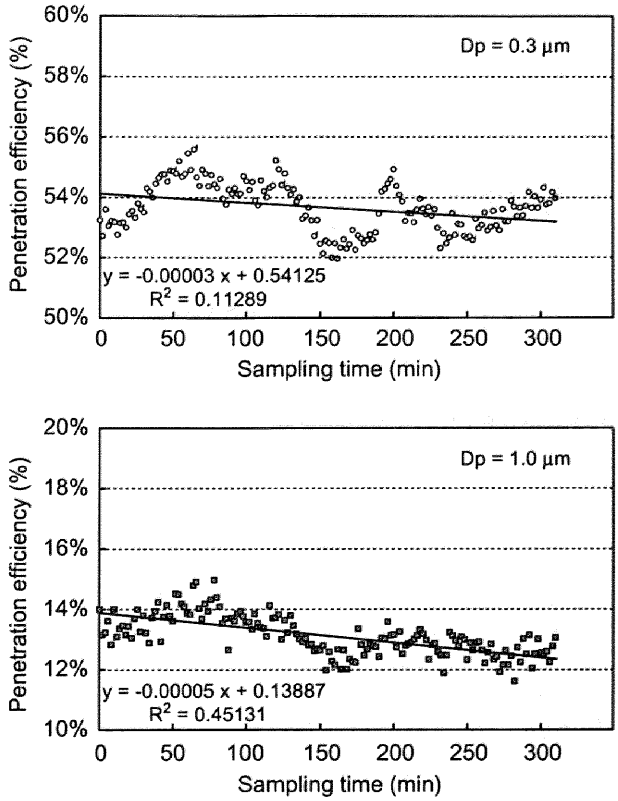

Fig. 4. Penetration efficiencies of 0.3 and 1.0 μm standard particles through a capillary filter of 2.0 μm pores with addition of 2.0 μm particles, $q = 0.48\ \mathrm{cm\,s^{-1}}$.

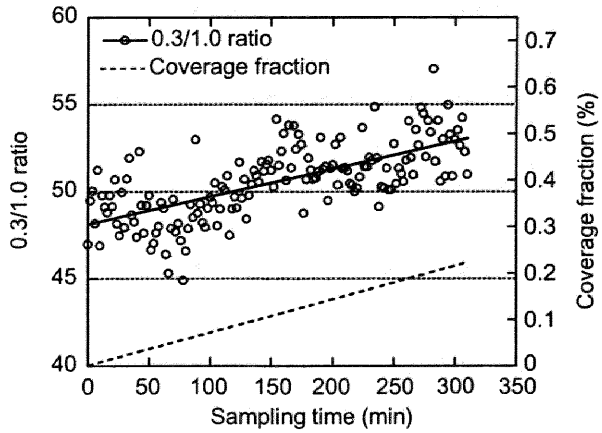

Fig. 5. Number ratios of 0.3 to 1.0 μm standard particles penetrating through a capillary filter of 2.0 μm pores with addition of 2.0 μm particles, and particle coverage fractions on filter.

were theoretically calculated. The results are summarized in Table 1. Although theoretical penetration efficiencies were slightly larger than the experimental values, the results were quite consistent across the entire particle sizes. Based on the model calculations, the contributions among each particle

Table 1
Constituent penetrations due to diffusion, interception and impaction alone, and their contributions to overall particle collection; capillary pore diameter = 2 μm, $q = 0.48$ cm s^{-1}

Particle diameter (μm)	Penetration efficiency (contribution to particle collection) (%)				
	Theoretical				Experimental
	Diffusion	Interception	Impaction	Overall[a]	Overall
0.3	99.7 (1.0)	72.3 (96.3)	99.2 (2.8)	71.5	55.2
1.0	100.0 (0.0)	25.0 (89.9)	91.6 (10.0)	22.9	17.4
2.0	100.0 (0.0)	0.0 (78.0)	71.8 (22.0)	0.0	0.0

[a]Overall penetration efficiencies are multiplications of constituent penetration efficiencies due to diffusion, interception and impaction alone.

collection mechanism were calculated (Table 1). While interception was a dominant collection mechanism for all particle sizes because of relatively large N_R used in our study, diffusion was almost negligible. Impaction also became important for the 2.0 μm particles. Interception, the most predominant collection mechanism in the present filtration condition, occurs when the center of a particle passes within a distance of particle radius from the rim of the pore. Therefore, particle depositions were expected to be denser around the rims of pores than on the face and on the pore walls of a filter. Intense particle accumulation around the rims of capillary pores might alter the aerodynamic properties of the filter, resulting in the shift of the size distribution of penetrated particles.

Throughout the first experiment, approximately 1.2×10^7 and 1.9×10^6 particles with 0.3 and 1.0 μm diameters, respectively, were collected on the filter while approximately 1.0×10^7, 1.6×10^6 and 1.0×10^5 particles with 0.3, 1.0 and 2.0 μm diameters, respectively, were collected through the second experiment. The calculated coverage area fractions by collected particles were approximately 0.23% and 0.22% on the filter surfaces for the first and second experiments, respectively (Figs. 3 and 5), although particles might be more densely deposited around the rims of pores due to the significance of interception. It is noteworthy that even small amount of particles on the filter (coverage fractions less than 1% on the filter surface) significantly altered the penetration characteristics of a capillary filter. In addition, no distinct difference between two experiments with and without addition of clogging particles of 2.0 μm diameter was observed. These facts indicate time-integrated samplings using capillary pore membrane filters could result in unintended shift of size distribution of collected particles even before particle clogs became important, possibly due to intense accumulation around the rims of capillary pores. In fact, while penetration efficiencies of both 0.3 and 1.0 μm particles were slightly decreased, the size distributions of penetrated particles were shifted significantly to the smaller side (Figs. 3 and 5).

3.3. Time dependency of penetration of actual ambient particles

The time course shifts of penetration efficiencies of actual ambient particles, calculated by dividing filtered concentrations by non-filtered concentrations, are shown in Fig. 6. Penetration efficiencies decreased approximately by 5% for all particle size groups although the initial efficiencies differed

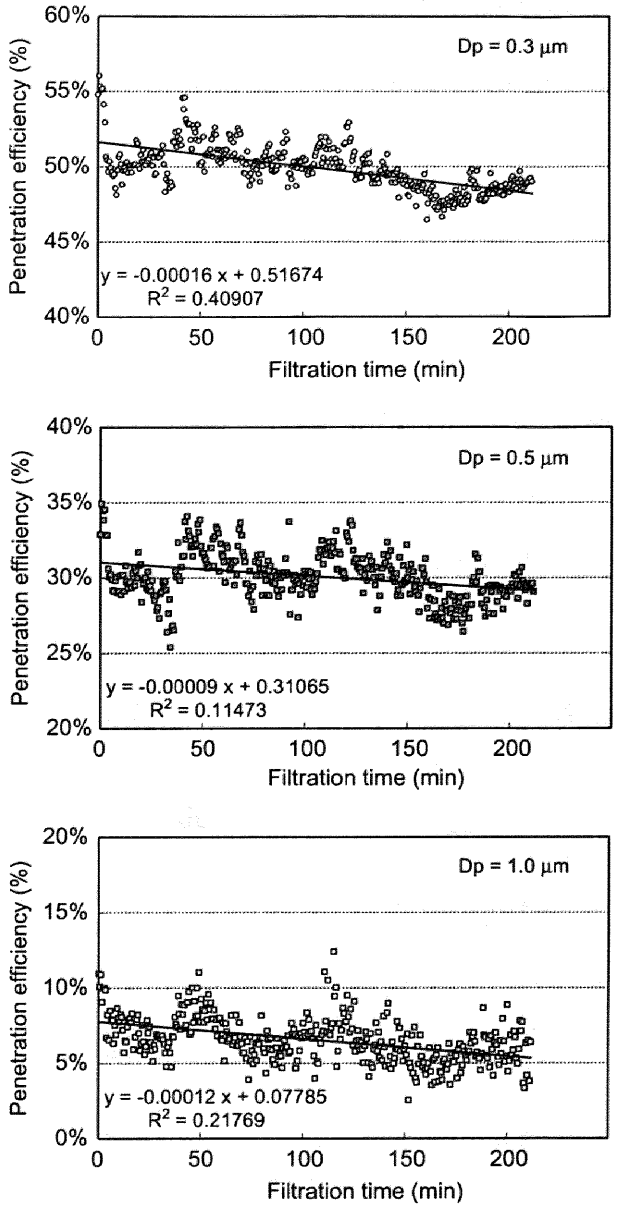

Fig. 6. Penetration efficiencies of ambient particles with 0.3, 0.5 and 1.0 μm diameters through a capillary filter with 2.0 μm pores, $q = 0.48\ \mathrm{cm\,s^{-1}}$.

among sizes. To investigate the time course shift in size distributions of the penetrated particle, the relative ratios of penetration efficiencies of 0.3 to 1.0 μm particles were calculated (Fig. 7). The initial ratio was standardized to 1, meaning the original penetration characteristics. Since the sampling was conducted alternately with and without filtration, the filtration time instead of sampling time was used. The ratios appeared to increase with filtration time, suggesting larger particles became selectively captured by the filter. This indicates the filtration using capillary pore membrane filters

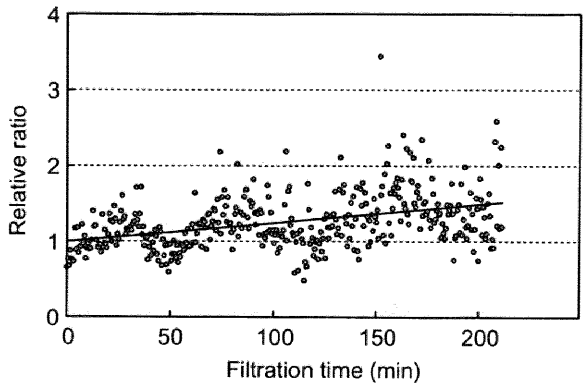

Fig. 7. Relative ratios of ambient particles with 0.3 to 1.0 μm diameters penetrating through a capillary filter with 2.0 μm pores. Initial ratio standardized to 1.0.

could result in shift in size distribution of collected particles. In the real sampling situation, in particular, this could result in biased chemical concentrations due to inherent size dependency of their compositions in actual ambient aerosols.

4. Summary and conclusions

The time course shift in penetration efficiencies of the mixtures of the standard particles with 0.3 and 1.0 diameters through the 2.0 μm capillary filter was monitored. Two types of experiments, with and without addition of the clogging particles with 2.0 μm diameter, were performed to examine the role of particle clogs. In both experiments, penetration efficiencies of the 0.3 and 1.0 μm particles decreased with time while the larger particles (1.0 μm) became selectively captured by the filter. It is notable that even small amount of collected particles (coverage fractions less than 1% on the filter surface) altered the penetrated particle size distributions. No distinct difference by adding the clogging particles (2.0 μm) was observed. These indicate the change in penetration characteristics could be initiated even before particle clogs became important, possibly due to intense particle accumulation around the rims of capillary pores. Penetration efficiencies of actual ambient particles showed approximately 5% decreases of all particle size groups although the initial efficiencies differed among their sizes. The result showed the size distribution of particles collected by the filter was shifted to the larger side, indicating time-integrated samplings using capillary pore membrane filters could result in the shift in size distribution of collected particles. In the real sampling situation, in particular, this could result in the biased chemical concentrations due to inherent size dependency of chemical compositions of actual ambient aerosol.

Acknowledgements

This work was funded in part by the Steel Industry Foundation for the Advancement of Environmental Protection Technology, Japan.

References

Caroff, M., Choudhary, K. R., & Gentry, J. W. (1973). Effect of pore and particle size distribution on efficiencies of membrane filters. *Journal of Aerosol Science, 4*, 93–102.

Gentry, J. W., Spurny, K. R., & Schoermann, J. (1982). Diffusional deposition of ultrafine aerosols on nuclepore filters. *Atmospheric Environment, 16*, 25–40.

Kanaoka, C., Emi, H., & Aikura, T. (1979). Collection efficiency of aerosols by micro-perforated plates. *Journal of Aerosol Science, 10*, 29–41.

Manton, M. J. (1978). The impaction of aerosols on a nuclepore filter. *Atmospheric Environment, 12*, 1669–1675.

Manton, M. J. (1979). Brownian diffusion of aerosols to the face of a nuclepore filter. *Atmospheric Environment, 13*, 525–531.

Montassier, M., Dupin, L., & Boulaud, D. (1996). Experimental study on the collection efficiency of membrane filters. *Journal of Aerosol Science, 27*(Suppl. 1), S637–S638.

Pich, J. (1964). Impaction of aerosol particles in the neighborhood of a circular hold. *Collection of Czechoslovak Chemical Communication Collect, 29*, 2223–2227.

Smutek, M., & Pich, J. (1974). Impaction of particles on the surface of membrane filters. *Journal of Aerosol Science, 5*, 17–24.

Spurny, K. R., Lodge, J. P., Frank, E. R., & Sheesley, D. C. (1969a). Aerosol filtration by means of nuclepore filters, structural and filtration properties. *Environmental Science & Technology, 3*, 453–464.

Spurny, K. R., Lodge, J. P., Frank, E. R., & Sheesley, D. C. (1969b). Aerosol filtration by means of nuclepore filters, aerosol sampling and measurement. *Environmental Science & Technology, 3*, 464–468.

APPENDIX A.3.

N. Yamamoto et al., *J. Aerosol Sci.* 35, 1225 (2004)

ELSEVIER

Aerosol Science 35 (2004) 1225–1234

Journal of
Aerosol Science

www.elsevier.com/locate/jaerosci

Particle size distribution quantification by microscopic observation

Naomichi Yamamoto[a,*], Yohei Shinozuka[b], Kazukiyo Kumagai[a], Minoru Fujii[c], Yukio Yanagisawa[a]

[a] *Department of Environmental System, Graduate School of Frontier Sciences, Institute of Environmental Studies, The University of Tokyo, Hongo 7-3-1, Bunkyo-ku, Tokyo 113-8656, Japan*
[b] *Department of Oceanography, University of Hawaii at Manoa, 1000 Pope Road, Honolulu, Hawaii 96822, USA*
[c] *National Institute for Environmental Studies, Onogawa 16-2, Tsukuba-Shi, Ibaraki 305-8506, Japan*

Received 29 February 2004; received in revised form 19 May 2004; accepted 20 May 2004

Abstract

The particle size distributions measured by the optical microscope (OPM) were compared with those by the light scattering particle counter (PC) to validate the microscopic method for particle size distribution quantification. While the OPM concentrations increased with the PC concentrations, the OPM concentrations tended to be higher than those by the PC. To explain the difference between the two methods, we estimated their relationship based on the Mie scattering theory. The calculation roughly estimated the particle geometric diameters in theory were 1.7–2.0 times as large as the corresponding PC readouts. Using these theoretical factors, the size ranges of the PC were converted to match with the OPM measurements (PC*). Overall, the OPM concentrations were lower than the PC* concentrations. The advantage in the OPM method particularly for ambient aerosols lied in its accuracy of particle sizing although the counting efficiency might be lowered due to its intrinsic limitations such as inability of counting particles having the similar refractive index of the filter.

Keywords: Line-sensing optical microscope; Light scattering particle counter; Projected area diameter; Mie scattering theory; Refractive index

1. Introduction

Among many types of aerosol sampling methods, there are two types in general, direct-reading and time-integrated. Direct-reading instruments such as light scattering instruments (Kerker, 1997),

* Corresponding author. Tel.: +81-3-5841-7335; fax: +81-3-5841-8583.
E-mail address: naomichi.yamamoto@yy.t.u-tokyo.ac.jp (N. Yamamoto).

0021-8502/$ - see front matter
doi:10.1016/j.jaerosci.2004.05.005

time-of-flight monitors (Cheng, Barr, Marshall, & Mitchell, 1993), condensation nuclei counters (Agarwal & Sem, 1980) and electrical mobility analyzers allow us to measure particulate concentrations in a few minutes at sampling sites. Because they instantaneously measure particulate concentration, direct-reading instruments are widely used, for instance, in occupational hygiene surveys (Hinds, 1999) or clean room (Kalechits, Kirsch, Kulibaba, Maslakov, & Pavlov, 1994) for continuous and periodical particle detection. They are, however, occasionally less accurate because they rely measurements on observing the properties related to size such as light scattering, light absorption, mechanical mobility, or electrical mobility. Time-integrated instruments including filtration and impaction, on the other hand, determine aerosol concentration by directly measuring the particle mass collected on filters or substrates. A filter sample integrates particle mass to accurately provide the average aerosol concentration during a sampling period. Using a microbalance, collected particles are gravimetrically analyzed. They, however, often require long-term sampling duration to collect sufficient particles for gravimetric analysis although they are generally simple and low-cost.

An instantaneous filter sampling with semi-automated microscopic observation would complement shortcomings of these two types of instruments. A short-term filter sampling, a simple and low-cost method, provides particulate concentrations in a high time resolution. Unlike direct-reading instruments, sampled filters are preserved for subsequent microchemical analyses. Although short-term filtration samplings are often encountered with insufficient particle mass for gravimetric analysis, we anticipated the microscopic analysis enabled particle quantification of extremely low amount. Moreover, microscopic investigation can provide additional information such as particle shapes. The microscopic analysis is slow, tedious and often inaccurate due to operational error or bias if the visual investigation was manually performed. We recently reported the semi computer-automated optical microscope for particle counting (Yamamoto, Fujii, Endo, Kumagai, & Yanagisawa, 2002) to overcome these difficulties. Moreover, the limited scope of observable area in microscopes with fixed objective lens and slide, a line-sensing camera with a linear motor actuating slide enabled to capture most of particles on a wide substrate area at a time.

Although Lapuerta, Armas, and Gomez (2003) characterized the size distribution trends of diesel particles by digital analysis on the filter image taken by a scanning electron microscope, they noted that the particle number concentrations detected by their method was not representative of real flowing particle populations measured by direct-reading instruments. The present investigation aims to explore the possibility of particle number concentration quantification in addition to the particle size trend characterization by microscopic observation. The study compared particle size distributions collected on the filter and measured by the above-mentioned optical microscope (OPM) with those measured by the light scattering particle counter (PC). The concentrations by the OPM and PC were related for each size-fractionated particle group through several collocated measurements. Since the particle sizes identified by light scattering methods generally differ from the actual geometries due to difference in scattering properties between calibration and measured particles, the conceptual aspects of particle size difference characterized between two different methods are also discussed.

2. Methods

Millipore membrane filters (Millipore Corp., MA, USA; 0.45 μm pore size, 47 mm diameter, mixtures of cellulose acetate and cellulose nitrate) were used for the filtration sampling. The 3.1-mm

interval black grids of the white filter facilitated the concentration calculation by counting the particles on the known fraction of effective filtration surface. The filter paper was placed in an aluminum filter holder with a stainless-steel support (SKC Inc., PA, USA) connected with a silicone tube to a vacuum pump (Model SIP-32L, Sibata Scientific Technology Ltd., Tokyo, Japan), and the sampling flow rate was adjusted at $10\,l\,min^{-1}$. A light scattering particle counter (PC) with the channels of > 10, > 20, > 30, > 50 and > 100 μm (Model KC-20, RION Ltd., Tokyo, Japan; laser diode with wavelength λ of 780 nm, sideway light-scattering method with collection angle θ from 70 to 150°), for which particle size calibrations were performed using standard spherical glass bead particles (refractive index; $m = 1.56$), was collocated with the filtration sampling. Twelve collocated filtration and PC samplings for durations of 30–60 min were taken indoors and outdoors. Indoor and outdoor samplings were taken during August–October 2003 in and out of the sixth floor room of the building (approximately 20 m from the ground level) of the University of Tokyo in Bunkyo-ku, located in the central part of Tokyo. There was no characteristic emission source of coarse micron-size particles around the sampling site. Therefore, the measured particles were expected to be wind blown soil or plant particles suspended near the sampling site. In addition, there was no peculiar indoor particulate source during the samplings.

The OPM with a line sensor camera, Dot Analyzer DA-6100/LS (Oji Scientific Instruments, Hyogo, Japan), was used to capture the image of particles collected on the filter. Its line-sensing mechanism with a linear motor actuating slide enabled observations of broad ranges of target materials (approximately 5.5×16.2 mm) at a time. Captured images were imported to a graphic software (Adobe Photoshop 5.0, Adobe System Inc.) to erase image noises, and then segmented into black and white pixels (2.7×2.7 μm/pixel) by an image analysis software, DA-6000, bundled with the OPM (Oji Scientific Instruments, Hyogo, Japan) to process sizes and numbers of collected particles (Fig. 1). The sizing accuracy of the OPM was confirmed using the black-colored polystyrene latex particles with 10 and 100 μm diameters (Duke Scientific Corp., CA, USA) of the National Institute of Standards and Technology (NIST) traceable. The standard black-colored particles originally suspended in water were diluted and collected on the membrane filters by suction filtration for the subsequent OPM analysis. To prevent particle coagulation, the particle suspensions were added with 0.5% (w/w) sodium hexametaphosphate as a dispersant and ultra-sonicated in advance of the suction filtration.

3. Results and discussion

3.1. Particle sizing accuracy by the OPM

The sizing accuracy of the OPM by observation of the standard black-colored particles is summarized in Table 1. The resolution of the digital image taken by the OPM is 2.7×2.7 μm/pixel. The particle diameters observed by the OPM were defined as the diameters of the circles that had the same projected area as the particle silhouettes comprised from each pixel.

3.2. Particle size distributions by the OPM and PC

The particle size distributions by the OPM and PC methods are shown with that by the PC with the particle size conversion (PC*) (Fig. 2). The method of the particle size conversion, required

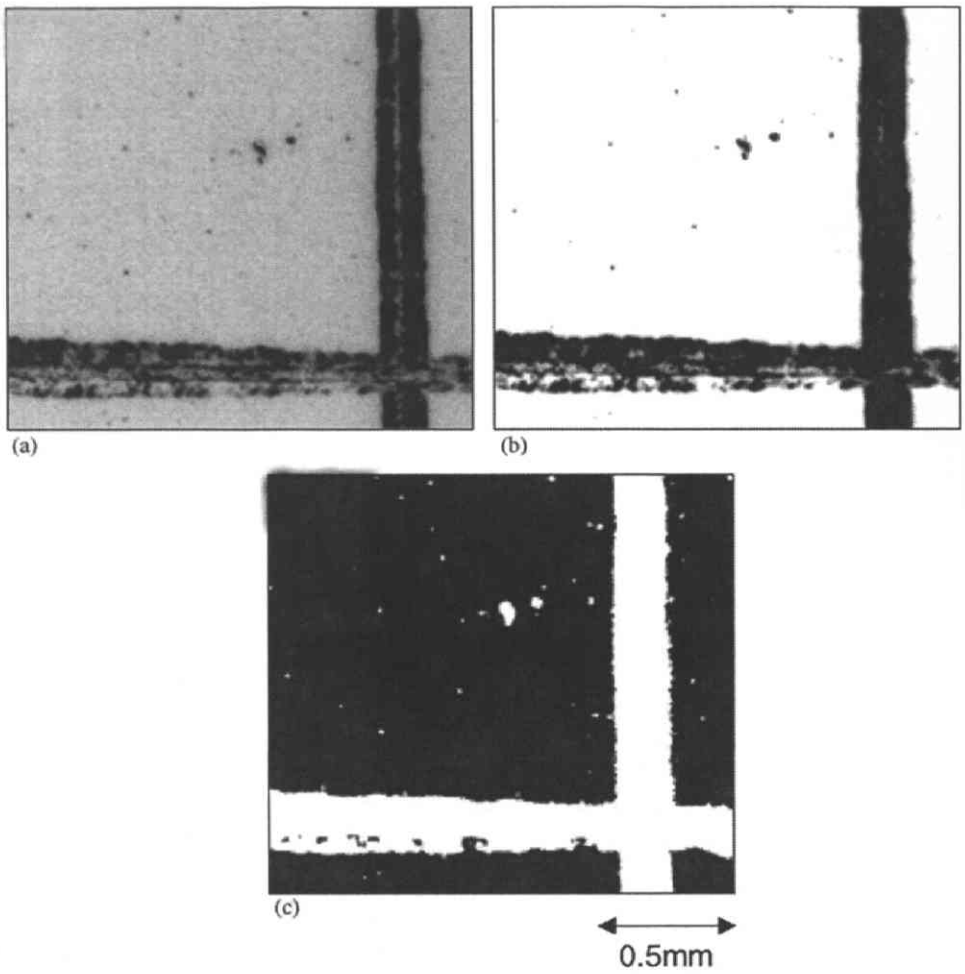

Fig. 1. A captured image (a), imported to a graphic software to erase image noises (b), and segmented into black and white pixels by an image analysis software (c).

Table 1
Analytical results of the standard black-colored polystyrene latex particles measured by the present OPM method

	Particle diameter (μm)	
Measured[a]	10.1 ± 6.6 ($n = 1568$)	99.0 ± 9.0 ($n = 16$)
Information value[b]	10.0 ± 0.1	100.0 ± 1.7

[a]Mean and 1 standard deviation.
[b]Certified value.

due to difference in scattering properties between calibration and measured particles by the PC, will be described in the following section. The relationship of particle number concentrations measured through twelve collocated samplings by the PC and OPM are shown in Fig. 3. The PC measured the

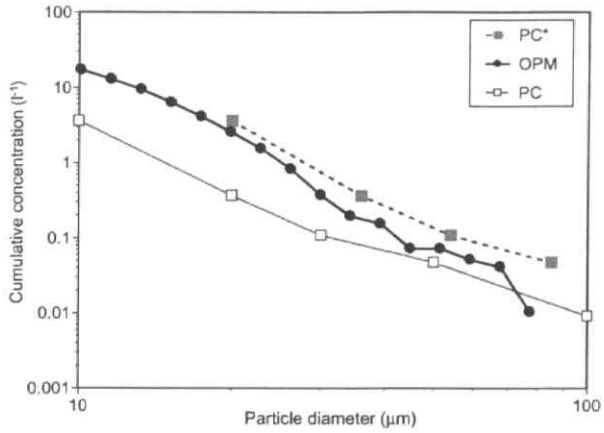

Fig. 2. Particle number distributions by the OPM, PC and PC*. Concentrations are accumulated from the largest to smaller particle size fractions.

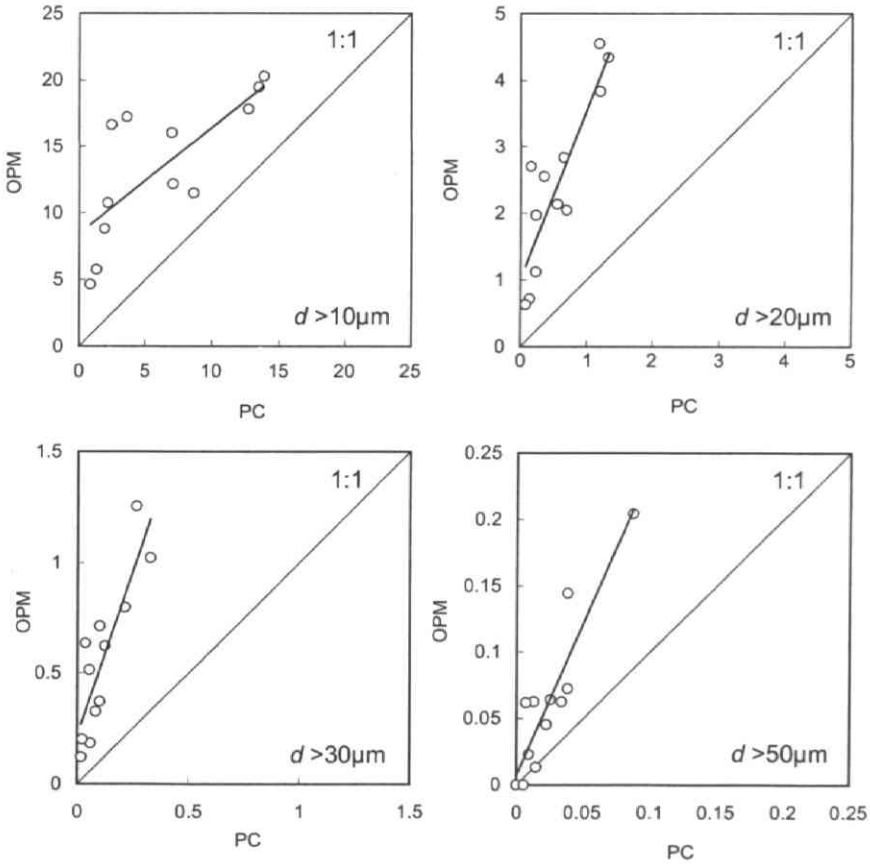

Fig. 3. Particle number concentrations (l^{-1}) by the PC and OPM.

particle concentrations by the particle diameter categories of $d > 10$, > 20, > 30 and > 50 μm while the OPM counted and measured the particles with continuous size. Therefore, the OPM concentrations were calculated based on particle size categories by the PC for comparison. To calculate the OPM concentrations, approximately 500–1900 particles of diameters larger than 10 μm were counted for each observation.

While the OPM concentrations increased with the PC concentrations, the OPM concentrations tended to be higher than those by the PC. The discrepancy between the PC and OPM size distributions was thought to result from the following reasons: (1) particle overlapping on the filter; (2) counting loss by the PC; (3) underestimate of the particle sizes by the PC. The coverage area fractions by collected particles on the filters were relatively small (0.04–0.15%). Therefore, particle overlapping was expected to be insignificant to explain the difference of the two size distributions. In addition, since the particle counting efficiency of the PC is known to be generally high (e.g., Mäkynen, Hakulinen, Kivistö, & Lehtimäki, 1982), it was inferred that the particle sizes characterized by the PC were smaller than the actual particle geometries.

3.3. Particle sizing by the OPM and PC

We first computed the PC response back from the particle diameter measured by the PC, d_{PC}, and looked for the diameter characterized by the OPM, d_{OPM}, that would result in the same PC response from the measured particles. The PC response, or the light intensity received by the instrument, was computed for d_{PC}, the refractive index of calibration particles, the wavelength and the detection angle range. In computing the angular scattering intensity, we used the Mie theory that was appropriate for particles in sizes comparable to the wavelength. We used the Wiscombe's code for homogeneous spheres (Wiscombe, 1996). Briefly, the diameter adjustment method is represented by the following equation:

$$\int_{70°}^{150°} s(m_{cal}, \lambda, d_{PC}, \theta)\,\mathrm{d}\theta = \int_{70°}^{150°} s(m_{meas}, \lambda, d_{PC^*}, \theta)\,\mathrm{d}\theta, \tag{1}$$

where s is the angular scattering intensity, m_{cal} is the calibration refractive index (=1.56), and m_{meas} is the refractive index of the measured particles. Given an estimated m_{meas}, the above equation relates the d_{PC} to the theoretical geometric diameter d_{PC^*}. We linked an array of geometric diameters to PC response in the same manner but for the urban aerosol with $m_{meas} = 1.56–0.087i$ (Ozkaynak, Schatz, Thurston, Isaacs, & Husar, 1985; Hinds, 1999). The values of refractive indices used for this calculation are summarized in Table 2. Both the calibration and urban aerosol PC response curves were smoothed over ±0.17 of common logarithm of diameter, to eliminate their fluctuations insignificant relative to the measurement precision. Interceptions of these two curves at a given light intensity specified corresponding d_{PC} and d_{PC^*} (Fig. 4). For example, a particle whose diameter was identified as 10.0 μm by the PC turned out to be 19.7 μm geometric large (hence particle size conversion factor C^* of 1.97), as these two curves had an identical light intensity of 11.1. The calculation for the entire PC diameter range shows that the d_{PC^*} were 1.7–2.0 times as large as the corresponding d_{PC} (Fig. 5). It should be noted that the C^* in Fig. 5 was based on the assumed particle refractive index of $1.56–0.087i$ and varied with assumptions of refractive index.

Table 2
Refractive index

Material	Refractive index
Air	1.00028
Urban aerosol (avg.)[a]	1.56–0.087*i*
Glass (standard particles)[b]	1.56
Membrane filter[c]	1.51

[a]Ozkaynak et al. (1985); Hinds (1999).
[b]Manufacturer of the particle counter.
[c]Mixture of cellulose acetate and cellulose nitrate, manufacturer of the filter.

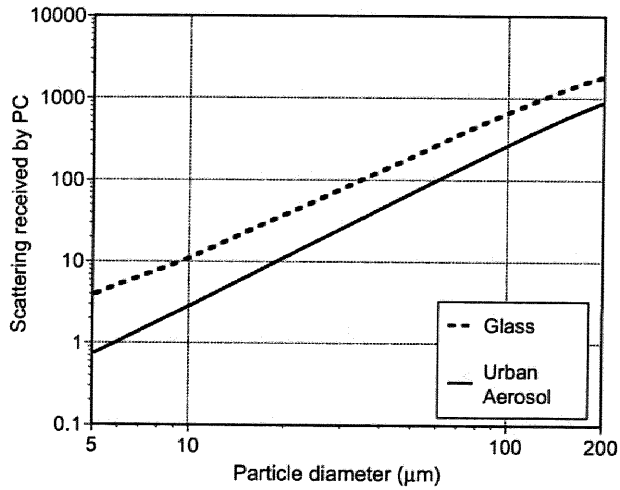

Fig. 4. Simulated PC responses to glass ($m_{cal} = 1.56$) and urban aerosols ($m_{meas} = 1.56–0.087i$).

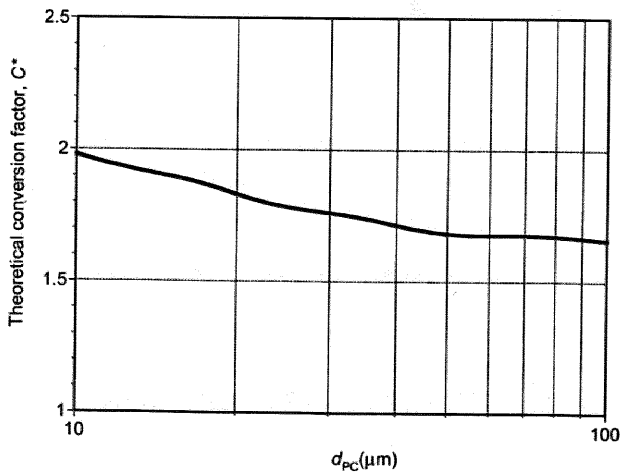

Fig. 5. Theoretical factors for particle size conversion. Glass ($m_{cal} = 1.56$) and urban aerosols ($m_{meas} = 1.56–0.087i$) were assumed for calibration and measured particles, respectively.

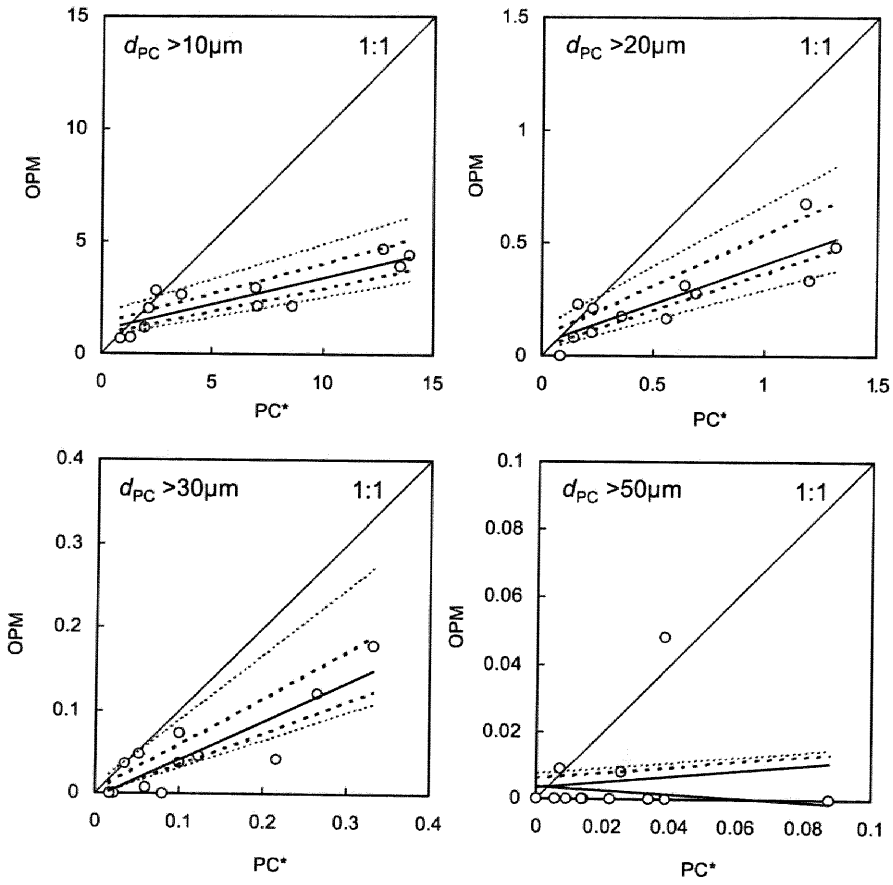

Fig. 6. Particle number concentrations (l^{-1}) by the PC* and OPM. Thin and thick dotted lines indicating roughly estimated uncertainty ranges of the assumed refractive index specified in text.

Using the theoretical conversion factors C^*, the particle diameter characterized by the PC was related to the theoretical geometric diameter:

$$d_{PC^*} = C^* \times d_{PC}. \tag{2}$$

Therefore, the size ranges by the PC were converted from $d_{PC} > 10$, > 20, > 30 and > 50 μm to $d_{PC^*} > 20$, > 36, > 54 and > 85 μm, respectively, to define the theoretical geometric size ranges by the PC observation. The concentrations recalculated based on these converted size ranges (PC*) are shown in Fig. 2. The PC* concentrations remain to be equal to corresponding PC concentrations although the defined particle sizes are different due to the particle size conversion. The relationship of particle number concentrations through twelve collocated results by the PC* and OPM are shown in Fig. 6. Some points in the diagram of $d_{PC} > 50$ μm came to zero because there was no particle sized by the OPM within the shifted PC* size range ($d_{PC^*} > 85$ μm). It is important to note that the current particle size conversion was based on the assumed particle refractive index of $1.56–0.087i$. Therefore, the converted PC* size ranges on d_{PC^*} could be varied depending on the refractive index assumed. To compare the OPM results based on the variable PC* size ranges, the original PC size ranges as a function on d_{PC} remained to be used although the converted ranges on d_{PC^*} are actually

different from the notated values on d_{PC} and varied even in the same diagram depending on the refractive index assumed.

3.4. Uncertainties in particle sizing

Since the results could be affected by the uncertainty of the assumed refractive index, the parametric sensitivity to choice of the refractive index was roughly assessed. For the purpose of the sensitivity assessment, we arbitrarily took the uncertainty range of 2% in the real part, 1.53–1.59, and a factor of two in the imaginary part, 0.044–0.174, (thick dotted lines) as well as the expanded uncertainty range of 4% in the real part, 1.50–1.62, and a factor of three in the imaginary part, 0.029–0.261 (thin dotted lines). Dotted lines in Fig. 6 indicate the uncertainty ranges of the regression lines between which the values could take. The lower solid line in the diagram of $d_{PC} > 50$ μm is the two dotted lines coincided. In fact, most of the shift was due to variation in the real part, while the little dependence was shown for the imaginary part over the supermicron diameter range. Overall, particle number concentrations by the OPM method are lower than those by the PC* within these uncertainty ranges of the refractive index. Provided the above-mentioned assumption of the refractive index was valid, the lower OPM concentrations are probably due to the following intrinsic limitation of the OPM. That is particles having the similar refractive index of the filter (Table 2) were hardly visible by the OPM. Since the particle counting efficiency by the PC is relatively high, the ratios of the OPM to PC* concentrations approximates the OPM particle counting efficiencies due to the intrinsic OPM limitations. Further investigation is required to examine the measured aerosol speciation to confirm this view.

It should be stressed that refractive index for the observed particles might take values out of the above assumed ranges, depending on their chemical components. For instance, while Marley et al. (2001) obtained the refractive indices of size-fractionated ambient aerosols ranging 1.41–2.31 for real part and 0.30–0.86 for imaginary part measured at the three cities in the US, Ohta, Murao, and Moriya (1990) reported the monthly mean imaginary part of the complex index of refraction of aerosols in Sapporo, Japan, ranging from 0.024 to 0.047. Since the refractive indices of urban aerosol are found to vary with their sizes (Marley et al., 2001), the use of single value through the entire size range can cause an additional uncertainty. Particle nonsphericity also disables accurate computation of the PC response, thereby contributing to uncertainty in the PC method. Thus, while the PC enable quick and easy assessment of aerosol size distribution, its accuracy in sizing is lowered by our limited knowledge in scattering properties of aerosol species. In the mean time, the OPM can capture the actual geometries of observed particles without these biases (Table 1). This also highlights the advantage in the OPM method particularly for aerosols of unknown compositions.

4. Summary and conclusions

The present study compared the particle size distributions collected on the filter and measured by the OPM with those by the PC to validate the microscopic method for particle size distribution quantification. We found that the microscopic method can measure particle number concentrations with relatively low amount on the filter although the particle size distributions characterized by the OPM and PC methods were different. While the OPM concentrations increased with the PC concentrations, the OPM concentrations tended to be higher. Since diameters identified by the PC differed

from the diameters observed by the OPM due to difference in scattering properties between calibration and measured particles, we roughly calculated their relationship based on the Mie scattering theory to explain the size distribution difference. The calculation showed that the theoretical geometric diameters were 1.7–2.0 times as large as the corresponding d_{PC}. Using these theoretical factors, the size ranges by the PC observation were converted (PC*). The result indicated that the OPM concentrations tended to be lower than those by the PC*. Although the particle counting efficiency by the PC is relatively high, its accuracy in particle sizing is lowered by our limited knowledge in scattering properties of aerosol species. In the meantime, the advantage in the OPM method particularly for aerosols of unknown compositions lies in its accuracy of particle sizing although the counting efficiency may be of concern.

Acknowledgements

This work was funded in part by the Suzuki Foundation, Japan. Naomichi Yamamoto thanks for the support by the grant for 21 Century COE Program, Ministry of Education, Culture, Sports, Science and Technology, Japan. Yohei Shinozuka is grateful for the combined support provided under TRACE-P (NASA NCC-1-416) and ACE-Asia (NSF ATM00-02070).

References

Agarwal, J. K., & Sem, G. J. (1980). Continuous flow, single-particle-counting condensation nucleus counter. *Journal of Aerosol Science, 11*, 343–357.

Cheng, V. S., Barr, E. B., Marshall, I. A., & Mitchell, J. P. (1993). Calibration and Performance of an API Aerosizer. *Journal of Aerosol Science, 24*, 501–514.

Hinds, W. C. (1999). *Aerosol technology: Properties, behavior, and measurement of airborne particles* (2nd ed.). New York: Wiley.

Kalechits, V. I., Kirsch, A. A., Kulibaba, V. I., Maslakov, O. Y., & Pavlov, Y. V. (1994). 15.P.10 aerosol control and monitoring system LADA. *Journal of Aerosol Science, 25*(Suppl. 1), S207–S208.

Kerker, M. (1997). Light scattering instruments for aerosol studies: An historical overview. *Aerosol Science and Technology, 27*, 522–540.

Lapuerta, M., Armas, O., & Gomez, A. (2003). Diesel size distribution estimation from digital image analysis. *Aerosol Science and Technology, 37*, 369–381.

Mäkynen, J., Hakulinen, J., Kivistö, T., & Lehtimäki, M. (1982). Optical particle counters: Response, resolution and counting efficiency. *Journal of Aerosol Science, 13*, 529–535.

Marley, N. A., Gaffney, J. S., Baird, C., Blazer, C. A., Drayton, P. J., & Frederick, J. E. (2001). An empirical method for the determination of the complex refractive index of size-fractionated atmospheric aerosols for radiative transfer calculations. *Aerosol Science and Technology, 34*, 535–549.

Ohta, S., Murao, N., & Moriya, T. (1990). Evaluation of absorption properties of atmospheric aerosols at solar wavelengths based on chemical characterization. *Atmospheric Environment, 24*, 1409–1416.

Ozkaynak, H., Schatz, A. D., Thurston, G. D., Isaacs, R. G., & Husar, R. B. (1985). Relationship between aerosol extinction coefficients derived from airport visual range observations and alternate measures of airborne particle mass. *Journal of the Air Pollution Control Association, 35*, 1176–1185.

Wiscombe, W. J. (1996). Mie scattering calculations: Advances in technique and fast, vector-speed computer codes. NCAR/TN-140+STR, NCAR TECHNICAL NOTE June 1979 (edited/revised August 1996). ftp://climate.gsfc.nasa.gov/pub/wiscombe/

Yamamoto, N., Fujii, M., Endo, O., Kumagai, K., & Yanagisawa, Y. (2002). Broad range observation of particle deposition on greased and non-greased impaction surfaces using a line-sensing optical microscope. *Journal of Aerosol Science, 33*, 1667–1679.

APPENDIX A.4.

A.4. N. Yamamoto et al., *Atmos. Environ.* 39, 3675 (2005)

Available online at www.sciencedirect.com
SCIENCE DIRECT®
Atmospheric Environment 39 (2005) 3675–3685
ATMOSPHERIC ENVIRONMENT
www.elsevier.com/locate/atmosenv

Size-dependent collection of micrometer-sized particles using nylon mesh

Naomichi Yamamoto[a,*], Kazukiyo Kumagai[a], Minoru Fujii[b], Derek G. Shendell[c], Osamu Endo[d], Yukio Yanagisawa[a]

[a]*Department of Environmental System, Institute of Environmental Studies, Graduate School of Frontier Sciences, The University of Tokyo, Hongo 7-3-1, Bunkyo-ku, Tokyo 113-8656, Japan*
[b]*National Institute for Environmental Studies, Onogawa 16-2, Tsukuba-shi, Ibaraki 305-8506, Japan*
[c]*Community Action to Fight Asthma (California State Coordinating Office), 1515 Clay Street, Suite 1700, Oakland, CA 94612, USA*
[d]*National Institute of Public Health, Shirokanedai 4-6-1, Minato-ku, Tokyo 108-8638, Japan*

Received 13 September 2004; received in revised form 21 February 2005; accepted 4 March 2005

Abstract

Our study explored the size-dependent collection characteristics for micron-sized particles using several kinds of commercially available woven nylon net filters. The particle concentrations with and without the filter were compared to determine the filtration characteristics. The theoretical efficiencies based on a single-fiber theory and a hole model were also computed. Although the theoretical efficiencies were generally consistent with the experimental results, the non-uniformity of air velocity profile within a mesh hole, and a particle's detachment from or bounce off the filters, should be further investigated in future research. Overall, the present study revealed the size-fractionation capability of the nylon wire mesh filters for micron-sized particles from experimental and theoretical points of view. Unlike impactors, the size-fractionation characteristics of the nylon wire mesh filter were determined by particle size, mesh fiber diameter, and a combination of different particle collection mechanisms including impaction, interception, and gravitational settling. Each mechanical process appears interdependently governed in part by the filter dimensions such as filter mesh size (diameter of opening) as well as related variables such as packing density and fiber diameter.

Keywords: Coarse particles; Filtration; Size distribution; Woven net filter; Mesh size

1. Introduction

The nylon net filter is a type of wire-mesh screen filter composed of woven nylon nets with known sizes (diameters) of mesh openings. Filtration using this type of filter is achieved by means of mechanical particle collection processes including impaction, interception, and Brownian diffusion. While impaction occurs when the particle crosses the abruptly changing streamlines near the filter fiber and hits the fiber because of its inertia, interception occurs when the center of a particle passes within a distance equal to the particle radius from the rim of the filter fibers. Brownian diffusion is an irregular wiggling motion of particles caused by the persistent collision by gas molecules. As a result, the particle collides with a fiber while traveling through it on a non-intercepting streamline (Hinds, 1999). Although

*Corresponding author. Tel.: +81 3 5841 7335; fax: +81 3 5841 8583.
E-mail address: naomichi.yamamoto@yy.t.u-tokyo.ac.jp (N. Yamamoto).

1352-2310/$ - see front matter © 2005 Elsevier Ltd. All rights reserved.
doi:10.1016/j.atmosenv.2005.03.001

interception and impaction are generally important mechanisms to collect supermicron particles with a filter, diffusion is the predominant mechanism for submicron particles. Therefore, when filtration sampling is conducted, particles of two different size ranges are collected with similar efficiency although the collection mechanisms differ.

Even though the collection efficiency of a filter is not uniquely related to the size of the particles to be collected, the size-fractionation technique using a nylon wire-mesh screen filter may be useful for large airborne particulate species such as of biological origin, like allergenic house dust generally in the coarse size range (e.g., 10–40 μm diameter dust mite fecal particles, a major type of house dust allergens) (Tovey et al., 1981). In particular, uniform collection of culturable biological particles, such as airborne fungi, on a filter is of interest because the conventional cascade impactors for the purpose of particle size fractionation may result in the overload of culturable organisms underneath the impaction nozzle, causing a single colony to grow from multiple depositions of organisms (McCartney et al., 1997). Since airborne fungal particles are in the range of 0.5 to 30 μm in size (Hinds, 1999), a size range for which diffusion can be neglected, the aforementioned complexity of size-fractionation measurement may be ignored for these particulate species.

The goal of the present study is to explore the possibility of a size-fractionation technique for micron-sized particles using several kinds of the commercially available woven nylon net filters. Although the particle collection mechanism with fine wire-mesh screen filters as diffusional batteries has been extensively studied to characterize fine particle removal (Sinclair and Hoopes, 1975; Cheng and Yeh, 1980; Yeh et al., 1982; Cheng et al., 1985), few studies have been conducted to establish a size-fractionation technique for measuring supermicron airborne particles of biological or chemical (combustion) origin. To determine the size-fractionation characteristics, ratios of the airborne particle concentrations with filtration to without filtration, measured by light-scattering particle counters, were calculated to obtain filtration efficiencies. The theoretical efficiencies calculated based on a single-fiber theory and a hole model were then compared with the experimental results.

2. Experimental

2.1. Filters

Nylon net filters with 11, 20, 60, 100 and 160 μm mesh sizes (Millipore Corp., Tokyo, Japan; 47 mm diameter, nylon 6,6 (Millipore, 2002)) were used. The filters consisted of woven nylon nets with opening area fractions of 6, 14, 42, 44 and 53% on a filter surface for the 11, 20, 60, 100 and 160 μm mesh filter sizes, respectively; filter thicknesses were 65, 55, 50, 80 and 100 μm, respectively. The packing density, α, was calculated by the following equation given by Cheng and Yeh (1980):

$$\alpha = \frac{\text{volume of solid}}{\text{total volume}} = \frac{4m_s}{\pi d_s^2 h \rho_s}, \quad (1)$$

where m_s is mass of filter, d_s is filter diameter, h is filter thickness, and ρ_s is density of the filter material ($= 1.14\,\mathrm{g\,cm^{-1}}$ for nylon 6,6). The filter mass was determined using a microbalance (Model AG204, Mettler Toledo Inc., USA). The fraction of a filter's surface area with mesh openings, ε, was equal to the projected area ratio of a mesh opening to a double-cross of axes of proximate nylon net fibers. Therefore, the diameter of a nylon fiber, d_f, is given by

$$d_f = \left(\frac{l^2}{\varepsilon}\right)^{0.5} - l, \quad (2)$$

where l is filter mesh size. The dimensions of the filters are also summarized in Table 1.

Table 1
Dimensions of the woven nylon net filters

Mesh size[a] l (μm)	Mesh opening[a] ε (%)	Thickness[a] h (μm)	Filter mass m_s (SD, in mg)[b]	Packing density[c] α	Fiber diameter[d] d_f (μm)
11	6	65	71.4 (0.3)	0.56	34
20	14	55	60.3 (0.5)	0.55	33
60	42	50	31.9 (0.5)	0.32	33
100	44	80	45.5 (0.2)	0.29	51
160	53	100	52.8 (0.1)	0.27	60

[a]Information values.
[b]Weighed by a microbalance ($n = 3$); SD = standard deviation.
[c]Calculated by Eq. (1).
[d]Calculated by Eq. (2).

2.2. Particle filtration efficiency

The particle concentrations with and without the filter (C_{out} and C_{in}, respectively) were compared to obtain the particle filtration efficiency. The ratio of C_{out} to C_{in} was defined as the penetration efficiency, Pt, of the filter. Therefore, the particle collection efficiency, E, was given by

$$E = 1 - Pt = 1 - \frac{C_{out}}{C_{in}}. \quad (3)$$

To prevent static charge buildup on the nylon net filter and to minimize the effect of electrostatic forces, an aluminum filter holder with a stainless-steel support (SKC Inc., PA, USA) was used. The filter holder faced upward during sampling. The face velocity of gas through the filter, q, was adjusted to be 0.48 cm s^{-1}.

2.3. Experiment I: Particles smaller than 5 μm

Airborne particles smaller than 5 μm in aerodynamic diameter were monitored using a light-scattering particle counter with size channels of 0.3, 0.5, 1, 2 and 5 μm (Model KC-01B, RION Ltd., Tokyo, Japan; halogen lamp, 70° sideway light-scattering method), for which particle size calibrations were performed using standard spherical polystyrene latex particles (refractive index = 1.59). A monitoring of cycle of 6 min of filtration and 3 min of non-filtration was repeated five times. The mean concentration of a non-filtration monitoring cycle before and after a filtration monitoring cycle was computed to determine how C_{in} and C_{out} were defined. The collection efficiencies for each sampling cycle were calculated by Eq. (3), and the means and standard deviations (SDs) of the efficiencies through five sampling cycles were calculated. The flow rate was adjusted to 500 ml min^{-1} ($q = 0.48$ cm s^{-1}) as specified for the Model KC-01B particle counter. Air samplings were taken indoors in the room on the sixth floor room of a building in the central part in Tokyo in February 2004.

2.4. Experiment II: Particles larger than 10 μm

To generate sufficient and controlled numbers of airborne particles larger than 10 μm in aerodynamic diameter, soil particles were actively resuspended in a bottle by accelerated air introduced through a nozzle (Fig. 1). The soil was collected in the yard in a central part in Tokyo, and then dried and sieved by a 500 μm mesh stainless-steel screen. The resuspended particles were introduced to the glass adaptor with or without filtration, diluted by clean air from a vacuum pump, and measured by a particle counter. A light-scattering particle counter with size channels of 10, 20, 30, 50 and 100 μm (Model KC-20, RION Ltd., Tokyo, Japan; laser diode with wavelength of 780 nm, 70° sideway light-scattering method), for which particle size calibrations were performed using standard spherical glass bead particles (refractive index = 1.56), was used to monitor resuspended particles. Dilution was necessary to regulate the face velocity of gas through the 47 mm diameter filter at 0.48 cm s^{-1} (0.51 min^{-1}), since the total airflow volume specified by the manufacturer for the Model KC-20 particle counter, at least 15 l min^{-1}, was too high. The mean concentrations from sampling 10 to 20 min from the initiation of each particle resuspension experiment were used to calculate the filtration efficiencies. Concentrations with the filter were measured three times for each type of filter and the concentration without the filter was measured six times. Concentrations measured in three filtration experiments for each mesh size filter were compared with those measured in the six non-filtration experiments to calculate filtration efficiencies. The SDs of the efficiencies were calculated using an error propagation formula with information on

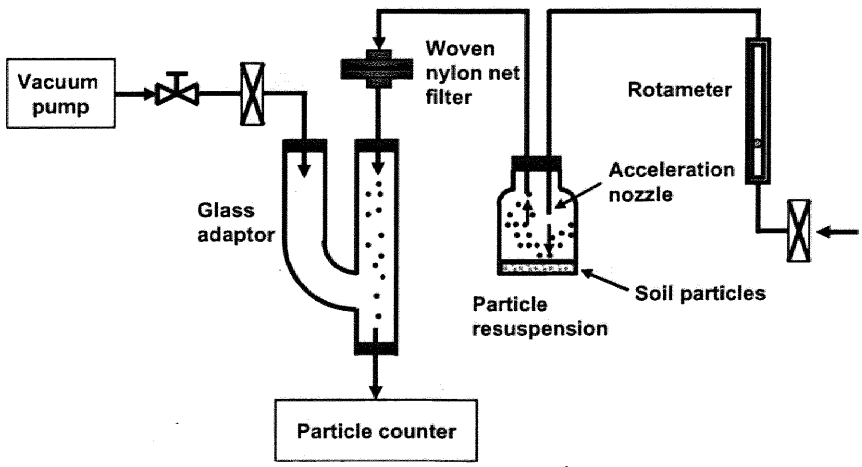

Fig. 1. Experimental setup for a large particle generation and measurement system (Experiment II).

the concentrations and SDs from the filtration and non-filtration experiments.

3. Model

3.1. Model description

Since all of the air entering a pore of a filter exits through the pore, a particle following an air streamline should also exit the pore. Nevertheless, the particles are collected on the filter fibers by one of several mechanisms. Within the structure of the filter, the air streamlines abruptly change their directions near the fibers of the filter. Consequently, a particle departing from the abruptly changing air streamline due to its inertia eventually hits the filter fiber and is collected (impaction). A particle not captured by impaction and following the air streamline can still be collected by the filter if the particle happens to encounter the surface of the fiber because of the particle's size (interception). For a large particle, settling due to gravity plays an important role in overcoming the abruptly changing air streamlines, resulting in particle collection on the filter fiber (gravitational settling).

In the present model analysis, the structure of nylon net filters was approximated in the middle of a sequence of single fibers and an array of collimated square holes (Fig. 2). While a single-fiber theory was used to calculate particle collection efficiencies by impaction and gravitational settling, the efficiency by interception was calculated using a hole model for which an array of collimated square holes was assumed.

Since a single-fiber theory defines the collection efficiency of a fiber for the fraction of particles approaching the fiber in a region defined by the projected area of the fiber that is ultimately collected on the fiber (Hinds, 1999), the collection efficiency of a filter by impaction or gravitational settling was approximated as the product of the single-fiber efficiency and the projected area fraction of fibers on a filter ($= 1 - \varepsilon$). Therefore, when the centers of the particles pass further away from the rim of the filter fibers, the particles were captured neither by impaction nor by gravitational settling. Nevertheless, the particles may be captured on a filter by interception when the particles happen to come within one particle radius of the rim of a fiber. To account for particle collection by interception, a hole model was used in conjunction with the single-fiber theory. Thus, while a single-fiber model for impaction and gravitational settling defines the collection efficiency of particles in the region defined by the projected area of the fiber, a hole model for interception characterizes the efficiency of particles flowing into the mesh hole.

Theoretical collection efficiencies due to each of these mechanical processes were separately calculated, and then combined to obtain the overall filter efficiency:

$$E_\Sigma = 1 - (1 - E_R)(1 - E_I)(1 - E_G), \tag{4}$$

where E_R, E_I and E_G are the particle collection efficiencies due to interception, impaction and gravitational settling, respectively. In this study, the particle collection efficiencies for impaction and gravitational settling were calculated based on a single-fiber model summarized by Hinds (1999), while those for interception were calculated based on a hole model given by the

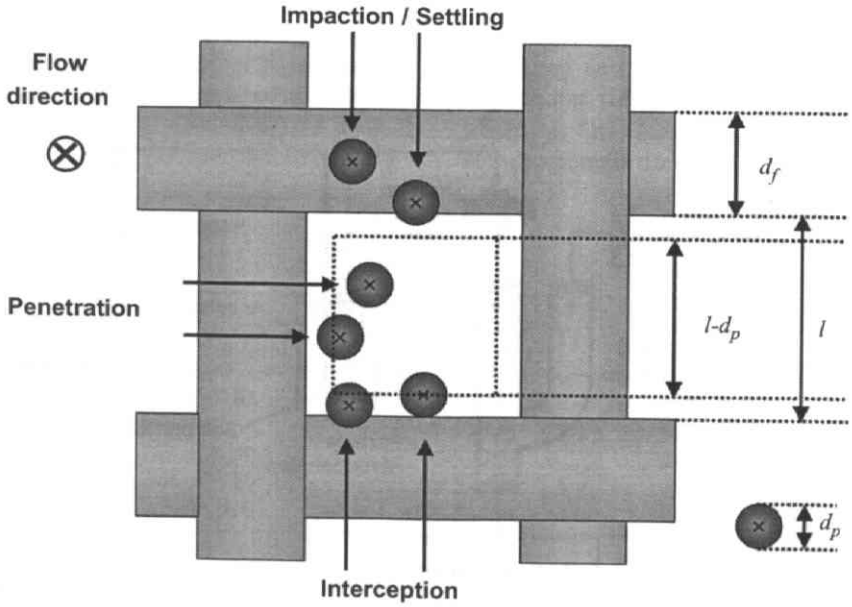

Fig. 2. Schematic diagram of particle collections on the wire-mesh screen filter.

Natanson expression (Spurny et al., 1969). The detailed calculation methods will be described in the following sections.

Diffusion and diffusion–interception interaction were not taken into account since the large particles for which diffusion could be neglected were investigated in this study. Solid spherical particles with unit density were assumed for calculations.

3.2. Impaction

Particle collection due to inertial impaction alone, E_I, was calculated using the following equation (Yeh and Liu, 1974; Hinds, 1999):

$$E_I = (1-\varepsilon)\frac{(\mathrm{Stk})J}{2\mathrm{Ku}^2}, \tag{5}$$

$$\text{where } \mathrm{Stk} = \frac{\rho_p d_p^2 C_c q}{18\eta d_f}, \tag{6}$$

$$J = (29.6 - 28\alpha^{0.62})R^2 - 27.5R^{2.8}, \quad \text{for } R<0.4,$$

$$J = 2.0, \quad \text{for } R>0.4, \tag{7}$$

$$\mathrm{Ku} = -\frac{\ln\alpha}{2} - \frac{3}{4} + \alpha - \frac{\alpha^2}{4}, \tag{8}$$

where ρ_p is particle density, d_p is particle diameter, C_c is Cunningham correction factor, η is gas viscosity, and

$$R = \frac{d_p}{d_f}, \tag{9}$$

The Cunningham correction factor, a factor accounting for the effect of slip, was calculated by the following equation (Allen and Raabe, 1985):

$$C_c = 1 + \frac{\lambda}{d_p}\left[2.34 + 1.05\ \exp\left(-0.39\frac{d_p}{\lambda}\right)\right], \tag{10}$$

where λ is the mean free path for air. Although the factor of $1-\varepsilon$ in Eq. (5) was not included in the original form referenced, this factor was necessary to apply the single-fiber theory to obtain the efficiency by an entire filter. For the same reason, the factor was necessary to calculate the efficiency by gravitational settling. Although the value of $(\mathrm{Stk})J/2\mathrm{Ku}^2$ in Eq. (5) can become larger than the theoretical maximum of efficiency (= 1.0) with the increase of particle size, the theoretical maximum of 1.0 was used once the value became larger than 1.0.

3.3. Gravitational settling

Particle collection due to gravitational settling alone, E_G, was calculated using the following equation (Stechkina et al., 1969; Hinds, 1999):

$$E_G \approx (1-\varepsilon)G(1+R), \tag{11}$$

$$\text{where } G = \frac{V_{TS}}{q} = \frac{\rho_p d_p^2 C_c g}{18\eta q}, \tag{12}$$

V_{TS} is terminal settling velocity, and g is acceleration due to gravity. This equation is applicable when q and V_{TS} are in the same direction, i.e., downward airflow. As was the case with Eq. (5), the theoretical maximum of the efficiency (= 1.0) was used once the value of $G(1+R)$ in Eq. (11) became larger than 1.0.

3.4. Interception

To calculate E_R, the Natanson expression originally developed for cylindrical holes perpendicular to the filter (Spurny et al., 1969) was modified for square holes (Fig. 2). E_R was computed using the following modified equation:

$$E_R = 1 - Pt_R = 1 - \frac{(l-d_p)^2}{l^2}, \tag{13}$$

where Pt_R is penetration efficiency due to interception alone. Since interception occurs when the center of a particle following a streamline passes within a distance $d_p/2$ from the rim of the hole (Fig. 2), a particle must pass inside a square with side length of $l-d_p$ to penetrate through the hole. Thus, the value of Pt_R derived from this expression represented the area ratio of the square with a side length of $l-d_p$ to a square mesh opening with side length of l. For this calculation, a uniform velocity profile within the hole was assumed.

4. Results and discussion

The experimental results are summarized in Tables 2–7. The collection efficiencies of the $>5\,\mu m$ particles for the filter with 160 μm mesh often showed negative values in some sampling cycles (Table 6), which were expected due to fluctuation of the monitored indoor particle concentrations throughout the measurement cycles. Since the concentrations of the $>5\,\mu m$ particles were relatively low and unstable compared to those of smaller particles, the efficiency calculations were sensitively influenced for the $>5\,\mu m$ size range. Concentrations shown in Table 7 were those converted to express the concentrations through the filter holder before dilution by clean air, and not readouts of the particle counter. Fig. 3 presents the overall theoretical particle collection efficiencies with the efficiencies due to each of the three investigated collection mechanisms. The theoretical particle diameters for 50% collection efficiencies, d_{50}, defined as particle diameters producing the theoretical values at 50% efficiency (Fig. 3), are presented in Table 8.

To compare with experimental results, values of theoretical efficiencies were organized in terms of

Table 2
Experimental results for the woven nylon net filters with 11 μm mesh size (Experiment I)

Sampling cycle	Concentrations with (C_{out})/without (C_{in}) the filter, each with units of l^{-1}					Collection efficiency[a] E				
	0.3–0.5 μm	0.5–1 μm	1–2 μm	2–5 μm	>5 μm	0.3–0.5 μm	0.5–1 μm	1–2 μm	2–5 μm	>5 μm
1	23 400/24 700	2690/2880	309/359	55.0/72.0	3.25/7.83	0.05	0.07	0.14	0.24	0.59
2	23 400/24 800	2790/2930	321/353	48.0/72.0	2.57/9.67	0.06	0.05	0.09	0.33	0.73
3	23 900/25 100	2890/3010	331/349	51.1/59.0	1.57/6.67	0.05	0.04	0.05	0.13	0.76
4	24 600/25 400	2910/3030	340/356	42.6/58.0	2.57/5.50	0.03	0.04	0.05	0.27	0.53
5	24 900/25 500	2960/3050	324/355	48.7/62.0	2.71/5.33	0.02	0.03	0.09	0.21	0.49
Average (SD)[b]						0.04 (0.01)	0.04 (0.01)	0.08 (0.04)	0.24 (0.07)	0.62 (0.12)

[a]Calculated by Eq. (3).
[b]SD = standard deviation.

Table 3
Experimental results for the woven nylon net filters with 20 μm mesh size (Experiment I)

Sampling cycle	Concentrations with (C_{out})/without (C_{in}) the filter, each with units of l^{-1}					Collection efficiency[a] E				
	0.3–0.5 μm	0.5–1 μm	1–2 μm	2–5 μm	>5 μm	0.3–0.5 μm	0.5–1 μm	1–2 μm	2–5 μm	>5 μm
1	20 100/20 600	2070/2120	316/319	80.7/85.8	6.43/10.67	0.03	0.03	0.01	0.06	0.40
2	20 000/20 500	2000/2080	293/301	60.3/74.8	4.29/7.79	0.02	0.04	0.03	0.19	0.45
3	19 900/20 500	1980/2080	291/299	59.0/65.6	3.86/6.13	0.03	0.04	0.02	0.10	0.37
4	20 000/20 500	2040/2060	280/294	58.4/55.3	3.71/4.83	0.02	0.01	0.05	−0.06	0.23
5	20 400/20 700	2070/2090	271/289	54.1/54.5	2.57/4.83	0.01	0.01	0.06	0.01	0.47
Average (SD)[b]						0.02 (0.01)	0.03 (0.02)	0.03 (0.02)	0.06 (0.09)	0.38 (0.09)

[a]Calculated by Eq. (3).
[b]SD = standard deviation.

Table 4
Experimental results for the woven nylon net filters with 60 μm mesh size (Experiment I)

Sampling cycle	Concentrations with (C_{out})/without (C_{in}) the filter, each with units of l^{-1}					Collection efficiency[a] E				
	0.3–0.5 μm	0.5–1 μm	1–2 μm	2–5 μm	>5 μm	0.3–0.5 μm	0.5–1 μm	1–2 μm	2–5 μm	>5 μm
1	25 400/25 600	3140/3070	366/357	57.3/60.3	3.71/5.13	0.01	−0.02	−0.02	0.05	0.28
2	25 100/25 500	3060/3120	351/354	56.5/59.0	6.25/5.83	0.02	0.02	0.01	0.04	−0.07
3	26 100/26 100	3170/3230	372/368	59.4/62.7	4.14/7.83	0.00	0.02	−0.01	0.05	0.47
4	26 600/26 800	3270/3310	357/376	55.0/64.8	4.71/6.00	0.01	0.01	0.05	0.15	0.21
5	27 500/28 300	3310/3370	368/374	51.7/66.0	3.43/4.67	0.03	0.02	0.02	0.23	0.27
Average (SD)[b]						0.01 (0.01)	0.01 (0.02)	0.01 (0.03)	0.11 (0.08)	0.23 (0.20)

[a]Calculated by Eq. (3).
[b]SD = standard deviation.

Table 5
Experimental results for the woven nylon net filters with 100 μm mesh size (Experiment I)

Sampling cycle	Concentrations with (C_{out})/without (C_{in}) the filter, each with units of l^{-1}					Collection efficiency[a] E				
	0.3–0.5 μm	0.5–1 μm	1–2 μm	2–5 μm	>5 μm	0.3–0.5 μm	0.5–1 μm	1–2 μm	2–5 μm	>5 μm
1	33 600/33 800	4200/4240	572/583	154/168	11.3/16.8	0.00	0.01	0.02	0.09	0.33
2	30 900/31 300	3730/3860	562/575	185/191	20.6/21.2	0.01	0.03	0.02	0.03	0.03
3	28 700/29 100	3500/3580	596/587	205/227	24.9/25.8	0.02	0.02	−0.02	0.10	0.04
4	27 200/27 300	3260/3370	610/614	224/264	27.1/28.7	0.01	0.03	0.01	0.15	0.05
5	25 100/25 400	3140/3170	649/677	295/306	35.1/34.9	0.01	0.01	0.04	0.03	−0.01
Average (SD)[b]						0.01 (0.01)	0.02 (0.01)	0.02 (0.02)	0.08 (0.05)	0.08 (0.14)

[a]Calculated by Eq. (3).
[b]SD = standard deviation.

Table 6
Experimental results for the woven nylon net filters with 160 μm mesh size (Experiment I)

Sampling cycle	Concentrations with (C_{out})/without (C_{in}) the filter, each with units of l^{-1}					Collection efficiency[a] E				
	0.3–0.5 μm	0.5–1 μm	1–2 μm	2–5 μm	>5 μm	0.3–0.5 μm	0.5–1 μm	1–2 μm	2–5 μm	>5 μm
1	23 100/23 300	1950/1940	477/477	168/176	16.0/12.0	0.01	−0.01	0.00	0.04	−0.33
2	23 400/23 600	1920/1930	457/457	164/161	11.6/10.7	0.01	0.00	0.00	−0.02	−0.08
3	24 300/24 600	2060/2070	456/452	161/149	9.1/11.2	0.01	0.01	−0.01	−0.08	0.18
4	25 300/25 800	2100/2220	449/459	148/148	8.9/11.7	0.02	0.05	0.02	0.00	0.24
5	26 300/26 700	2220/2280	453/432	137/140	9.6/10.0	0.02	0.03	−0.05	0.02	0.04
Average (SD)[b]						0.01 (0.01)	0.02 (0.02)	−0.01 (0.03)	−0.01 (0.05)	0.01 (0.23)

[a]Calculated by Eq. (3).
[b]SD = standard deviation.

particle size ranges. The value of the efficiency in the particle size range between a and b, E_{ab}, was integrated over its range weighted by the concentration fractions of each particle size. The equation used was

$$E_{ab} = \frac{\int_a^b E(d_p)C(d_p)dd_p}{\int_a^b C(d_p)dd_p}, \quad (14)$$

where $E(d_p)$ and $C(d_p)$ were the collection efficiency and concentration within an interval of particle sizes between d_p and $d_p + dd_p$, respectively. Although values of $E(d_p)$ were determined by the aforementioned theoretical calculations, values of $C(d_p)$ were estimated by interpolation of the concentrations measured across size channels of the particle counter. Based on the experimental results demonstrating uneven concentration distributions across the size channels (Tables 2–7), the particle size distributions were expected to be uneven within a size channel. In the present analysis, the concentration gradient in the size channel ranging from a to b was approximated by the following equation:

$$\frac{dC(d_p)}{dd_p} \approx \frac{C_{bc} - C_{ab}}{\Delta d_{ab}}, \quad (15)$$

where Δd_{ab} was the width of the size channel, and C_{ab} and C_{bc} were readouts from size channels ranging from a to b and from b to c, respectively. The particle size ranges for the channels of >5 and >50 μm were assumed to be 5–10 and 50–100 μm, respectively, and the concentrations were presumed to approach zero at particle sizes of 10 and 100 μm, respectively. The frequency distribution within each size channel was also estimated. Since concentrations measured by a size channel were integrated over its size range, the size distribution of $C(d_p)$ in a particle counter's size channel

Table 7
Experimental results (Experiment II)

Mesh size l (μm)	No. of experiments	Concentration[a] (l^{-1}) (SD)[c]				Collection efficiency[b] E (SD)[b]			
		10–20 μm	20–30 μm	30–50 m	> 50 μm	10–20 μm	20–30 μm	30–50 μm	> 50 μm
11	3	4.70	0.100	0.000	0.100	1.00	1.00	1.00	0.96
		(1.14)	(0.087)	(0.000)	(0.173)	(0.00)	(0.00)	(0.00)	(0.07)
20	3	150.2	0.200	0.250	0.050	1.00	1.00	0.99	0.98
		(24.4)	(0.229)	(0.312)	(0.087)	(0.00)	(0.00)	(0.01)	(0.03)
60	3	25 000	101.2	1.80	0.100	0.51	0.85	0.93	0.96
		(10 400)	(33.7)	(1.04)	(0.173)	(0.24)	(0.06)	(0.05)	(0.07)
100	3	28 700	216	5.40	0.400	0.44	0.68	0.79	0.84
		(11 700)	(127)	(2.21)	(0.087)	(0.27)	(0.21)	(0.11)	(0.07)
160	3	32 600	254	7.60	0.350	0.36	0.63	0.70	0.86
		(10 200)	(126)	(2.17)	(0.312)	(0.26)	(0.21)	(0.13)	(0.13)
No filter	6	50 900	684	25.60	2.550	—	—	—	—
		(13 300)	(194)	(8.17)	(0.910)	—	—	—	—

[a]Concentrations through the filter holder either with or without the filter, not readouts of the particle counter.
[b]Calculated by Eq. (3).
[c]SD = standard deviation.

ranging from a to b should meet the following equation:

$$\int_a^b C(d_p)dd_p = C_{ab}. \quad (16)$$

To meet conditions given by Eqs. (15) and (16), values of theoretical efficiencies for each size channel were calculated with Eq. (14). The theoretical and experimental efficiencies are shown in Fig. 4.

Overall, the theoretical collection efficiencies were consistent with the experimental results. The theoretical efficiencies were, however, slightly higher than the experimental values for the collection of particles smaller than 5 μm by filters with 11 and 20 μm mesh sizes. For instance, while the experimental collection efficiency for 2–5 μm particles by 20 μm mesh was 0.06 ± 0.09, the theoretical efficiency was 0.47. The reported differences between theory and experiment for the smaller particles with finer mesh sizes were expected due to the non-uniform velocity profile within a hole (John et al., 1978; Gentry et al., 1982), which was more pronounced for finer mesh openings. If the air velocity is sufficiently higher in the inner region of the mesh opening because of the slip where the flowing air contacts the inner wall of the mesh hole, particles traveling through the hole would become concentrated in the inner region of the mesh hole because of the larger volumetric flow in that region. As a result, the particles would less likely be captured by interception because most particles would pass sufficiently further from the rim of the filter fibers. This tendency becomes more distinct for the smaller particles because the ratio of the relative size of particles to the size of a mesh becomes smaller, resulting in decreased probability of particle interception. Therefore, although we assumed a uniform velocity profile for the theoretical calculation of interception, these calculations might be overestimates for the smaller particles if the actual air velocity was higher in the inner region of the mesh opening.

In addition, larger theoretical collection efficiencies for filters with 100 and 160 μm mesh sizes were observed for larger particles. For instance, while the experimental collection efficiency for 30–50 μm particles by 100 μm mesh was 0.78 ± 0.11, the theoretical efficiency was 0.92. Although we assumed particles adhered to filter fibers permanently once they contacted the fibers, they might have detached from the fibers and been re-entrained in the aerosol stream or have bounced off the mesh fibers. Thus, our theoretical efficiency calculations may have overestimated values compared to true particle collection efficiency. Corn and Stein (1965) observed a greater probability of particle detachment in flowing air with increasing particle size, and Mausa and Umhauer (1996) suggested the importance of bounce off the fibers for biological particles in the larger than 5 μm size range.

Particle sizes characterized by light-scattering particle counters were generally different from those observed by microscopes, depending on the optical properties of measured and calibration particles. While glass bead or polystyrene latex particles known to be non-absorbing were used to calibrate the particle counters, measured particles might have absorbed light. If measured particles absorbed light, which was reported for urban aerosol (Ozkaynak et al., 1985), the size distributions

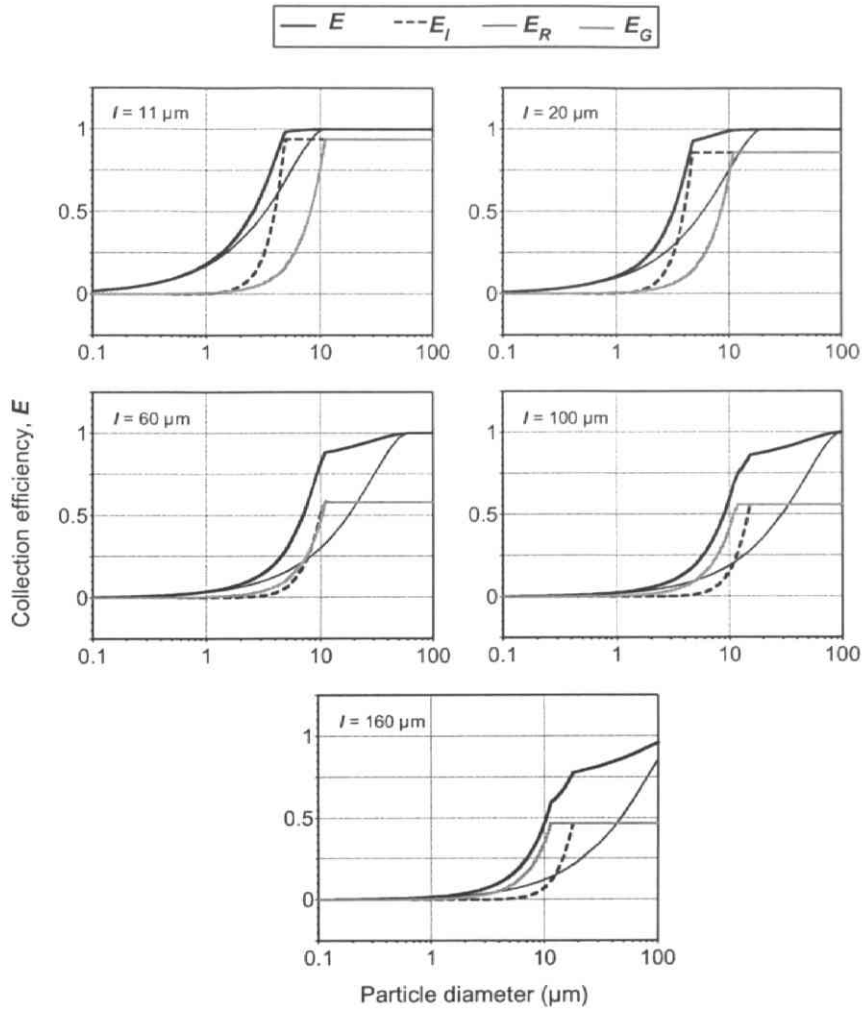

Fig. 3. Theoretical particle collection efficiencies by woven nylon net filters with various mesh openings. $q = 0.48\,\mathrm{cm\,s^{-1}}$ of downward airflow.

Table 8
Theoretical particle diameters for 50% collection efficiencies by nylon net filters

Mesh size (μm)	Theoretical d_{50}[a] (μm)
11	2.5
20	3.2
60	6.9
100	8.8
160	10.4

[a]Defined as particle diameters that give theoretical values of 50% collection efficiency in Fig. 3.

characterized by the particle counters were on the smaller side compared to those observed with microscopes (Yamamoto et al., 2004). Although the light-scattering properties of ambient and soil particles measured in this study were unknown, the experimental efficiency curves (Fig. 4) might be on the larger side in case the measured particles absorbed light. This observation suggested our theoretical calculations were possibly higher than the results shown in Fig. 4.

Although we assumed spherical particles for the theoretical efficiency calculations, particle shape may have to be taken into account. The non-spherical indoor air particles investigated in the present study were thought to be more resistive in air because irregular particles have dynamic shape factors generally greater than 1.0 (Hinds, 1999). Therefore, these non-spherical particles would be less likely to be collected by means of impaction and gravitational settling due to decreased settling velocity, but the collection efficiency due to interception would be expected to increase. Provided the irregular particles settled in random orientation (Davies, 1979; Hinds, 1999), they were more likely intercepted by the filter fibers compared to spherical particles.

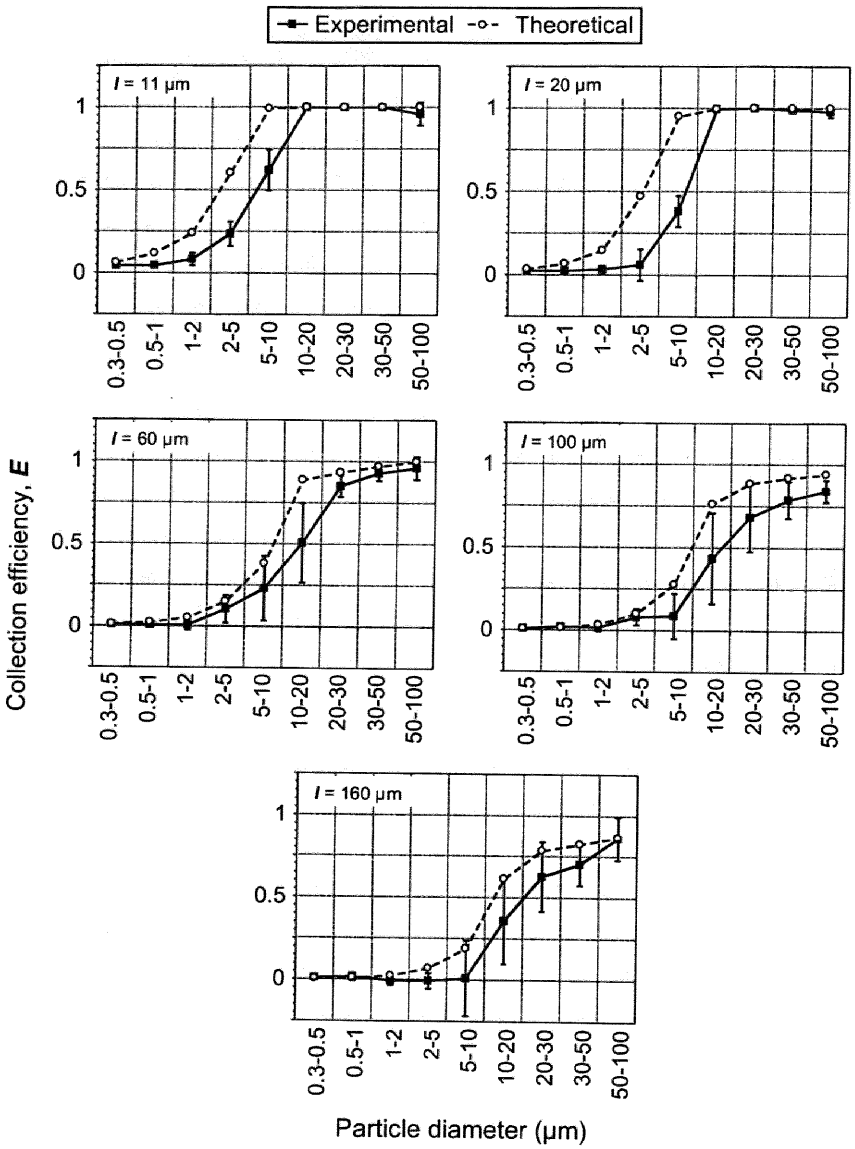

Fig. 4. Theoretical and experimental collection efficiencies.

In addition, electrostatic forces were not taken into account for the theoretical calculations. Given experimental efficiencies were consistently lower than the theoretical values, not incorporating attractive forces between the filter and the particles due to static charges did not appear to lead to underestimation of overall theoretical collection efficiencies. Repulsive forces among similarly charged particles accumulated on the filter fibers, however, may have reduced the filter's particle collection efficiency, resulting in lower experimental values (Fig. 4). For these mechanical viewpoints, future research should further develop models to understand better the roles of these mechanisms.

The present study indicated the efficiency was a product of the values for multiple particle collection mechanisms (Fig. 3). Thus, unlike impactors, which fractionate particles by size based solely on inertial impaction, size-fractionation by the nylon wire mesh screen filters appears determined by a combination of various mechanical processes including impaction, interception, and gravitational settling. Each mechanical process appears interdependently governed by filter dimensions such as filter mesh size (diameter of opening), as well as related variables such as packing density and fiber diameter. While impaction and gravitational settling depend on mesh fiber diameter and not directly on mesh size, the fiber diameter was calculated from the filter dimensions including the filter mesh size and fraction of mesh openings, which are interdependently related due to the filter structure.

5. Summary and conclusions

The present study explored the size-dependent collection characteristics for micron-sized particles using several kinds of commercially available woven nylon net filters. We determined size-fractionation characteristics by measuring particle concentrations, with and without the filter, with light-scattering particle counters to calculate collection efficiencies. Theoretical efficiencies calculated based on a single-fiber theory and a hole model were compared with the experimental results. Overall, the theoretical efficiencies were generally consistent with the experimental results. The differences between theoretical and experimental collection efficiencies for smaller particles, i.e. $d_p < 5\,\mu m$, for filters with finer mesh sizes, i.e. $l = 11$ and $20\,\mu m$, were expected in part due to non-uniform air velocity profiles within the mesh hole. Discrepancies observed for larger particles, i.e. $d_p > 20\,\mu m$, for filters with coarser mesh sizes, i.e. $l = 100$ and $160\,\mu m$, were expected in part due to particle detachment from the filter fibers and particles bouncing off fibers. Unlike with impactors, size-fractionation characteristics appeared to be determined by combination of different particle collection mechanisms. Each mechanical process appears interdependently governed by filter dimensions such as filter mesh size (diameter of opening) as well as their related variables such as packing density and fiber diameter. Future research should further develop models to understand better the roles of these mechanisms, because this measurement technique could have broader applications in indoor air quality and health effects investigations concerning particles and bioaerosols.

Acknowledgements

This work was supported in part by a Sasakawa Scientific Research Grant from The Japan Science Society. Naomichi Yamamoto also received support through a grant from the 21 Century COE Program, Ministry of Education, Culture, Sports, Science and Technology, Japan.

References

Allen, M.D., Raabe, O.G., 1985. Slip correction measurements of spherical solid aerosol particles in an improved Millikan apparatus. Aerosol Science and Technology 4, 269–286.

Cheng, Y.S., Yeh, H.C., 1980. Theory of a screen type diffusion battery. Journal of Aerosol Science 11, 313–320.

Cheng, Y.S., Yeh, H.C., Brinsko, K.J., 1985. Use of wire screens as a Fan model filter. Aerosol Science and Technology 4, 165–174.

Corn, M., Stein, F., 1965. Re-entrainment of particles from a plane surface. American Industrial Hygiene Association Journal 26, 325–336.

Davies, C.N., 1979. Particle–fluid interaction. Journal of Aerosol Science 10, 477–513.

Gentry, J.W., Spurny, K.R., Schoermann, J., 1982. Diffusional deposition of ultrafine aerosols on Nuclepore filters. Atmospheric Environment 16, 25–40.

Hinds, W.C., 1999. Aerosol Technology: Properties Behavior and Measurement of Airborne Particles, second ed. Wiley, New York.

John, W., Reischl, G., Goren, S., Plotkin, D., 1978. Anomalous filtration of solid particles by Nuclepore filters. Atmospheric Environment 12, 1555–1557.

Maus, R., Umhauer, H., 1996. Collection and adhesion efficiency of biological particles on single fibers. Journal of Aerosol Science 27 (Suppl. 1), S255–S256.

McCartney, H.A., Fitt, B.D.L., Schmechel, D., 1997. Sampling of bioaerosols in plant pathology. Journal of Aerosol Science 28, 349–364.

Millipore, 2002. Catalogue for Membrane Discs and Filter Holders.

Ozkaynak, H., Schatz, A.D., Thurston, G.D., Isaacs, R.G., Husar, R.B., 1985. Relationship between aerosol extinction coefficients derived from airport visual range observations and alternate measures of airborne particle mass. Journal of the Air Pollution Control Association 35, 1176–1185.

Sinclair, D., Hoopes, G.S., 1975. A novel form of diffusion battery. American Industrial Hygiene Association Journal 39–42.

Spurny, K.R., Lodge, J.P., Frank, E.R., Sheesley, D.C., 1969. Aerosol filtration by means of Nuclepore filters. Environmental Science and Technology 3, 453–464.

Stechkina, I.B., Kirsch, A.A., Fuchs, N.A., 1969. Studies on fibrous aerosol filters—iv. Calculation of aerosol deposition in model filters in the region of maximum penetration. The Annals of Occupational Hygiene 12, 1–8.

Tovey, E.R., Chapman, M.D., Platts-Mills, T.A.E., 1981. Mite faeces are a major source of house dust allergens. Nature 289, 592–593.

Yamamoto, N., Shinozuka, Y., Kumagai, K., Fujii., M., Yanagisawa, Y., 2004. Particle size distribution quantification by microscopic observation. Journal of Aerosol Science 35, 1225–1234.

Yeh, H.C., Liu, B.Y.H., 1974. Aerosol filtration by fibrous filters. Journal of Aerosol Science 5, 191–217.

Yeh, H.C., Cheng, Y.S., Orman, M.M., 1982. Evaluation of various types of wire screens as diffusion battery cells. Journal of Colloid and Interface Science 86, 12–16.

APPENDIX B.

Patent

APPENDIX B.1.

Patent application number: JPN 2005-193740 (in Japanese)

【書類名】　特許願
【整理番号】　05P082
【あて先】　特許庁長官殿
【国際特許分類】　G01N 1/23
【発明者】
　【住所又は居所】　東京都文京区本郷７丁目３番１号　東京大学工学部５号館
　【氏名】　柳沢　幸雄
【発明者】
　【住所又は居所】　東京都文京区本郷７丁目３番１号　東京大学工学部５号館
　【氏名】　山本　尚理
【発明者】
　【住所又は居所】　東京都台東区池之端３丁目１番２５号　柴田科学株式会社内
　【氏名】　柴田　真利
【発明者】
　【住所又は居所】　東京都台東区池之端３丁目１番２５号　柴田科学株式会社内
　【氏名】　小山　博巳
【発明者】
　【住所又は居所】　東京都台東区池之端３丁目１番２５号　柴田科学株式会社内
　【氏名】　彦野　政治
【特許出願人】
　【識別番号】　000181767
　【氏名又は名称】　柴田科学株式会社
【代理人】
　【識別番号】　100064539
　【弁理士】
　【氏名又は名称】　右田　登志男
【代理人】
　【識別番号】　100103274
　【弁理士】
　【氏名又は名称】　千且　和也
【手数料の表示】
　【予納台帳番号】　196598
　【納付金額】　16,000円
【提出物件の目録】
　【物件名】　特許請求の範囲　1
　【物件名】　明細書　1
　【物件名】　図面　1
　【物件名】　要約書　1

【書類名】特許請求の範囲
【請求項１】
　被捕集物質を捕集可能な捕集基質を曝した状態で装着することが可能である被捕集物質捕集器本体と、
　該被捕集物質捕集器本体の外縁よりも大きな内縁を有する第１リング部材と、
　該第１リング部材の外縁よりも大きな内縁を有する第２リング部材と、を備え、
　前記被捕集物質捕集器本体は、その垂直方向に延びる中心軸と直交する第１軸を中心に、前記第１リング部材に対して傾動可能に取り付けられているとともに、前記第１軸よりも下方に重心を有し、
　前記第１リング部材は、前記中心軸及び前記第１軸に直交する第２軸を中心に、前記第２リング部材に対して傾動可能に取り付けられていることを特徴とする被捕集物質捕集器。
【請求項２】
　前記被捕集物質捕集器本体は、前記捕集基質を上方に向けて曝した状態で装着可能であることを特徴とする請求項１記載の被捕集物質捕集器。
【請求項３】
　前記第２リング部材を他の部材に取り付けることを可能とする取付部材を少なくとも１以上備えることを特徴とする請求項１または２記載の被捕集物質捕集器。

【書類名】明細書
【発明の名称】被捕集物質捕集器
【技術分野】
【０００１】
本発明は、被捕集物質を捕集可能な捕集基質を装着可能である被捕集物質捕集器に関するものである。
【背景技術】
【０００２】
現在、日本人の約４０００～５０００万人が何らかのアレルギー症状を抱えており、その数も年々増加傾向にある。例えば、日本国における喘息医療費は、労働損失など間接費を含めると、年間約６４００億円にものぼることが報告されている。花粉症患者は、全国で約１３００万人、経済損失は年間約２９００億円と推定され、問題の早期解決が望まれる。また、欧米においても最近の１０年間で、アレルギー性疾患の罹患率が２０～５０％の率で増加していると報告されており、対策が急務とされている。
【０００３】
気管支喘息やアレルギー性鼻炎など呼吸器系アレルギー疾患においては、吸入性アレルゲン（ダニ、カビ、スギ花粉など）による曝露の寄与が大きいと言われているものの、呼吸器系アレルギー疾患の発症機構の詳細については未解明な部分も多く、広範かつ体系的な曝露評価調査や疫学調査を行うことによって、その発症機構の詳細を解明する必要がある。
【０００４】
呼吸器系アレルギー疾患の発症機構の詳細の解明は、ポンプなどの動力を利用したアクティブ型捕集器によって、吸入性アレルゲンを含む浮遊粒子状物質を捕集することによって行なうことができる。例えば、複数のアクティブ型捕集器を室内外の様々な場所に設置して、これら複数のアクティブ型捕集器によって捕集された吸入性アレルゲンに基づいて、個人曝露量を推定することが行われている。しかしながら、このような方法は、あくまでも推定の域を脱しておらず、吸入性のアレルゲンの個人曝露評価について、被験者を取り囲む極めて局域的な空気中濃度についてまで考慮されているものではない。また、このようなアクティブ型捕集器を各被験者に取り付けて運搬させることによって、極めて曲域的な空気濃度測定するということが考えられるが、そのポンプが重いなどの理由から、持ち運びには適していない（特許文献１）。
【０００５】
一方、このようなアクティブ型捕集器の他に吸入性のアレルゲンを捕集するものとして、ポンプを用いないパッシブ型捕集器が用いられている（特許文献２）。パッシブ型捕集器は、通常、気体透過性の捕集基質（拡散フィルタ）を張った容器、又は気体透過性材質により作成された捕集基質（拡散フィルタ）中に、吸着剤をコーティングした充填剤を満たしたサンプラーからなり、これらフィルタに被捕集物を捕集するように構成されている。窒素酸化物（ＮＯｘ）や揮発性有機化合物（ＶＯＣｓ）など、ガス相の物質に対しては、物質固有の拡散係数を用いることにより、パッシブ型捕集器を用いて捕集した物質量から比較的容易に空気中濃度を算出することができる。一方、固体である浮遊粒子状物質（吸入性アレルゲンを含む）は、粒子の大きさにより、空気中における慣性運動、沈降速度、ブラウン拡散の寄与割合が著しく異なることから、パッシブ捕集した粒子全体量から空気中濃度を換算することは、理論的に不可能である。しかし、例外的に、粗大なアレルゲン粒子のみを対象とすれば、ブラウン拡散の影響を十分に無視することができる。したがって、重力沈降のみを考慮した比較的単純化された計算式を用いることにより、浮遊粒子状物質の空気中濃度の計算が可能となる。このような粒径１０μm以上の粗大アレルゲン粒子としては、ダニ、カビ、スギ花粉が含まれており、重要な粒径域の粒子種であるといえる。このため、パッシブ型捕集器により粗大なアレルゲン粒子を捕集して、空気中濃度を計算することができる。
【０００６】

パッシブ捕集した粒子より導かれる空気中の粒子個数濃度の算出方法は、以下の通りである。

【０００７】

アレルゲン粒子の捕集メカニズムとして、重力沈降を想定すると、粒径d_p（m）を有する粒子の重力沈降速度V_{TS}（$m \cdot s^{-1}$）は数１により表される。

【０００８】

【数１】

$$V_{TS} = \rho_p d_p^2 g / 18\eta$$

【０００９】

ここで、ρ_p（$kg \cdot m^{-3}$）：粒子密度、g（$m \cdot s^{-2}$）：重力加速度、η（$kg \cdot m^{-1} \cdot s^{-1}$）：空気の粘性である。また、重力方向に対し垂直方向に配される表面積A（m^2）の捕集基質表面にN個の粒子が重力沈降捕集された場合、重力沈降による粒子フラックスJ（$m^{-2} \cdot s^{-1}$）は、数２により表される。

【００１０】

【数２】

$$J = N / At$$

【００１１】

ここで、t（s）：捕集時間である。また、当該空間における粒子の個数濃度C（m^{-3}）は、フラックスJおよび重力沈降速度V_{TS}の情報より、数３により表される。

【００１２】

【数３】

$$C = J / V_{TS}$$

【００１３】

したがって、粒子個数濃度Cは、数１～数３より、数４によって表される。

【００１４】

【数４】

$$C = 18N\eta / At\rho_p d_p^2 g$$

【００１５】

ここで、測定条件および測定粒子を数えることによって、N、η、A、tおよびgを得ることができる。一方、ρ_pおよびd_pは、各アレルゲン粒子で異なる未知数をとることから、粒子密度ρ_pに関しては文献値（例：花粉８５０$kg \cdot m^{-3}$）より情報を得て、粒子径d_pに関しては重力沈降捕集した粒子を顕微鏡観察することにより情報を得ることが可能である。

【００１６】

このようなパッシブ型捕集器は、ポンプを必要としないので、軽量である。このため、

被験者に持ち運ばせることにより、個人曝露捕集器として利用することが考えられる。
【００１７】
【特許文献１】特開２００４－３７２３０
【特許文献２】特開２００４－１９１１２０
【発明の開示】
【発明が解決しようとする課題】
【００１８】
しかしながら、パッシブ型被捕集物質捕集器を被験者に装着させる場合、被験者の動きにより、粒子を捕集する捕集基質面が傾く場合があり、算出される空気中の粒子個数濃度にその傾きによる誤差が生じるという問題がある。すなわち、上述のように捕集基質上に重力沈降捕集した粒子から空気中の濃度を計算することは可能であるが、計算精度をより上げるためには、測定時の捕集基質面の重力方向に対する傾きを一定の角度に維持する必要がある。また、重力沈降する浮遊粒子以外の被捕集物質、例えばアルデヒドやケトンなどのガスを捕集する場合であっても、測定時の捕集基質面の重力方向に対する傾きを一定の角度に維持する必要がある。
【００１９】
そこで、本発明は、このような問題に鑑みてなされたものであって、被験者が携帯可能な程度に軽量であり、その被験者の動きによる誤差を可及的に防止することができるパッシブ型被捕集物質捕集器を提供することを目的とする。
【課題を解決するための手段】
【００２０】
以上の目的を達成するため、本発明に係る被捕集物質捕集器は、被捕集物質を捕集可能な捕集基質を曝した状態で装着することが可能である被捕集物質捕集器本体と、該被捕集物質捕集器本体の外縁よりも大きな内縁を有する第１リング部材と、該第１リング部材の外縁よりも大きな内縁を有する第２リング部材と、を備え、前記被捕集物質捕集器本体は、その垂直方向に延びる中心軸と直交する第１軸を中心に、前記第１リング部材に対して傾動可能に取り付けられているとともに、前記第１軸よりも下方に重心を有し、前記第１リング部材は、前記中心軸及び前記第１軸に直交する第２軸を中心に、前記第２リング部材に対して傾動可能に取り付けられていることを特徴とする。
【００２１】
以上のように本発明に係る被捕集物質捕集器によれば、被捕集物質捕集器本体が下方に重心を有し、第１リング部材と傾動可能であって、この第１リング部材は、第２リング部材と傾動可能であるので、被捕集物質捕集器本体は、重力方向に対して常に一定の方向に維持し、これにより、装着された捕集基質の面を重力方向に対して一定の角度に維持することができる。
【００２２】
本発明に係る被捕集物質捕集器において、前記被捕集物質捕集器本体は、前記捕集基質を上方に向けて曝した状態で装着可能であることが好ましく、このように捕集基質を上方に向けて曝した状態で装着する場合、被捕集物質として重力沈降する浮遊粒子を捕集することができる。すなわち、上記数２及び数４のＡの値を定置することにより、パッシブ捕集した粒子量から空気中濃度への換算を経験又は統計的にではなく、物質移動論などに基づき解析的に行なうことができる。
また、前記捕集基質の面の角度は、様々な角度になるように捕集基質を装着しても良く、例えば捕集基質の面が垂直な状態になるように捕集基質を装着した場合、ガスなどの捕集に用いることができる。
【００２３】
また、本発明に係る被捕集物質捕集器は、前記第２リング部材を他の部材に取り付けることを可能とする取付部材を少なくとも１以上備えることが好ましく、このように取付部材を設けることにより、被験者に取り付けることができる。さらに、本発明に係る捕集物質捕集基は、被験者に携帯させて利用する他、静置して用いても良い。この場合、上述の

ように捕集基質の面を一定の角度に維持することができるので、傾斜面に設置した場合であっても、重力方向に垂直な角度など所望の角度を保つことができる。

【発明の効果】

【００２４】

以上のように、本発明によれば、被験者が携帯可能な程度に軽量であり、その被験者の動きによる誤差を可及的に防止することができるパッシブ型被捕集物質捕集器を提供することができる。

【００２５】

このように、このパッシブ型捕集器を持ち運び可能な携帯型にすることにより、被験者に常時携帯してもらうことが可能となり、これにより被験者を取り囲む極めて局域的な空気中濃度について常時測定することができ、より現実に即した形で対象物質への個人暴露を評価することが可能となる。そして、これにより、アレルギー患者に関するより精緻な曝露評価調査および疫学調査が促進され、これまで未解決な部分も多かったアレルギー疾患の発症機構の詳細について、新たな知見を得ることが可能となる。また、乳幼児が携帯可能な数センチ大のパッシブ型捕集器を開発すれば、アレルギー疾患の発症において重要な乳幼児期におけるデータ収集が可能となる。

【発明を実施するための最良の形態】

【００２６】

次に、本発明に係る被捕集物質捕集器の第１実施例について、図面に基づいて説明する。第１実施例に係る被捕集物質捕集器は、重力沈降する浮遊粒子を捕集するものである。図１は、第１実施例に係る被捕集物質捕集器の正面図であり、図２は、その平面図であり、図３は、その側面図であり、図４は、図２のＡ－Ａ線に沿った断面図であり、図５は、図２のＢ－Ｂ線に沿った断面図である。

【００２７】

第１実施例に係る被捕集物質捕集器１０は、捕集基質１２を装着することが可能な被捕集物質捕集器本体１４と、被捕集物質捕集器本体１４の外縁よりも大きな内縁を有する第１リング部材１６と、第１リング部材１６の外縁よりも大きな径の内周面からなる開口部１８Ａを上方に有するハウジング部材１８と、を備えている。

【００２８】

被捕集物質捕集器本体１４は、上方に円状の開口１４Ａを有する有底円筒状に形成されており、その開口１４Ａには、その全域を覆うように円盤状の捕集基質１２を装着することができる。すなわち、開口１４Ａの内周面の上端には、開口１４Ａよりも大きな径を有する段差１５が形成されており、その段差１５の上面に捕集基質１２の外縁が載置される。したがって、捕集基質１２の径は、段差１５の内径と同じであることが好ましく、少なくとも段差１５の内径よりも小さく、開口１２Ａの内径よりも大きい必要がある。この捕集基質１２の上方には、リング状のゴムパッキン２０を介して、捕集基質１２とほぼ同径な円盤状の網目部材２２が載置される。さらに、リング状の蓋部材２４を被捕集物質捕集器本体１４に螺着することによって、網目部材２２及びゴムパッキン２０を段差１５の方向に押圧し、これにより、捕集基質１２を被捕集物質捕集器本体１４に固定することができる。網目部材２２は、捕集の目的とするダニ、カビ、スギ花粉などの浮遊粒子が透過可能に構成されている。

【００２９】

被捕集物質捕集器本体１４は、垂直方向下方に突出する突出部１４Ｂを有する。また、被捕集物質捕集器本体１４は、その垂直方向の軸線ａ－ａに垂直な位置の軸線ｂ－ｂを中心に、第１リング部材１６に対して傾動可能に取り付けられている。すなわち、被捕集物質捕集器本体１４の軸線ｂ－ｂ上には、外周面から中心に向かって一対のねじ穴２６、２６が形成されており、このねじ穴２６、２６に後述する取付ねじ２８、２８が螺合されることにより、被捕集物質捕集器本体１４を第１リング部材１６に対して傾動可能に取り付けている。そして、被捕集物質捕集器本体１４の突出部１４Ｂは、垂直方向下方に突出することによって、被捕集物質捕集器本体１４の重心を軸線ｂ－ｂよりも下方に形成するこ

とができ、これにより例え第１リング部材１６が傾いたとしても、被捕集物質捕集器本体１４は、第１リング部材１６に対してその傾いた方向と反対方向に相対的に傾動し、その上下方向の軸を軸線ａ－ａと一致させることができるので、捕集基質１２は、重力方向に対して垂直な位置を維持することができる。

【００３０】

第１リング部材１６は、上述のように被捕集物質捕集器本体１４のねじ穴２６、２６に螺合可能な取付ねじ２８、２８によって被捕集物質捕集器本体１４を傾動可能に取り付けている。第１リング部材１６と被捕集物質捕集器本体１４の間の取付ねじ２８、２８の外周には、テフロン（登録商標）など摩擦係数の少ない素材で構成された円筒状のスペーサ３０、３０が介在しており、このスペーサ３０、３０によって、第１リング部材１６に対する被捕集物質捕集器本体１２の傾動を可能としている。また、第１リング部材１６は、上述した軸線ａ－ａ及び軸線ｂ－ｂに対して垂直な軸線ｃ－ｃを中心に、ハウジング部材１８の開口部１８Ａに対して傾動可能に取り付けられている。すなわち、第１リング部材１６の軸線ｃ－ｃ上には、外周面から中心に向かって一対のねじ穴３２、３２が形成されており、このねじ穴３２、３２に後述する取付ねじ３４、３４が螺合されることにより、第１リング部材１６をハウジング部材１８の開口部１８Ａに対して傾動可能に取り付けている。

【００３１】

ハウジング部材１８は、上述のように第１リング部材１６のねじ穴３２、３２に螺合可能な取付ねじ３４、３４によって、開口部１８Ａに第１リング部材１６を傾動可能に取り付けている。ハウジング部材１８と第１リング部材１６の間の取付ねじ３４、３４の外周には、テフロン（登録商標）など摩擦係数の少ない素材で構成された円筒状のスペーサ３６、３６が介在しており、このスペーサ３６、３６によって、ハウジング部材１８に対する第１リング部材１６の傾動を可能としている。したがって、このハウジング部材１８の開口部１８Ａは、第２リング部材として機能している。

【００３２】

また、ハウジング部材１８は、断面Ｕ字状に形成されており、取付ねじ３４、３４の上方に突出して延在する一対の突出部１８Ｂ、１８Ｂを有する。この突出部１８Ｂ、１８Ｂの一方には、取付鎖３８の一端がねじ４０によって傾動可能に取り付けられており、他方には、取付鎖３８の他端がねじ４０によって傾動可能に取り付けられている。この取付鎖３８は、被験者の首に掛けるのに十分な長さを有する。また、このような取付鎖３８を取り付ける代わりに被験者のベルトなどに引っ掛けるためのフック４２を設けても良い。このフック４２は、例えばＬ字状に形成して、ハウジング部材１８の底面にねじ４４によって固定しても良い。

【００３３】

次に、第１実施例に係る被捕集物質捕集器において、捕集基質１２の面を重力方向に直交した状態に維持可能であることについて説明する。先ず、被捕集物質捕集器本体１４は、突出部１４Ｂによって中心下部に重心を有する。したがって、図１に示すように、被捕集物質捕集器１０が軸線ｂ－ｂを中心に方向Ｍｂに傾く場合、第１リング部材１６は、ハウジング部材１８と一体に方向Ｍｂに傾くが、粒子捕集器本体１２は、突出部１２Ｂによる中心下部への重心により、軸線ｂ－ｂを中心に第１リング部材１６に対して、第１リング部材１６とハウジング部材１８が傾いた方向と反対方向に相対的に傾動され、捕集基質１２の面の重力方向に垂直な位置が維持される。また、図３に示すように、被捕集物質捕集器１０が軸線ｃ－ｃを中心に方向Ｍｃに傾く場合、ハウジング部材１８は、方向Ｍｃに傾くが、被捕集物質捕集器本体１４は、突出部１４Ｂによる中心下部への重心により、第１リング部材１６と一体となって、軸線ｃ－ｃを中心にハウジング部材１８に対して、ハウジング部材１８が傾いた方向と反対方向に相対的に傾動され、捕集基質１２の面の重力方向に垂直な位置が維持される。さらに、被捕集物質捕集器１０が軸線ｂ－ｂと軸線ｃ－ｃの間の軸を中心に傾く場合、ハウジング部材１８は、その傾いた方向に傾くが、粒子捕集器本体１４は、突出部１４Ｂによる中心下部への重心により、第１リング部材１６は、

軸線ｃ－ｃを中心にハウジング部材１８に対して、ハウジング部材１８が傾いたベクトルを軸線ｂ－ｂ方向と軸線ｃ－ｃ方向に分解した二つのベクトルのうち軸線ｂ－ｂ方向のベクトルの反対方向に相対的に傾動されるとともに、粒子捕集器本体１４は、軸線ｂ－ｂを中心に第１リング部材１６に対して、上述のように分解した二つのベクトルのうち軸線ｃ－ｃ方向のベクトルの反対方向に相対的に傾動され、捕集基質１２の面の重力方向に対して垂直な位置を維持することができる。

【００３４】

次に、実施例１に係る被捕集物質捕集器１０を用いたアレルゲン粒子の採取方法及びアレルゲン粒子の測定方法について説明する。

【００３５】

第１実施例に係る被捕集物質捕集器１０をスギ花粉の採取に使用する場合、ワセリンなどを塗布したスライドガラスを捕集基質１２として使用する。スライドガラス上に付着したスギ花粉はゲンチアナバイオレットなどの染色液で染色し、光学顕微鏡により、捕集基質１２上に付着した花粉を観察することによって１ｃｍ^{2}あたりの花粉の量を計算することができる。

【００３６】

第１実施例に係る被捕集物質捕集器１０を真菌や細菌の採取に使用する場合、ペトリ皿に寒天培地を固化させたものを捕集基質１２として使用する。寒天培地上に落下した真菌や細菌は、目視できるまで培養するのではなく、より短時間に成長した微小なコロニーを染色することにより判別し易くし、１０～２０倍の顕微鏡観察によって、コロニーを計数することができる。

【００３７】

上記に加えて、スギ花粉、真菌及び細菌などのアレルゲン粒子を識別する方法であるＥＬＩＳＡ染色法を使用してもよい。この染色法は、生体内にアレルゲンなどの異物（原体）が入り、生体内の免疫システムにより、その抗原にのみ特異的に作用、捕捉するタンパク（抗体）が生産されることを応用したものである。すなわち、アレルゲン粒子に付着した抗体に、発色基質（もしくは蛍光基質）を作用させることにより、アレルゲン粒子のみを選択的に発色染色（もしくは蛍光染色）するものである。これら染色されたアレルゲン粒子は、光学顕微鏡や蛍光顕微鏡を用いることで観測し、定量が行われる。

【００３８】

また、顕微鏡により取得した画像を、電子端末に取り込み画像解析ソフトを用いることにより、染色された粒子の色彩、粒径、形状、個数などについて解析を迅速に実効することも可能である。

【００３９】

例えば、文献値より密度ρ_p＝８５０ｋｇｍ^{3}を得て、球形アレルゲン粒子であると仮定した場合、顕微鏡観察によりアレルゲン粒径が３０μｍであると確定すれば、一つあたりのアレルゲン粒子の質量は４．５×１０$^{-16}$ｋｇ（０．４５ｐｇ）となる。したがって、顕微鏡観察を用いる本手法は、ｐｇレベルでのアレルゲン検出が可能な測定手段であるといえる。そして、その検出感度の高さから、より短時間で個人曝露測定が可能となる。また、従来法である吸光度測定方法はアレルゲンをバルクとして分析することから、粒子の粒径分布や形状などの情報を取得不可能である一方、本手法であれば、試料を顕微鏡観察することから、アレルゲン粒子の粒径分布や形状などの付加情報を得ることが可能になる。

【００４０】

また、浮遊粒子状物質の粒径及び形状は、呼吸器官における沈着部位、すなわち呼吸器官における炎症部位を決定する因子であるので、この付加情報が重要な役割を果たすこととなる。

【００４１】

また、実施例１に係る被捕集物質捕集器１０を用いてアクティブ捕集する場合、捕集時における捕集基質の空気表面速度U_0は、以下に示す数５により計算される。

【００４２】
【数５】

$$U_0 = 4Q / D_0^2 \pi$$

【００４３】
ここで、Ｑ：流量、Ｄ$_0$：捕集基質直径である。捕集基質直径、空気流量、及び粒子直径にもよるが、数１により算出されるパッシブ型における浮遊粒子の重力沈降速度Ｖ$_{TS}$は、粒子が粗大になるほど、アクティブ型における空気表面速度Ｕ$_0$を十分に上回ることが分かる。上記のようなスギ花粉、真菌及び細菌などのアレルゲン粒子は、捕集基質における空気表面速度と比較し、同程度の重力沈降速度である。したがって、これらのアレルゲン粒子を捕集対象物質として第１実施例の示す被捕集物質捕集器１０により採取することで、ポンプで空気を吸引するアクティブ型の被捕集物質捕集器と比較し同程度のアレルゲン量を、煩雑な機器類を用いることなく重力沈降のみを用い容易に捕集することが可能になる。
【００４４】
なお、第１実施例に係る被捕集物質捕集器１０は、被験者が持ち運んで使用する他に、静置させて用いることもできる。例えば、図６に示すように、三脚４６をハウジング部材１８の底面にねじによって取り付けることができる。この場合、第１実施例に係る被捕集物質捕集器１０を傾斜面４８上に置いたとしても、上述した構成から捕集基質１２の面を重力方向に垂直な位置に維持することができる。
【００４５】
次に、本発明に係る被捕集物質捕集器の第２実施例について説明する。第２実施例に係る被捕集物質捕集器は、ホルムアルデヒドなどのガスを捕集するものである。図７は、第２実施例に係る被捕集物質捕集器の正面図であり、図８は、図７に対応する被捕集物質捕集器の側面図である。第２実施例に係る被捕集物質捕集器１０’は、第１実施例と被捕集物質捕集器本体１４’の形状が異なる。この第２実施例に係る被捕集物質捕集器本体１４’は、捕集基質１２を垂直な状態、すなわち重力方向に平行な状態で装着可能に構成されている。このように捕集基質１２を垂直な状態で装着することにより、例えばホルムアルデヒドやケトンなどガスを捕集する場合であっても、一定の角度を保つことができるので、測定誤差が生じるのを可及的に防止することができる。
【００４６】
以上、発明の実施例について説明したが、本発明はこれらに限定されるものではない。例えば、第１実施例においては、捕集基質としてカバーガラス及び寒天培地等を説明したが、この他、ろ紙を使っても良い。また、捕集器基質の重力方向に対する角度は０°及び９０°に限られず、所定の角度に維持することが可能であれば良い。
【図面の簡単な説明】
【００４７】
【図１】本発明の第１実施例にかかる被捕集物質捕集器の正面図である。
【図２】本発明の第１実施例にかかる被捕集物質捕集器の平面図である。
【図３】本発明の第１実施例にかかる被捕集物質捕集器の側面図である。
【図４】本発明の第１実施例にかかる被捕集物質捕集器のＡ－Ａ断面図である。
【図５】本発明の第１実施例にかかる被捕集物質捕集器のＢ－Ｂ断面図である。
【図６】本発明の第１実施例にかかる被捕集物質捕集器の設置例を示す図である。
【図７】本発明の第２実施例にかかる被捕集物質捕集器の正面図である、
【図８】本発明の第２実施例にかかる被捕集物質捕集器の側面図である。
【符号の説明】
【００４８】

１０，１０’・・・被捕集物質捕集器
１２・・・捕集基質
１４，１４’・・・被捕集物質捕集器本体
１４Ａ・・・開口
１４Ｂ・・・突出部
１５・・・段差
１６・・・第１リング部材
１８・・・ハウジング部材
１８Ａ・・・開口部
１８Ｂ・・・突出部
２０・・・ゴムパッキン
２２・・・網目部材
２４・・・蓋部材
２６・・・ねじ穴
２８・・・取付ねじ
３０・・・スペーサ
３２・・・ねじ穴
３４・・・取付ねじ
３６・・・スペーサ
３８・・・取付鎖
４０・・・ねじ
４２・・・フック
４４・・・ねじ
４６・・・三脚
４８・・・傾斜面

【書類名】図面
【図１】

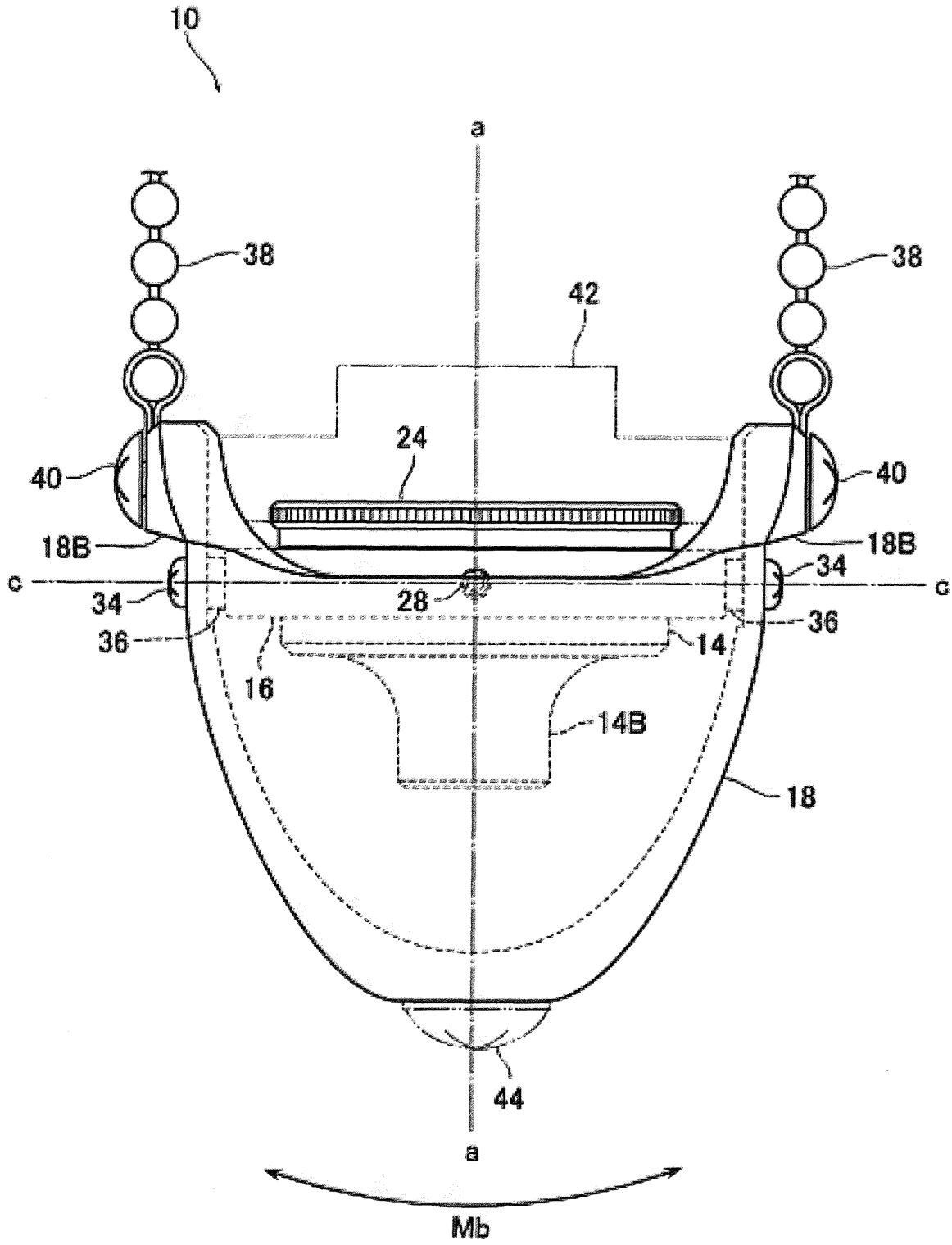

【図２】

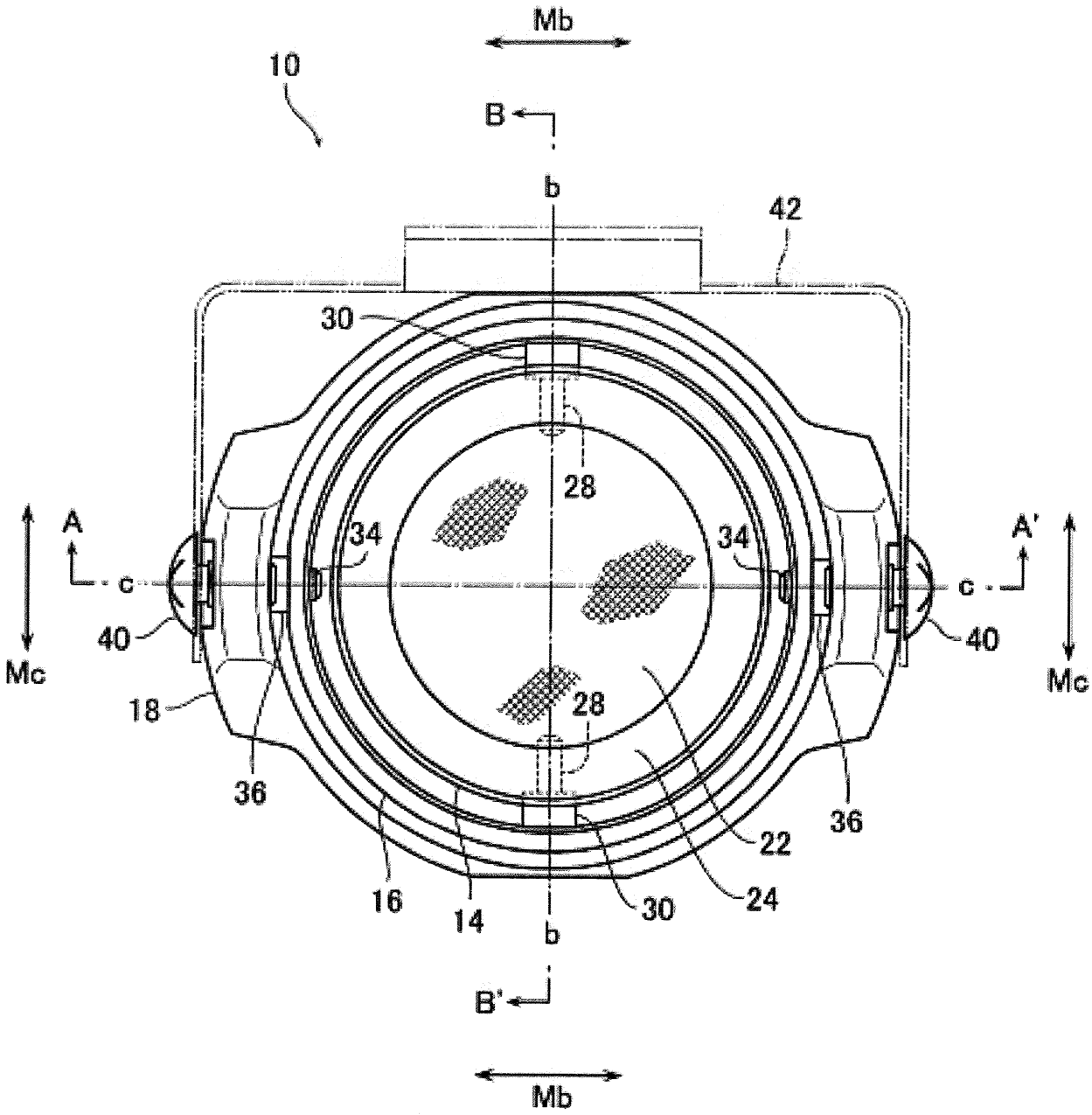
Mb
10
B
b
42
30
28
A
34
34
A'
c
c
40
40
Mc
Mc
18
28
36
36
22
16
14
30
24
b
B'
Mb

【図３】

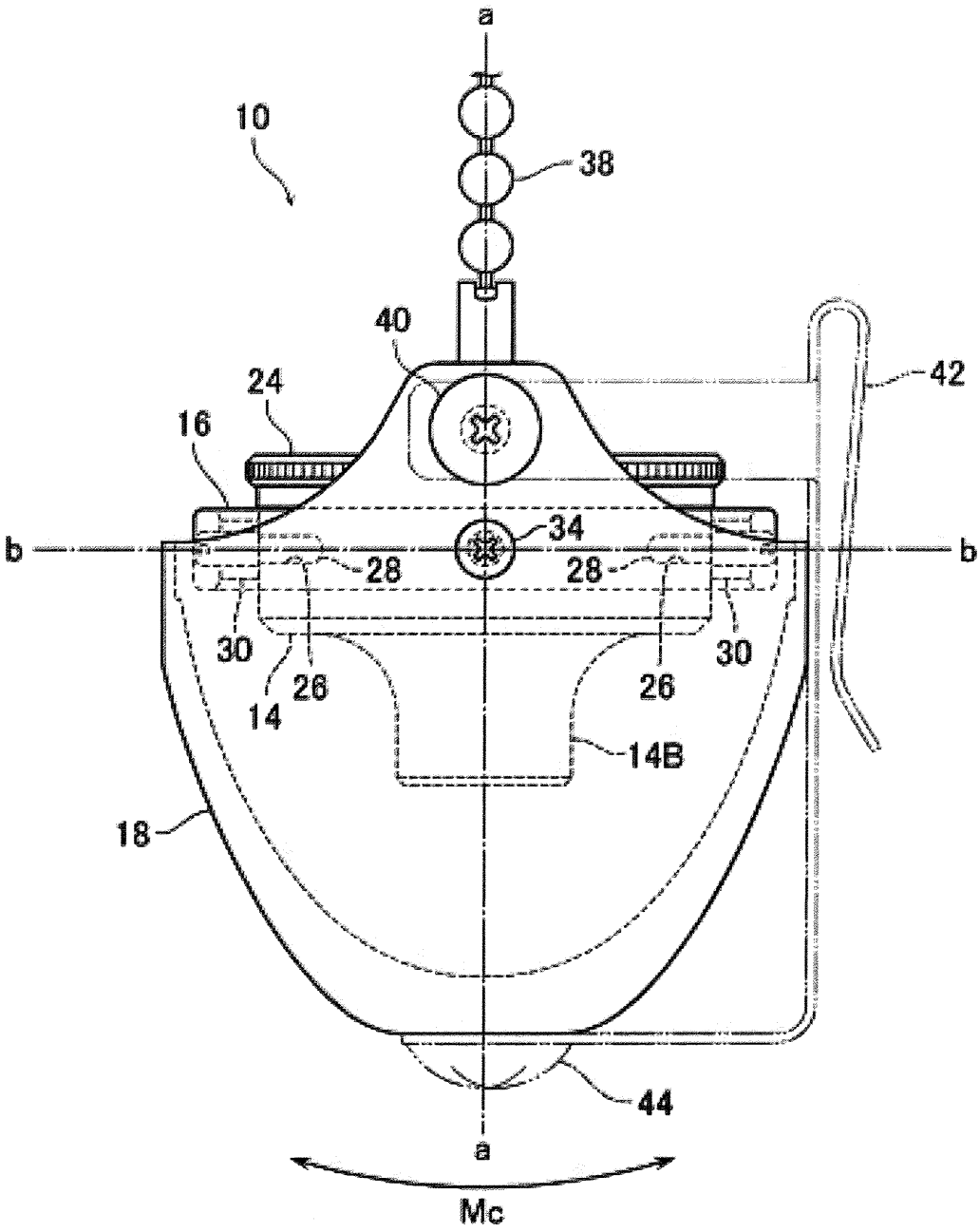

【図４】

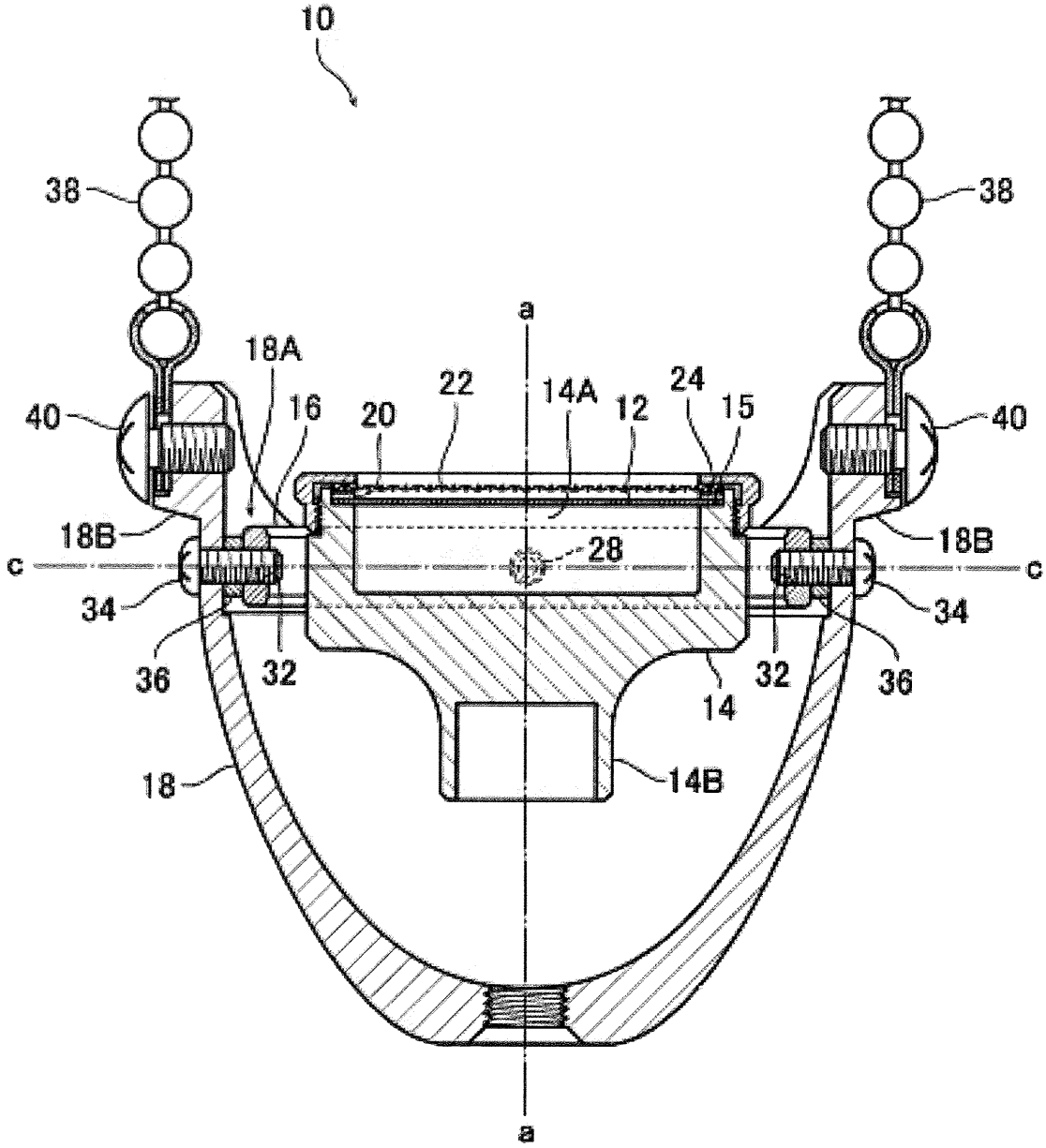
10
38
38
a
18A
22
14A
24
16
20
12
15
40
40
18B
18B
28
c
c
34
34
36
32
32
36
14
18
14B
a

A－A' 断面

【図５】

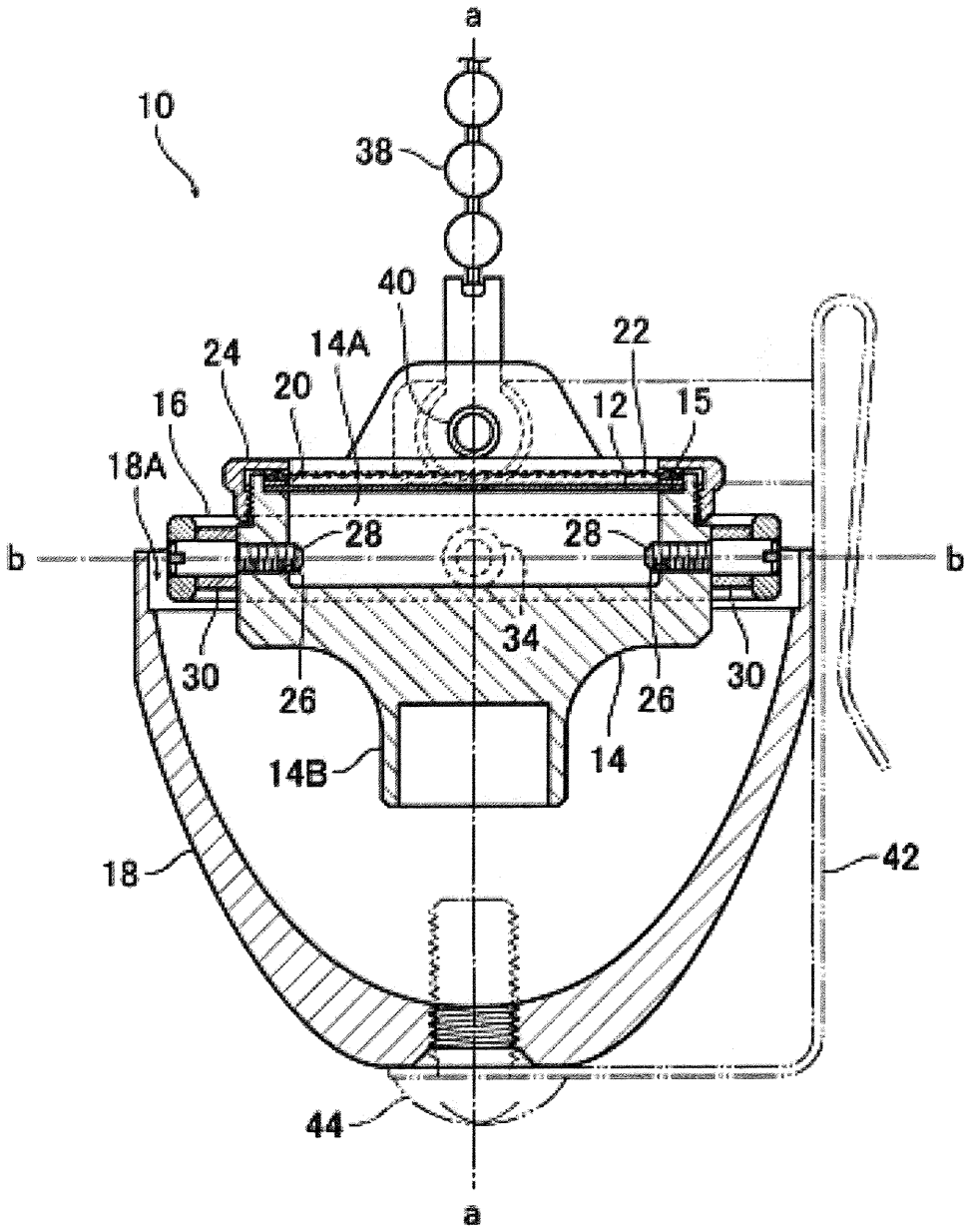
a
10
38
40
24
14A
20
22
16
12
15
18A
b
28
28
b
34
30
26
26
30
14B
14
18
42
44
a

B－B' 断面

【図６】

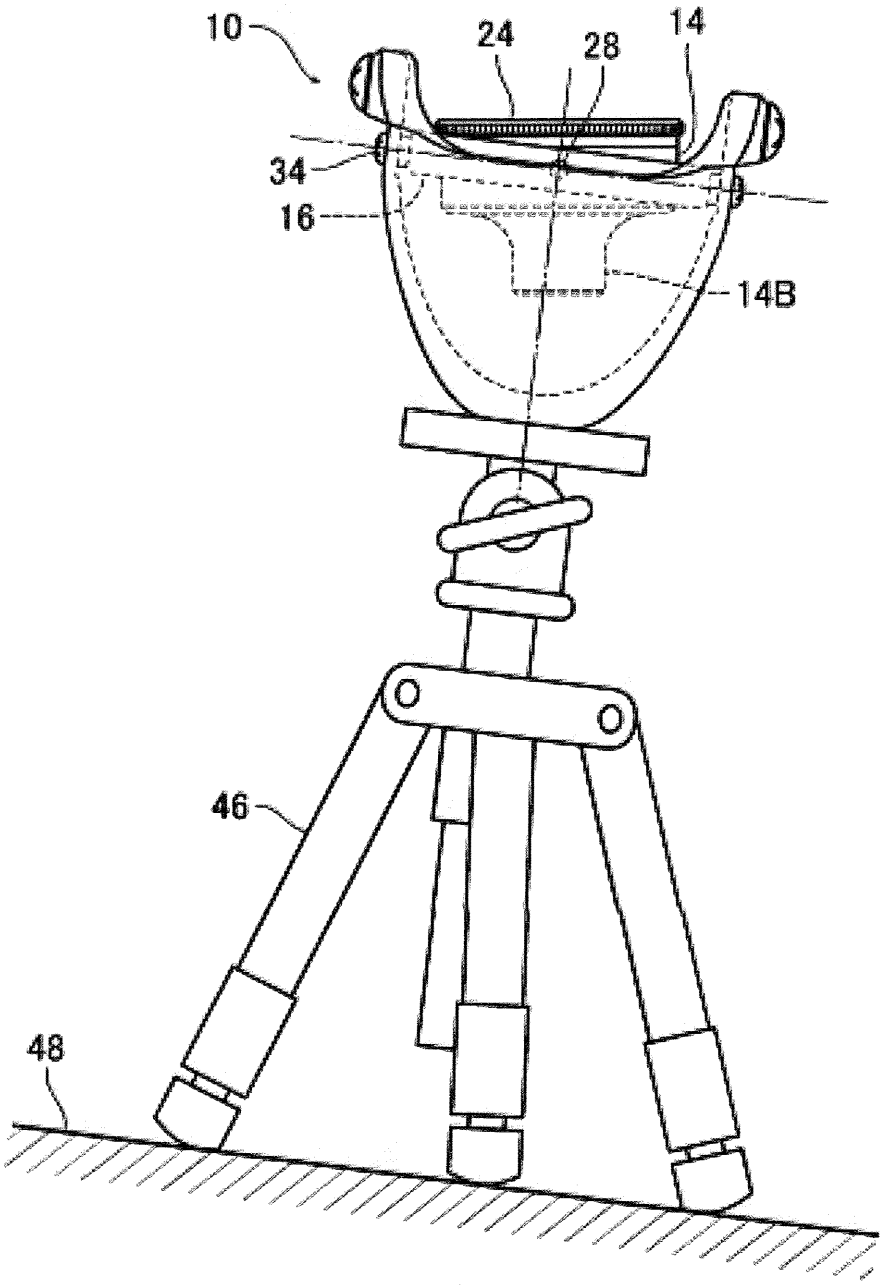

【図７】

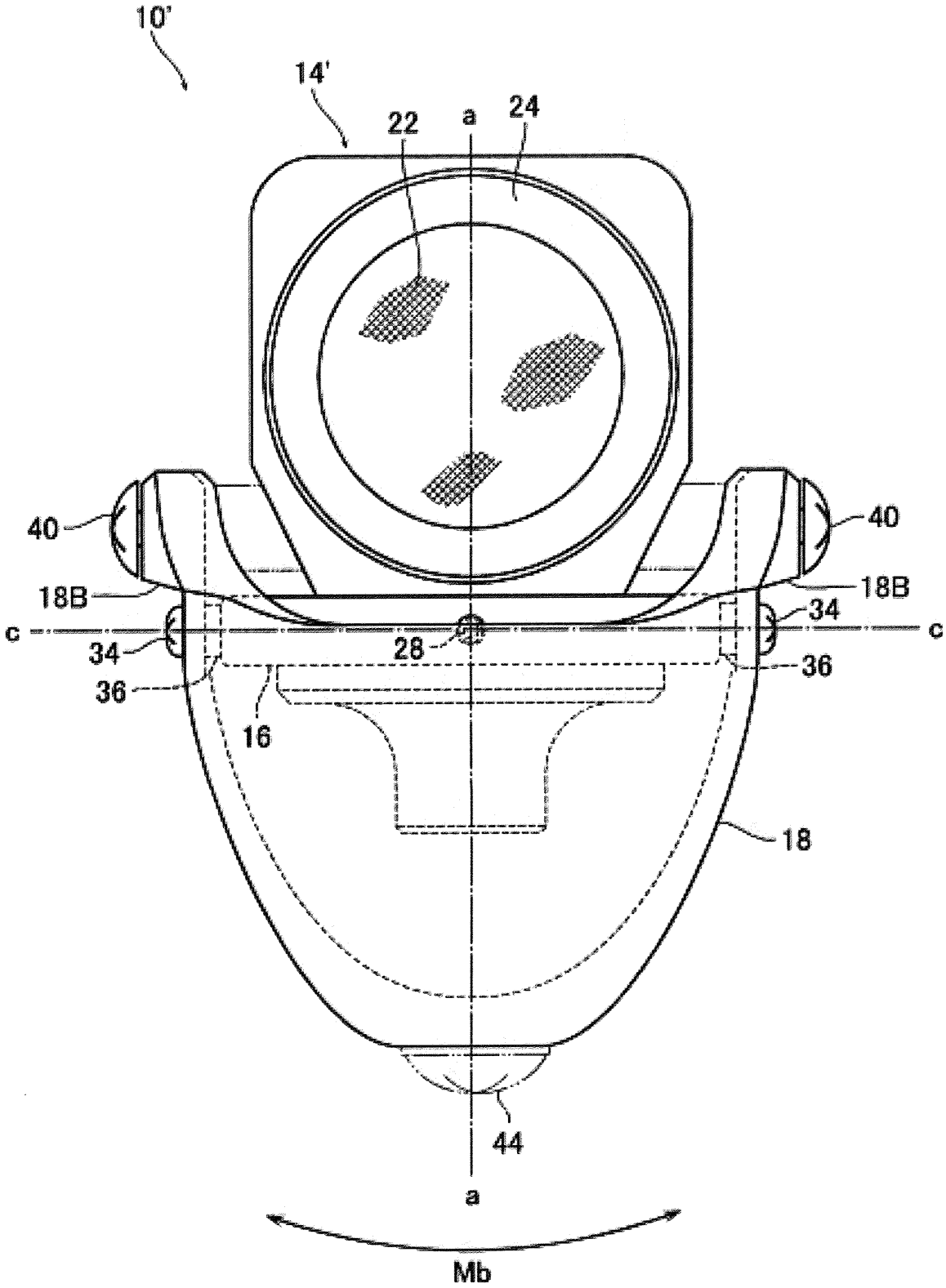

【図８】

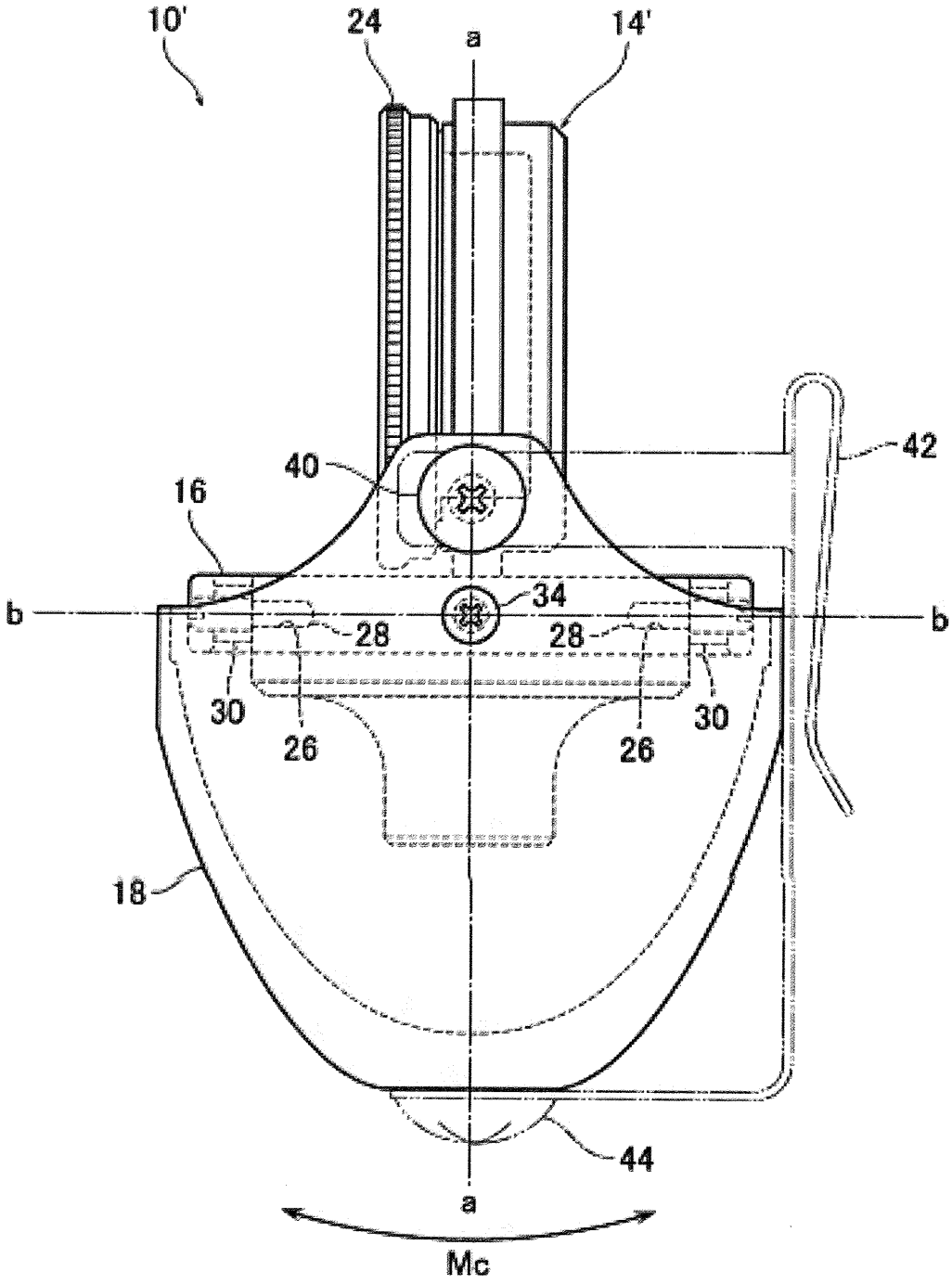

【書類名】要約書
【要約】
【課題】被捕集物質を捕集する面を常に重力方向に対し一定に維持する被捕集物質補集器を提供する。
【解決手段】被捕集物質を捕集可能な捕集基質１２を曝した状態で装着することが可能である被捕集物質捕集器本体１４と、該被捕集物質捕集器本体１４の外縁よりも大きな内縁を有する第１リング部材１６と、該第１リング部材１６の外縁よりも大きな内縁を有する第２リング部材１８と、を備え、前記被捕集物質捕集器本体１４は、その垂直方向に延びる中心軸ａ－ａと直交する第１軸ｂ－ｂを中心に、前記第１リング部材１６に対して傾動可能に取り付けられているとともに、前記第１軸ｂ－ｂよりも下方に重心１４Ｂを有し、前記第１リング部材１６は、前記中心軸ａ－ａ及び前記第１軸ｂ－ｂに直交する第２軸ｃ－ｃを中心に、前記第２リング部材１８に対して傾動可能に取り付けられていることを特徴とする被捕集物質捕集器１０を提供する。
【選択図】図１

APPENDIX C.

Sibata Scientific Technology Catalogues

APPENDIX C.1.
Personal Aeroallergen Sampler (PAAS)

SIBATA

Personal Aeroallergen Sampler (PAAS)

A passive sampler for aeroallergens

The PAAS can be used to collect large airborne particles such as aeroallergens including mite fecal particles, cedar pollens and fungal spores with diameters respectively ranging 10-40 μm, 25-60 μm and 2-60 μm. Particle collection can be sufficiently achieved by gravitational settlings since aeroallergens are relatively large. The sampler is designed to collect large airborne particles on the horizontalized collection surface by gravitational settlings. Even though the sampler is inclined, the effective gravitational settling area can be constant by means of the gyroscopic structure. This prevents distortion of the measurement result caused by inclination of the sampler. In consequence, the sampler can be used as a personal monitor continuously subjected to inclination and/or movement.

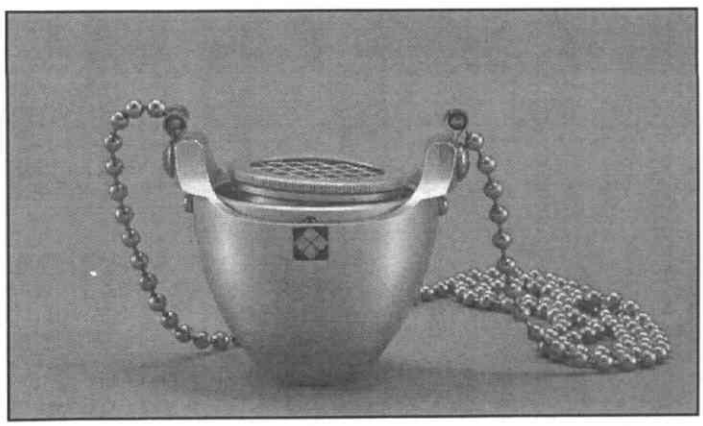

▽Descriptions

- The sampler consists of two planetary rings in different sizes which enables the substrate holder to rotate in all directions. A particle collection substrate is placed on the filter holder, covered by a protective mesh, and tightened with a stainless filter holder cap. The substrate holder is attached by an inner rotating shaft extending to the inner ring, and the inner ring is attached by an outer rotating shaft extending to the protective outer shell. The inner rotating shaft is oriented at an angle of 90 degrees relative to that of the outer shaft. An underlying structure resembling a gyroscope enables the particle collection surface to be continuously directed upward regardless of inclination of the sampler. To collect airborne particles around the human breathing area, the human subject should wear the passive sampler around his or her neck.

▽Applications

Suitable for personal monitoring of aeroallergens such as:

- Cedar pollens
- Airborne fungi
- House dust mite and so on

Particles gravitationally collected on the collection substrate can be analyzed by microscopic and/or culture methods. Bulk analyses are also applicable if sufficient amount of the sample is collected.

▽Specifications

Model	Personal Aeroallergen Sampler (PAAS)
Target substances	Large airborne particles Aeroallergens (pollens, fungi, house dust mite, and so on)
Power source	n/a (Passive method)
Dimensions	50 (W) × 40 (D)× 40 (H) mm
Diameter of particle collection surface	25 mm
Weight	Approx. 50 g

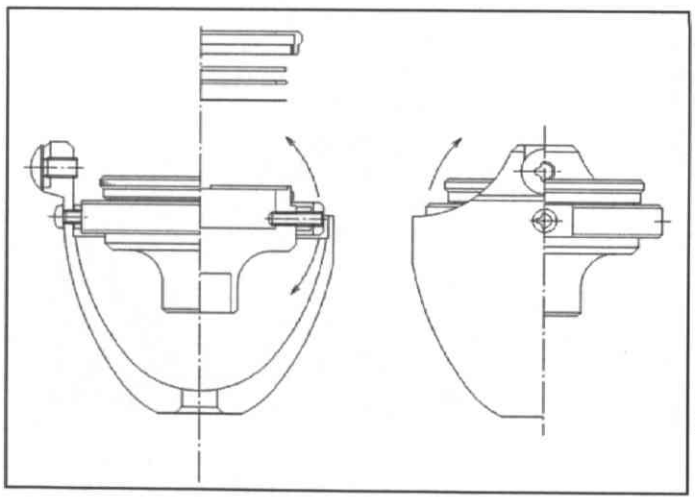

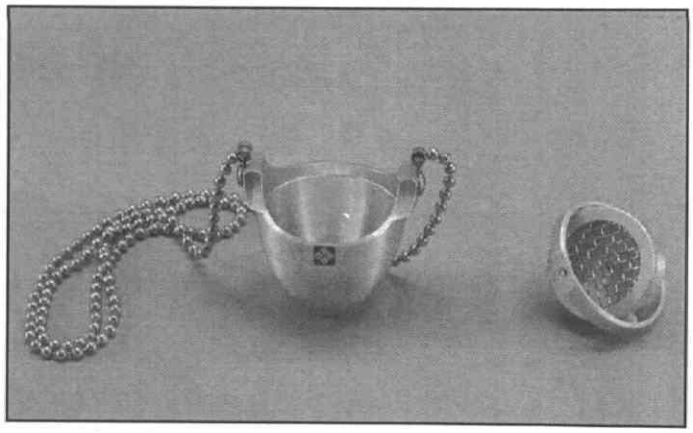

SIBATA

TOKYO Head Office
1-25, Ikenohata 3-chome,
Taito-ku, Tokyo, Japan 110-8701
Tel : 81-3-3822-2112
Fax : 81-3-5685-1394

BEIJING Office
Room No.3213, Beijing Hotel
33, Dong Chang An Jie,
Beijing China
Tel : 86-10-6513-7766 EXT.3213
Fax : 86-10-6513-7842

Yanagisawa Laboratory
University of Tokyo, Graduate School of Frontier Sciences
Address: Hongo 7-3-1, Bunkyo-ku, Tokyo 113-8656, JAPAN
Tel.: +81-3-5841-7335 Fax: +81-3-5841-8583 (N. Yamamoto)
E-mail: webmaster @yy.t.u-tokyo.ac.jp
URL: http://www.yy.t.u-tokyo.ac.jp

APPENDIX C.2.

Personal Aeroallergen Sampler (PAAS) (in Japanese)

参考資料

SIBATA

携帯型アレルゲン捕集装置

Personal Aeroallergen Sampler (PAAS)

A passive sampler for aeroallergens

気管支喘息や鼻炎などの呼吸器系アレルギー疾患では吸入性アレルゲンへの曝露が重要であると言われています。一方、発症機構の詳細ついては未解明な点も多く、広範かつ体系的な調査を行うことで、詳細について明らかにする必要があります。携帯型アレルゲン捕集装置（PAAS）は、浮遊粒子状物質の中でも比較的粗大な吸入性アレルゲン（ダニの糞: 10-40 μm、真菌の胞子: 0.5-30 μm、スギ花粉: 25-60 μm）を捕集対象としており、粒子の重力沈降を捕集の駆動力としていることから、ポンプ等を用いることなく、簡便に吸入性アレルゲンの曝露測定を行うことが可能です。PAAS は、重力沈降を粒子捕集に利用することから、被験者の動きによらず、粒子捕集面が常に上向きとなるよう、回転可能なジャイロスコープ型の捕集装置となっています。

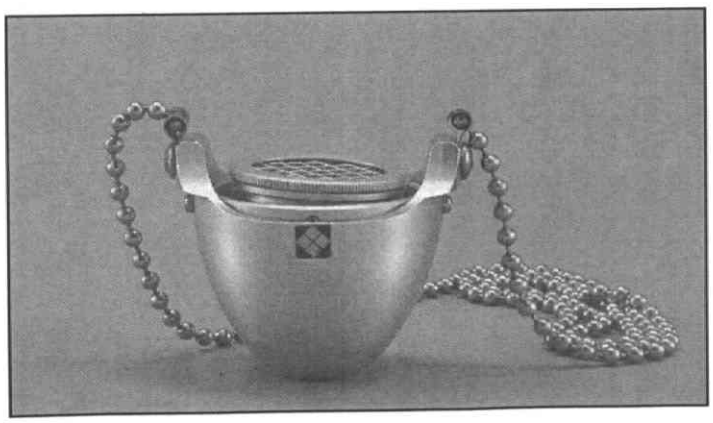

▽特徴

PAAS は、浮遊粒子状物質の中でも比較的粗大な吸入性アレルゲンを捕集対象としています。粒子の重力沈降をパッシブ捕集の駆動力として想定していることから、被験者の動きによらず、粒子捕集面が常に上向きとなるよう、回転可能なジャイロスコープ型の装置としました。また、被験者の呼吸域近傍で捕集が行えるよう、首からぶら下げるためのステンレス鎖を取り付けました。ポンプで空気を吸引ろ過するアクティブ型の測定装置と比較し、簡便な曝露評価調査が可能になります。

▽効果的な利用法

吸入性アレルゲン（スギ花粉、空中菌類、イエダニ等）の個人サンプリングに適しています。捕集した粒子は、光学顕微鏡や蛍光顕微鏡を用いて定性や定量をします。基質上に捕集した粒子を培養法などで計数することも出来ます。また、捕集粒子量が十分なら、既存の吸光度法（ELISA 法）などによる分析も可能です。

▽仕様

型式	携帯型アレルゲン捕集装置 Personal Aeroallergen Sampler (PAAS)
対象物質	粗大粒子 空気中アレルゲン（花粉、菌類、イエダニなど）
サンプリング	パッシブ式（沈降法）
寸法	50 (W) × 40 (D)× 40 (H) mm
粒子捕集面	25 mm
重量	約 50 g

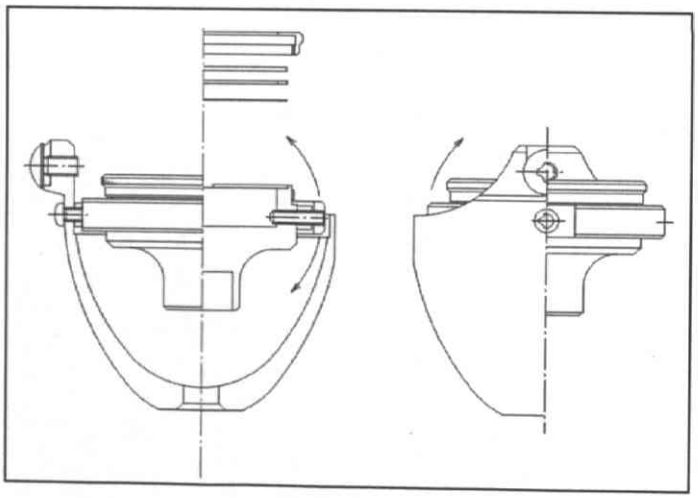

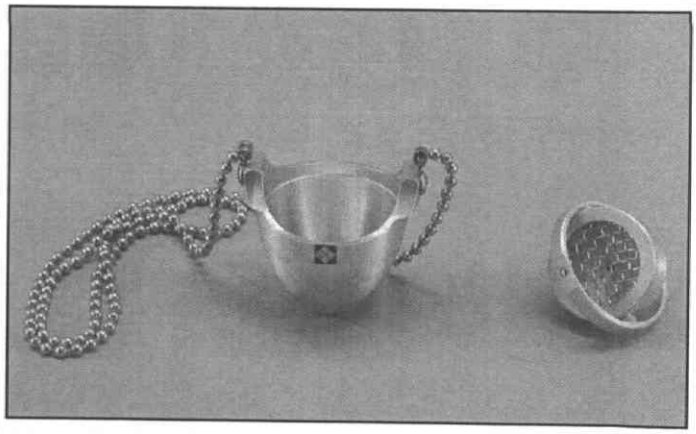

SIBATA SCIENTIFIC TECHNOLOGY LTD.
柴田科学株式会社
本　社　〒110-8701 東京都台東区池之端3-1-25
東京営業所 ☎(03) 3822-2111　福岡営業所 ☎(092) 471-5515
大阪営業所 ☎(06) 6356-8131　仙台営業所 ☎(022) 308-6341
名古屋営業所 ☎(052) 263-9310
ホームページURL=http://www.sibata.co.jp/

東京大学大学院新領域創成科学研究科
柳沢研究室
住所：東京都文京区本郷7-3-1　東京大学工学部5号館
Tel：03-5841-7335　Fax：03-5841-8583（担当：山本）
E-mail: webmaster @yy.t.u-tokyo.ac.jp
URL: http://www.yy.t.u-tokyo.ac.jp

APPENDIX D.

Standard operating procedure for the DA-6100/LS (in Japanese)

王子計測機器ドットアナライザー（DA-6100/LS）
標準操作手順（SOP）

1. 画像取り込み

1.1. 専用のドングル(ハードウェアキー)が使用するPCのプリンターポートに接続されていることを確認する。
1.2. Windows NTを起動する。
1.3. \\C\PM2.5 動作プログラム\test.vbpを開く。
1.4. Microsoft Visual Basicが起動するので、実行ボタン(▶)をクリックすると、図1にある顕微鏡画像の取り込みソフトが起動する。
1.5. 試料を対物レンズの下に設置する。
1.6.「画像取込」ボタンをクリックすると、図1のディスプレイに画像が現れる。
1.7. ディスプレイに縦縞が現れるよう、顕微鏡の照明強度を調節する。
1.8. ディスプレイの縦縞が最も細くなるよう、顕微鏡の右側に付いている、フォーカシングユニットのレボルバーを回転させ、焦点を調節する。
1.9. リニアステージを「移動」ボタンにより移動させることで、通常の顕微鏡画像の取得が可能になる。
1.10. ステージが右端もしくは左端に行き過ぎないよう、適宜「停止」ボタンを用いることで、注意する。
1.11. 試料が対物レンズの直下を移動する直前に、「1 shot」ボタンをクリックする。
1.12. 画像が固定されるので、「画像保存」ボタンをクリックし、画像(tif 形式)をファイルに保存する。
1.13. Windows NTをシャットダウンし、Windows 2000を起動する。
1.14. USBポートにフラッシュメモリーなどの媒体を取り付け、画像を媒体に保存する。
(ネットワーク経由で画像を保存することも可能であるが、Windows NTのメンテナンスおよびセキュリティの問題を考慮し、当該PCはスタンドアロンとして使うことが望ましい。なお、現在あるソフトウェアは、Windows NT上でしか動作しない。また、画像処理および解析については、処理速度の速い他のPCを使うことが望ましい)

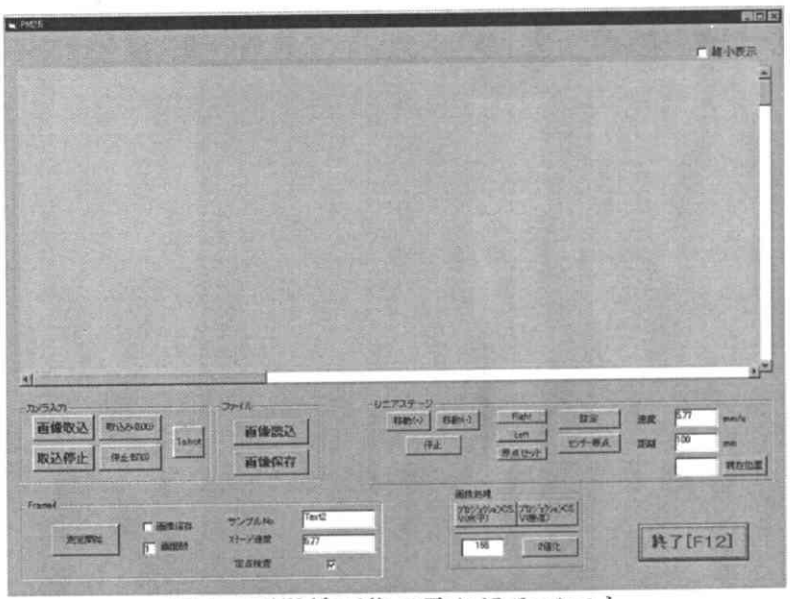

図1. 顕微鏡画像の取り込みソフト

2. 画像処理

2.1. Adobe Photoshop により、顕微鏡画像ファイル(tifファイル)を開く。
2.2. ツールバーの「フィルタ」→「ノイズ」を選び、「輪郭以外をぼかす」の操作を 2 回行う。
2.3. 選択ツールをアクティブにし、選択ツールオプションの「矩形」「固定」を指定する(図 2)。
2.4. 縦横 6 × 1 mm の画像を選択できるよう、幅 362 pixel および高さ 2460 pixel を指定する(図 2)。
2.5. 画像の右端 1 mm の範囲は除外し、縦横 6 × 1 mm を範囲を選択ツールにて選択する。(6 mm の縦方向の長さを確保できない場合、それ以下の長さでもかまわない)(図 2、3)
2.6. 選択した画像は、ツールバーの「イメージ」→「色調補正」→「2 階調化」により、二値化を行う。
2.7. 輝度ヒストグラムの左の裾野を二値化の閾値として選び、画像の二値化を行う(図 4)。
2.8. 二値化画像を bmp 形式で保存する。

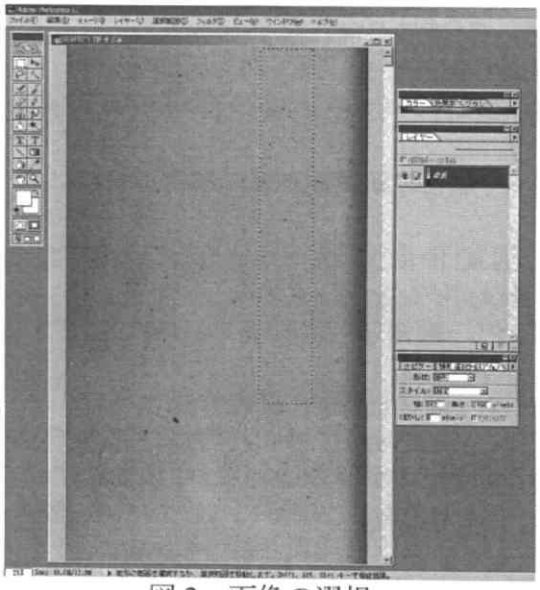

図 2. 画像の選択

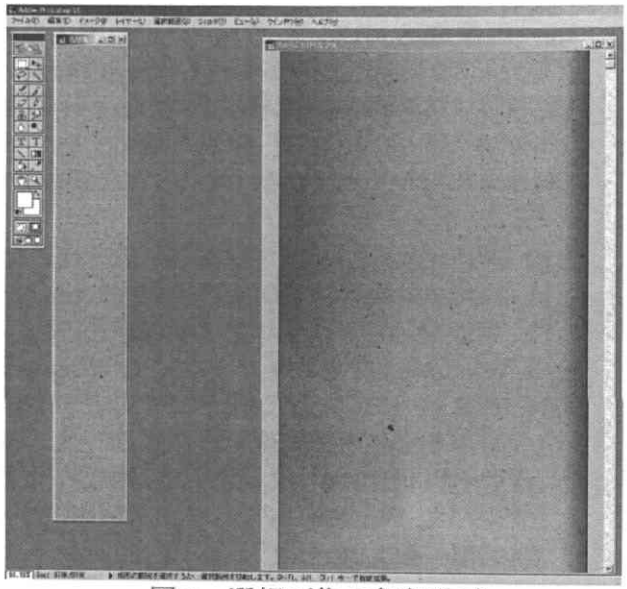

図 3. 選択画像の新規作成

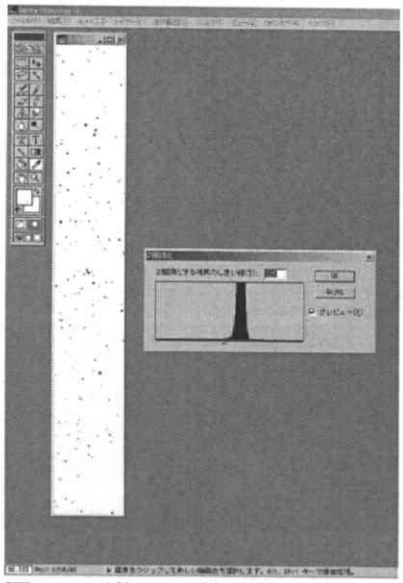

図 4. 画像の二値化閾値の設定

3. 画像解析

3.1. DA6000 の起動
3.1.1. 専用のドングル（ハードウェアキー）が使用する PC のプリンターポートに接続されていることを確認する。
3.1.2. DA6000 を起動する。

3.2. スケーリング
3.2.1. ツールバーの「フィルタ」→「新規作成」を選び、「モノクロイメージ」を作成する。
3.2.2. 「ファイル」→「イメージファイル読込み」を選び、マイクロ目盛りなど、既知幅を持った顕微鏡画像のファイルを開く。
3.2.3. ツールバーの「編集」→「スケール」を選ぶ。
3.2.4. 既知の目盛り幅に合わせ、゛基準値゛および゛単位゛を設定する（図 5）。
3.2.5. 「測定」ボタンをクッリクし、始点および終点を定めることで、スケーリングを行う（図 6）。この場合、横方向にスケーリングすることを推奨する（理由については後述）。
3.2.6. 「設定」ボタンをクッリクし、スケールを決定する。

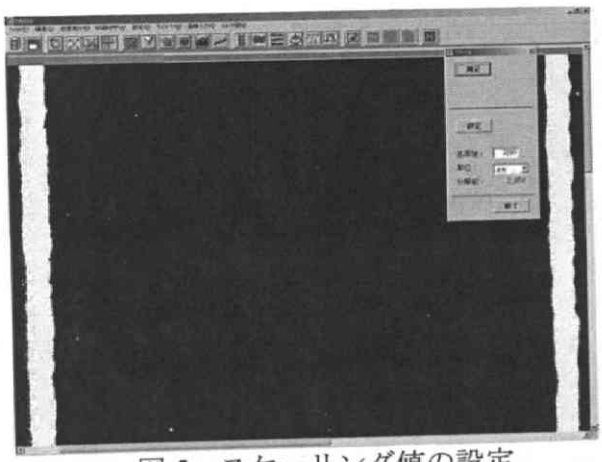
図 5. スケーリング値の設定

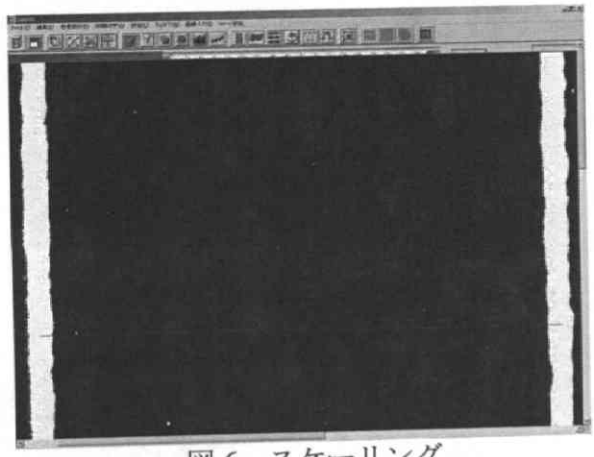
図 6. スケーリング

3.3. 粒子測定

3.3.1.「ファイル」→「イメージファイル読込み」を選び、粒子計測を行うファイルを開く。

3.3.2.「処理実行」→「二値化」を選択し、画像の二値化(反転)を行う。この際、しきい値は High のほうを 0 に設定しておき(図 7)、実行をクリックする。

3.3.3.「処理実行」→「粒子計測」のウィンドウを開き、面積、フェレ円相当径の項目を選択すし(図 8)、OK をクリックする(他の項目については、解析目的に応じて選択する)。

3.3.4. 計算結果が表示されるので(図 9)、計算結果(csv ファイル)を所定のフォルダーに保存する。

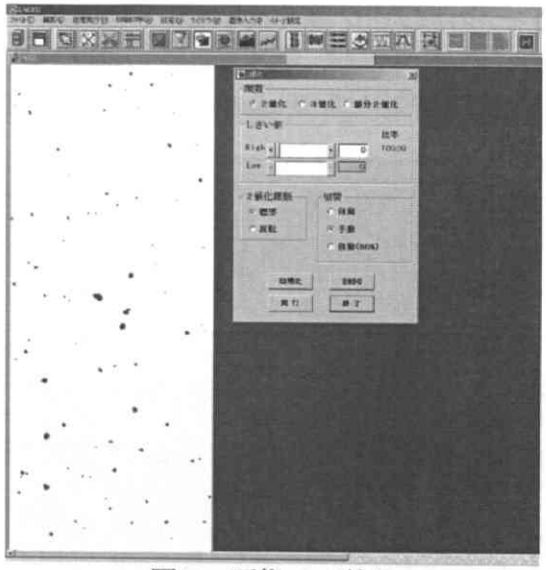

図 7. 画像の二値化

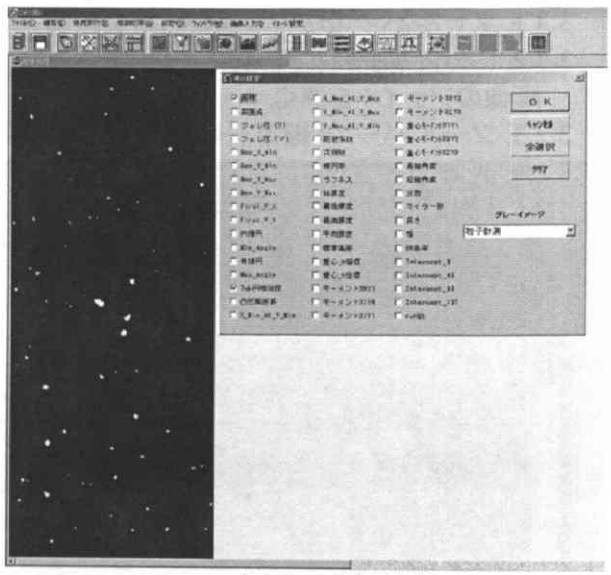

図 8. 画像解析

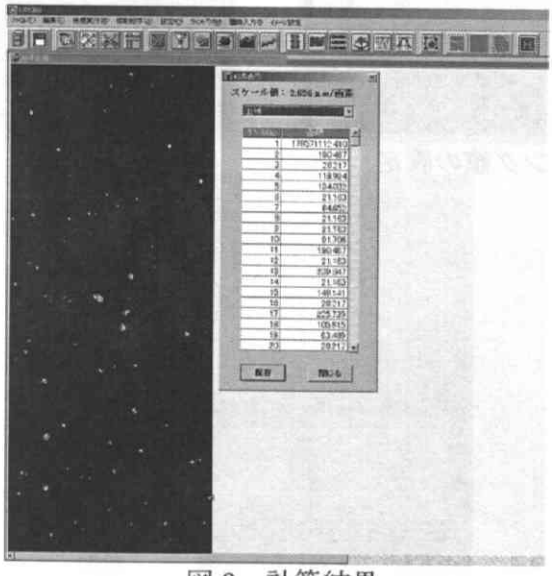

図 9. 計算結果

4. 粒径分布の算出

計算結果はcsvファイルとして保存されている。必要に応じてxlsファイルなどに変換する。また、顕微鏡画像(tifファイル)は、縦横比が410:362と縦長に取り込まれていることから、横方向にスケーリングした場合は縦方向に対して362/410倍し、また縦方向にスケーリングした場合は横方向に対して410/362倍する必要がある。

(粒子投影直径の算出)
Microsoft Excelの以下の関数により、粒子の投影直径が計算できる。

=2*(((362/410)*[面積])/PI())^0.5

ここで、[面積]は、画像解析ソフト(DA6000)により計算された粒子の面積。また、この式は横方向にスケーリングした場合の式となっている。

APPENDIX E.

Curriculum Vitae

NAOMICHI YAMAMOTO

Department of Environmental Systems
Institute of Environmental Studies
Graduate School of Frontier Sciences, The University of Tokyo
Hongo 7-3-1, Bunkyo-ku, Tokyo 113-8656, JAPAN
Tel: +81-3-5841-7335 Fax: +81-3-5841-7335
E-mail: naomichi.yamamoto@yy.t.u-tokyo.ac.jp
URL: http://www.yy.t.u-tokyo.ac.jp/yamamoto/

Education

The University of Tokyo, Graduate School of Frontier Sciences
Institute of Environmental Studies, Dept. of Environmental Systems
Ph.D. Student, Environmental Process Engineering Track (Advisor: Dr. Yukio Yanagisawa)
Ph.D. Thesis: *Microscopic method for airborne coarse particles: Application to a passive sampler*

University of California, Los Angeles, School of Public Health. 2000
Dept. of Environmental Health Sciences
M.S. in Environmental Health Sciences, Air Quality Track (Advisor: Dr. Arthur M. Winer)
Master's Report: *Samplers and instrumentation employed for indoor, outdoor and personal air monitoring and temperatures and relative humidity measured at the California sites of the RIOPA study*

Waseda University, School of Science and Engineering, Tokyo, Japan. 1997
Dept. of Applied Physics
Bachelor of Engineering (Advisor: Dr. Yoshimasa Hama)
Graduation Thesis: *Detection of quantum beats using the single photon counting method.*

Research Experiences

12/2001-present The University of Tokyo, Graduate School of Frontier Sciences, Institute of Environmental Studies
Ph.D. Student / COE Research Assistant (1/03-3/05) / Teaching Assistant (10/03-3/04)
Researcher (National Institute of Public Health) (4/04-present)

Established the microscopic method for particle size distribution quantification. Examined particle penetration characteristics through various type filters to explore novel size fractionation techniques for large airborne particles. Developed a personal aeroallergen sampler (PAAS), a passive sampler to assess personal exposures to aeroallergens.

1/2001-11/2001 University of California, Los Angeles, Southern California Particle Center and Supersite (SCPCS), Particle Instrumentation Unit (PIU)
Staff Research Associate

Operated various aerosol monitors including the Partisol, MOUDI, APS, SMPS, TEOM, DataRAM, and Aethalometer to identify the spatial, temporal, chemical and size fractional trends of particulate matters in several sampling locations in Los Angeles region. Managed and analyzed large data set to present for principal investigators.

10/1998-12/2000 University of California, Los Angeles, School of Public Health, Dept. of Environmental Health Sciences.
Master Student / Graduate Student Researcher (6/99-8/00)

Conducted field monitoring, laboratory research, and data analysis for the national Relationship Among Indoor, Outdoor, and Personal Air Concentrations (RIOPA) Study of PM2.5, aldehydes and air toxics. Identified spatial trends of air pollutant emission sources and traffic density in Los Angeles County using ArcView and ArcInfo GIS.

Grants

4/2004-3/2005 Sasakawa Scientific Research Grant, The Japan Science Society. Development of a separation technique for suspended particulate matters by chemical composition. Total amount of grant: ¥ 500,000.

12/2003 Travel Grant, The University of Tokyo. The 3rd Asian Aerosol Conference, Hong Kong, China. Total amount of grant: ¥ 60,000.

Grants (team award)

4/2003-3/2004 Fujii, M., Yamamoto, N., and Yanagisawa, Y., Suzuki Foundation. Development of a passive aerosol sampler using microscopic observation. Total amount of grant: ¥ 1,500,000

4/2002-3/2003 Yanagisawa, Y., Yamamoto, N., and Fujii, M., Steel Industry Foundation for the Advancement of Environmental Protection Technology. Development of a passive aerosol sampler using a line-sensing optical microscope and image analysis. Total amount of grant: ¥ 1,500,000.

7/1999-3/2000 Shendell, D.G., Sabin, L.D., Yamamoto, N., Guillebaud, C., Wilson Endowment Grant, Dept. of Community Health Sciences, University of California, Los Angeles. Improving public health in the Southern California.

Award

3/1996 University Chancellor's Award, Waseda University, Won the championship in the quadruple scull at the 1995 all Japan intercollegiate rowing competition.

Professional Society Affiliations

Member, American Association for Aerosol Research
Member, Japan Association of Aerosol Science and Technology
Member, Society of Indoor Environment, Japan

Certificate

10/2001 State of California Department of Consumer Affair, Engineer-in-Training (EIT) certificate

Patent

[1] Yanagisawa, Y., Yamamoto, Y., Shibata, M., Koyama, H., Hikono, M., A sampler for suspended particulate matters, JPN patent application number 2005-193740 (2005.07.01).

Journal Articles

[1] Yamamoto, N., Takahashi, Y., Yoshinaga, J., Tanaka, A., Shibata, Y., (2005). Size distributions of soil particles adhered to children's hands, *Archives of Environmental Contamination and Toxicology*, accepted.

[2] Yamamoto, N., Kumagai, K., Fujii, M., Shendell, D.G., Endo, O., Yanagisawa, Y., (2005). Size dependent collection of micrometer-sized particles using nylon mesh, *Atmospheric Environment 39*, (20) 3675-3685.

[3] Endo, M., Yamamoto, N., Yoshinaga, J., Yanagisawa, Y., Endo, O., Goto, S., Yoneda, M., Shibata, Y., Morita, M., (2004). ^{14}C measurement for size-fractionated airborne particulate matters, *Atmospheric Environment 38,* (36) 6263-6267.

[4] Yamamoto, N., Shinozuka, Y., Kumagai, K., Fujii, M., Yanagisawa, Y., (2004). Particle size distribution quantification by microscopic observation, *Journal of Aerosol Science 35,* (10) 1225-1234.

[5] Yamamoto, N., Fujii, M., Kumagai, K., Yanagisawa, Y., (2004). Time course shift in particle penetration characteristics through capillary pore membrane filters, *Journal of Aerosol Science 35*, (6) 731-741.

[6] Shinohara, N., Fujii, M., Kumagai, K., Yamamoto, N., Yamasaki, A., Yanagisawa, Y., (2004). Field validation of an active sampling cartridge as a passive sampler for long-term carbonyl monitoring, *Journal of the Air & Waste Management Association 54*, (4) 419-424.

[7] Shibata, K., Endo, M., Yamamoto, N., Yoshinaga, J., Yanagisawa, Y., Endo, O., Goto, S., Yoneda, M., Shibata, Y., Morita, M., (2004). Temporal variation of radiocarbon concentration in airborne particulate matter in Tokyo, *Radiocarbon 46*, (1) 485-490.

[8] Yamamoto, N., Fujii, M., Endo, O., Kumagai, K., Yanagisawa, Y., (2002). Broad range observation of particle deposition on greased and non-greased impaction surfaces using a line-sensing optical microscope, *Journal of Aerosol Science 33,* (12) 1667-1679.

Translation

[1] Handbook of Chemical Health and Safety, American Chemical Society (Edited by Alaimo, R.J.), Ch. 3 and 8 translated to Japanese by Yamamoto, N., Japanese version (Edited by Tamura, S.) published by Maruzen, Tokyo.

International Conferences

[1] Kumagai, K., Ni, Y., Yamamoto, N., Jona, M., Yamamoto, M., Nakai, S., Kouzaki, J., Yanagisawa, Y., The effect of lifestyle to indoor VOCs, Presented at the 14th Annual Conference of the International Society of Exposure Analysis, Philadelphia, Pennsylvania, 10/17-10/21, 2004.

[2] Yamamoto, N., Fujii, M., Endo, O., Kumagai, K., Yanagisawa, Y., Particle size distributions by collocated filtration and impaction -microscopic comparison-, Presented at the 3rd Asian Aerosol Conference, Hong Kong, China, 01/06-01/09, 2004.

[3] Shibata, K., Endo, M., Yamamoto, N., Yoshinaga, J., Yanagisawa, Y., Endo, O., Goto, S., Yoneda, M., Shibata, Y., Morita, M., Temporal variation of radiocarbon concentration in airborne particulate matter in Tokyo, Presented at the 18th International ^{14}C Conference, Wellington, New Zealand, 09/01-09/05, 2003.

[4] Jaques, P., Colome, S., Avol, E., Grant, B., Thurairatnam, S., Yamamoto, N., Zhu, Y., Hinds, W.C., Froines, J.A., Mobile particulate matter research laboratory for comprehensive aerosol measurement in the Los Angeles Basin. Presented at the Association for American Aerosol Research Annual Conference, Portland, Oregon, 10/15-10/19, 2001.

[5] Shendell, D.G., Colome, S.D., Winer, A.M., Sabin, L.D., Yamamoto, N., Guillebaud, C., Site selection methodology for randomized subject recruitment in Los Angeles County, CA for the Relationship Among Indoor, Outdoor, and Personal Air Concentrations Study of fine particles and air toxics. Presented at the 10th Annual Meeting of the International Society of Exposure Analysis, Monterey, California, 10/24-10/27, 2000.

Domestic Conferences and Lectures

[1] 山本尚理, 彦野政治, 小山博巳, 熊谷一清, 柳沢幸雄「携帯型アレルゲン捕集装置」室内環境学会, 平成 17 年 11 月 20-21 日, 福岡.

[2] 村本淳, 山本尚理, 吉永淳, 平林幹啓, 遠藤治, 長谷川就一, 田邊潔, 後藤純雄, 柴田康行「ディーゼル規制による大気粉塵中炭素起源組成への影響－放射性炭素同位体比を用いた検討－」大気環境学会, 平成 16 年 10 月 20-22 日, 秋田.

[3] 野口美由貴, 熊谷一清, 松村年郎, 河原純子, 山本尚理, 柳沢幸雄「熱蒸散型ピレスロイド系殺虫剤の空間部分特性」日本環境管理学会・室内環境学会 学術研究発表会, 平成 16 年 10 月 9-11 日, 東京(ポスター賞受賞).

[4] 山本尚理, 熊谷一清, 柳沢幸雄「室内活動によるハウスダスト粒子の空気中挙動に関する研究」日本環境管理学会・室内環境学会 学術研究発表会, 平成 16 年 10 月 9-11 日, 東京.

[5] 高橋祐子, 山本尚理, 吉永淳, 田中敦「小児の手に付着する土壌の粒径分布」環境化学討論会, 平成 16 年 7 月 7-9 日, 静岡.

[6] 水越厚史, 河原純子, 倪悦勇, 山本尚理「健康影響を考慮した室内材料最適化に関する基礎的研究」東京大学 COE(化学・材料系)「動的分子論に立脚したフロンティア基礎化学」化学を基盤とするヒューマンマテリアル創成」合同シンポジウム, 平成 16 年 6 月 26-27 日, 東京.

[7] 倪悦勇, 熊谷一清, 吉野博, 吉野泰子, 重野貴之, 吉永淳, 藤井実, 篠原直秀, 山本尚理, 柳沢幸雄「中国における居住環境中 VOC 実態調査－統計分析による室内発生源の推定－」室内環境学会, 平成 15 年 12 月 18-19 日, 東京.

[8] 山本尚理「私のキャリアパス」東京大学大学院新領域創成科学研究科「本音で語るキャリアデザイン in 柏キャンパス」第 15 回新領域創成フォーラム, 平成 15 年 11 月 29 日, 千葉.

[9] Yamamoto, N., Shinozuka, Y., Kumagai1, K., Fujii, M., Yanagisawa, Y., Microscopic filter observation for particle number concentration measurement for indoor low levels, 室内環境学会, 平成 15 年 12 月 18-19 日, 東京.

[10] 熊谷一清, 藤井実, 山本尚理, 瓜生務, 奥泉裕美子, 常名美貴, 高野聡子, 岡野卓, 塩尻一尋, 柳沢幸雄「東京大学大学院 新領域創成科学研究科 環境学専 攻 柳沢研究室紹介」第 6 回分析化学会東京シンポジウム 2002 機器分析東京討論会, 平成 14 年 9 月, 東京.